DOCTOR OF PHILOSOPHY

Optical OFDM with Multiple Information-carrying Dimensions for Elastic Access Networks

Al Halabi, Fadi

Award date:
2019

Awarding institution:
Bangor University

DOCTOR OF PHILOSOPHY

Optical OFDM with Multiple Information-carrying Dimensions for Elastic Access Networks

Al Halabi, Fadi

Award date:
2019

Optical OFDM with Multiple Information-carrying Dimensions for Elastic Access Networks

Fadi Al Halabi

A thesis submitted for the degree of

Doctor of Philosophy

School of Electronic Engineering

Bangor University

March 2019

Abstract

With the exponential data traffic growth associated with unprecedented emerging bandwidth-hungry network applications and services, the fifth generation (5G) of mobile networks is currently being adopted worldwide, which is targeted to provide significant increased signal transmission capacities, massive machine-type communications (MTC), and ultra-reliable low-latency (URLL) real-time services. The 5G network architecture that aims to support these targets adopts the cloud radio access network (C-RAN) where mobile fronthaul connects remote units (RUs) and virtual baseband units (vBBUs), whilst mobile backhaul connects a pool of vBBUs and data centre. To further increase the signal transmission bandwidth of mobile fronthaul/backhaul links in a cost-effective manner, passive optical networks (PONs) are considered as one of the most important candidates. Moreover, intensity-modulation and direct-detection (IMDD) is preferred in these networks to improve its cost-effectiveness and lower the transceiver architecture complexity. From the signal transmission technique point-of-view, the initial stage of 5G should have sufficient transparency to 4G. Since orthogonal frequency division multiplexing (OFDM) is widely used in 4G, thus OFDM is still a promising signal modulation technique for 5G. As such, this dissertation research aims to explore the feasibility of utilising digital signal processing (DSP)-enabled multiple information-carrying dimensions to improve the performance of optical OFDM (OOFDM) IMDD PON systems in terms of signal transmission capacity, system power budget, transceiver design flexibility and system performance adaptability.

A subcarrier index-power (SIP) information-bearing dimension is introduced into conventional OOFDM by setting the subcarrier power level at either low or high according to an incoming data sequence in order to convey an extra information bit per subcarrier. As a result, a novel signal transmission technique termed subcarrier index-power modulated optical OFDM (SIPM-OOFDM) is proposed for the first time. Compared with conventional OOFDM adopting similar signal modulation formats, this technique offers an increase of 17% in signal bit rate without compromising the minimum required optical signal-to-noise ratio (OSNR) for achieving a specific bit error rate (BER). Moreover, such improvement does not degrade the performance tolerance to both chromatic dispersion and fiber nonlinearity. As the usage efficiency of high power level subcarriers is not fully

maximised in SIPM-OOFDM, a technique termed SIPM-OOFDM with superposition multiplexing (SIPM-OOFDM-SPM) is proposed by applying the superposition multiplexing (SPM) operation for high power subcarriers. SPM passively adds different signal modulation format-encoded complex numbers and assigns the sum to a high power subcarrier. As a direct result, compared to SIPM-OOFDM, SIPM-OOFDM-SPM increases the signal bit rate by 28.6% without increasing the signal modulation formats. To further enhance the power usage efficiency of both high and low power subcarriers, an improved version of SIPM-OOFDM-SPM, termed SIPM-OOFDM with dual superposition multiplexing (SIPM-OOFDM-DSPM) is proposed. Compared to SIPM-OOFDM-SPM, SIPM-OOFDM-DSPM increases the signal bit rate by approximately 11% while using lower signal modulation formats. It should be noted that both SIPM-OOFDM-SPM and SIPM-OOFDM-DSPM are capable of improving the system power budget and performance tolerance to both chromatic dispersion and fiber nonlinearity compared to the SIPM-OOFDM technique operating at the same signal bit rate. To further increase the number of information bits conveyed per subcarrier in the above-mentioned techniques, multi-level SIPM-OOFDM (ML-SIPM-OOFDM) is proposed and investigated, in which the number of subcarrier power levels can be increased to a predefined multilevel (ML). As a direct result, compared to SIPM-OOFDM, ML-SIPM-OOFDM improves the signal bit rate by approximately 30%. Moreover, in terms of transceiver design, ML could be applied easily in SIPM-OOFDM, SIPM-OOFDM-SPM and SIPM-OOFDM-DSPM as the ML-associated operating principles, their DSP implementation procedures and corresponding performance advantages are very similar for these transmission techniques.

In all the above outlined signal transmission techniques, each individual subcarrier is regarded as a separate unit to carry extra information bits. To enable a group of subcarriers of various power levels to carry extra information bits, SIPM-OOFDM with subcarrier grouping (SIPM-SG-OOFDM) is proposed, where each symbol is divided into multiple subcarrier groups to bear extra user information bits in the subcarrier group (SG) information-bearing dimension. In addition, SIPM-SG-OOFDM is equipped with an additional capability of automatically detecting and subsequently correcting errors at the receiver without consuming any valuable transmission bandwidth. As a direct result, compared to SIPM-OOFDM, SIPM-SG-OOFDM not only increases the signal bit rate by 11%, but also improves the system power budget by 1.0dB. This implies SIPM-SG-OOFDM can improve performance capacity, adaptability and flexibility. Moreover, the

performances can also be further enhanced by combining the ML and SG operating principles in each of the above-mentioned signal transmission techniques which considerably increases the information-carrying dimension.

The above descriptions indicates that, compared to conventional OOFDM employing similar signal modulation formats, the proposed techniques are capable of providing cost-sensitive IMDD PON systems with improved signal transmission capacities and system power budgets. In terms of the transceiver architecture, the proposed techniques still maintain the exact same transceiver design as conventional OOFDM, except that slight modifications in the encoding/decoding DSP elements occur in each of these techniques. These different DSP elements can be implemented in the digital domain in parallel in the transceivers, thus depending upon the traffic requirements and network status, a suitable technique and/or their combination can be selected to improve both the transceiver performance flexibility and adaptability.

Acknowledgements

First of all, I would like to thank my supervisor, Prof. Jianming Tang, for his guidance during my research and study at Bangor University and also Dr. Roger Giddings for sharing his valuable time whenever I needed some additional assistance. I am also deeply grateful to Prof. Ali Hamié for introducing me to Bangor University and his recommendations while applying for a PhD course in the School of Electronic Engineering.

I also wish to extend my warmest thanks to all my colleagues in the optical communications research group. Together we shared many unforgettable and enjoyable memories and I wish them a bright future full of success and happiness.

Huge appreciation goes to my family for all their everlasting help, support and love. Together we shared an eventful journey.

This thesis is dedicated to the memory of my beloved uncle, Nazem Kafrouni.

Always in our hearts.

Abbreviations

ABL	Adaptive Bit Loading
ALA	Adaptive Loading Algorithms
APL	Adaptive Power Loading
ADC	Analogue to Digital Converter
AMOOFDM	Adaptively Modulated Optical OFDM
AWGN	Additive White Gaussian Noise
BER	Bit Error Rate
BPSK	Binary Phase Shift Keying
BPF	Bandpass Filter
CD	Chromatic Dispersion
CDF	Cumulative Distribution Function
CDM	Code Division Multiplexing
CP	Cyclic Prefix
CoMP	Coordinated Multi-Point
C-RAN	Cloud-Radio Access Network
DAC	Digital to Analogue Converter
DSP	Digital Signal Processing
DWDM	Dense Wavelength Division Multiplexing
EO	Electrical-to-Optical
FDM	Frequency Division Multiplexing
FEC	Forward Error Correction
FFT	Fast Fourier Transform
FPGA	Field Programmable Gate Array
FWM	Four-Wave Mixing
ICI	Inter-Channel-Interference

IFFT	Inverse Fast Fourier Transform
IMDD	Intensity-Modulation and Direct-Detection
IoT	Internet of Things
ISI	Inter-Symbol-Interference
LAN	Local Area Network
LED	Light-Emitting Diode
LPF	Low-pass Filter
LTE	Long-Term Evolution
MAN	Metropolitan Area Network
MCM	Multi-Carrier Modulation
MIMO	Multiple Input, Multiple Output
MMF	Multi-Mode Fiber
OE	Optical-to-Electrical
OFDM	Orthogonal Frequency Division Multiplexing
ONU	Optical Network Unit
OOFDM	Optical Orthogonal Frequency Division Multiplexing
OSNR	Optical Signal-to-Noise Ratio
PAPR	Peak-to-Average Power Ratio
PD	Photodiode
PDM	Polarization Division Multiplexing
PON	Passive Optical Network
P/S	Parallel-to-Serial
PSD	Power Spectral Density
PSK	Phase Shift Keying
QAM	Quadrature Amplitude Modulation
QPSK	Quadrature Phase Shift Keying
QoE	Quality of Experience
RAN	Radio Access Networks

RF	Radio Frequency
RU	Remote Unit
SDM	Space Division Multiplexing
SCN	Small-Cell Network
SSMF	Standard Single-Mode Fiber
SNR	Signal-to-Noise Ratio
S/P	Serial-to-Parallel
SRS	Stimulated Raman Scattering
TDM	Time Division Multiplexing
vBBU	virtual Baseband Unit
VoIP	Voice over IP
WDM	Wavelength Division Multiplexing
XPM	Cross-Phase Modulation

Contents

1. Introduction

1.1 Future Network Challenges

Over the past few decades, mobile communications has undergone a vast and rapid evolution to the point where it has become essential in our daily lives, as millions of people worldwide own mobile devices that support a wide range of applications and services such as image transfer, video call, video-on-demand, online banking, as well as cloud-based services including data storage/recovery and remote access. Users constantly use their mobile devices to post and share their everyday-activities via global multimedia social networking services such as Facebook, Twitter and Instagram. For example, as of January 2018, Facebook has more than 2.2 billion active users while WhatsApp, a worldwide dominant voice over IP (VoIP) service, supports more than 1.5 billion subscribers [1]. Moreover, a case study [2] shows that, compared to the number of smartphone in the United States in 2015, an approximately 40% increase to that is expected by 2021. It is also predicted [3] that an average smartphone user will download approximately one terabyte of data annually by 2020, leading to an over 30 times growth in current mobile data traffic. This trend will persist and become even more pronounced in the near future as it has to satisfy the users' needs at anytime, anywhere and through any method of connectivity.

To accommodate the trend of explosive mobile traffic, fifth generation (5G) of mobile networks is currently being adopted globally, which has the overall goal of ubiquitous connectivity for any kind of device and any kind of application that may benefit from being connected. In parallel with the escalated development of the Internet of Things (IoT), 5G will ultimately transform communications, drive efficiency and productivity, and it also create rich 5G ecosystems, thus enabling the 4^{th} industrial revolution. Technically speaking, 5G needs to offer an increase of approximately 10-100 times in signal bit rate compared to 4G. In terms of traffic density, which is the signal bit rate times the number of users per km^2, 5G should deliver a 1000 times increase around 2020 compared to that in 2010 [4, 5], as well as an improved quality of experience (QoE) for users compared with long-term evolution (LTE) [6]. Apart from the significantly improved signal transmission capacity, 5G must also provide ultra-reliable low-latency (URLL) real-time services. Such requirement is highly important for providing services including public safety sensors, devices monitoring patients and

connected transportation systems. In general, latency is the time duration between making a request for data at the transmitter and detecting it at the receiver [7]. Factors affecting latency includes transmission delay, queuing delay, processing/computing delay and re-transmissions (if required). Whereas, reliability refers to the ability of a system to perform its required functions under a stated condition within the required latency bound [5]. Specifically speaking, 5G aims to support an end-to-end latency within 1ms compared to 4G's 5ms latency and 5G reliability requirement should be as high as 99.99999% in terms of packet error rate [4, 8]. Another major target for 5G is massive machine-type communication (MTC) in which a massive number of machine-type devices are simultaneously connected to allow automated data generation, processing, transfer and exchange amongst them with minimum human interaction [4, 5]. In general, MTC has to support a wide range of applications, including automotive industry, transportation, public safety and healthcare [9, 10]. Moreover, with 50 billion connected devices expected by 2020 that need to access and share data anywhere and anytime, 5G aims to support a density of devices as high as 1 million/km^2 and 10 times extended battery life for low-powered massive MTC devices [11].

The 5G network architecture that aims to support the above-mentioned targets is presented in Fig.1.1 [12]. As shown in this figure, the 5G network adopts the cloud radio access network

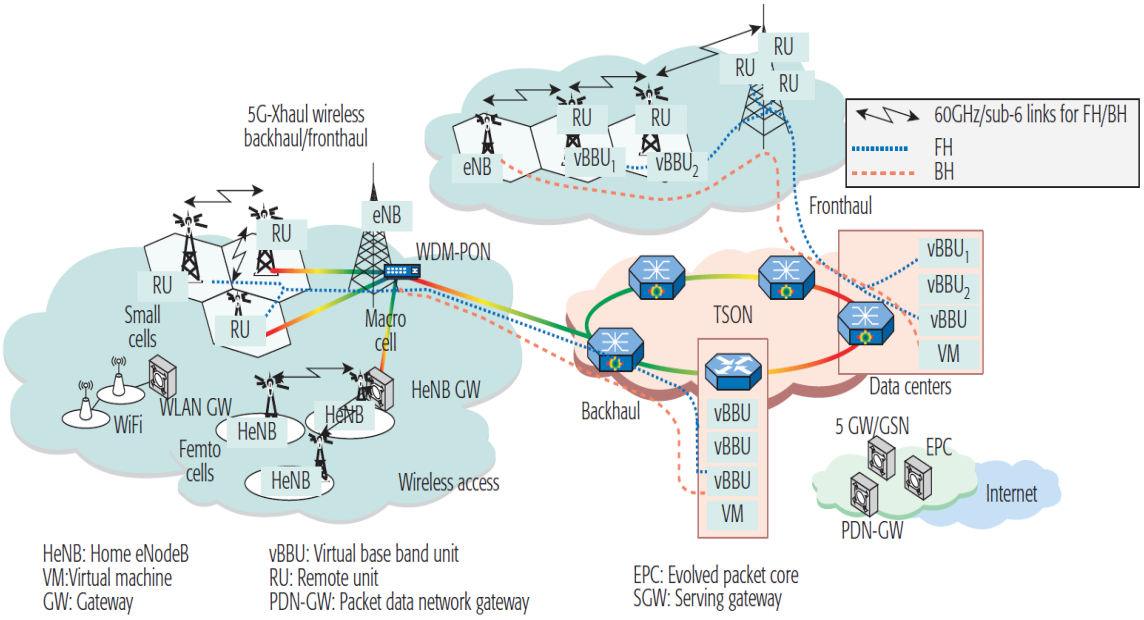

Fig. 1.1. 5G Network Architecture [12]

(C-RAN) where mobile fronthaul connects remote units (RUs) and virtual baseband units (vBBUs), whilst mobile backhaul connects a pool of vBBUs and data centre. The RUs perform radio functions such as power amplification, digital processing, analogue-to-digital conversion (ADC), digital-to-analogue conversion (DAC) etc. Whereas, the pool of vBBUs, located at a protected centralized site such as cloud or data centers, comprises of multiple vBBU nodes that have high computational and storage capabilities and are responsible for processing resources and dynamically allocating them to the corresponding RUs based on the current network requirements [13]. In typical existing mobile fronthaul/backhaul links, copper cables and millimetre wave (mmWave) [14] are often utilized.

To further increase the signal transmission bandwidth of mobile fronthaul/backhaul links in a cost-effective manner, passive optical networks (PONs) are considered as one of the most important candidates [15]. Not only do PONs provide low power consumption where the links between RUs and vBBUs avoid the need to install and maintain any additional power-driven devices, PONs also offer high reliability where a malfunction of one link does not affect the rest. Moreover, intensity-modulation and direct-detection (IMDD) transmission systems can be adopted in these networks as such systems have improved cost-effectiveness and offer a lower transceiver architecture complexity compared to other transmission systems e.g., coherent transmission systems [16]. In addition, it is also highly desirable to realize the fronthaul/backhaul links using wavelength division multiplexing PONs (WDM-PONs), which also provide more versatility and flexibility since each wavelength in a WDM-PON is effectively a point-to-point link, thus allowing each link to run at a different speed and with a different protocol [15].

Firstly, from the signal transmission technique point-of-view, the initial stage of 5G should have sufficient transparency to 4G. Since orthogonal frequency division multiplexing (OFDM) is widely used in 4G because of its unique features including high signal bit rate and spectral efficiency and excellent performance adaptability [17-20], thus OFDM is still a promising signal modulation technique for 5G. To further enhance the signal bit rates of OFDM transmission systems, a large number of technical approaches have been proposed by exploiting numerous signal multiplexing schemes, high-order signal modulation formats, and an appropriate combination of both. Sophisticated signal multiplexing schemes such as polarization division multiplexing (PDM) [21], code division multiplexing (CDM) [22, 23] and space division multiplexing (SDM) [24, 25] often require expensive optical components

and/or highly complex transceiver architectures. On the other hand, the utilisation of high-order signal modulation formats escalates the demand for optical signal-to-noise ratio (OSNR). Therefore, it is extremely beneficial if an energy-free extra information-bearing dimension is introduced into OFDM to considerably enhance both signal bit rate and spectral efficiency while avoiding the usage of high signal modulation formats and without increasing the OSNR and transceiver digital signal processing (DSP)/architecture complexity.

Secondly, from the network implementation point-of-view, numerous existent techniques have also been proposed to deliver the 5G targets, most notably, small-cell network (SCN) [26-28] and massive multiple-input/multiple-output (MIMO) [29, 30]. In SCNs, very dense low-powered RUs that have a smaller coverage range of approximately 10 meters to a few kilometers, compared to the conventional macro-cell (range up to 35 km), are considered and are located at typical outdoor hotspot locations. By shrinking the cell size, SCNs maximize the spectrum utilization efficiency by using the same frequency bands multiple times, thus improving the user signal bit rate per cell [26]. Compared to 4G-associated MIMO, massive MIMO is expected to be implemented to allow an increased number of antennas in both RUs and user devices resulting in further improved user signal bit rates [30].

Thirdly, in terms of massive MTC, to support high traffic density, both SCNs and massive MIMO are essential [11, 26], which require a large number of RUs to be deployed. For cost-sensitive 5G application scenarios, this imposes strong restrictions in terms of maintenance and overall system cost. Moreover, the large number of deployed RUs also causes interferences such as inter-cell interference that affects network users especially users located at the edges of the networks. To address such a technical problem, coordinated multi-point (CoMP) transmission can be employed, which uses dynamic sharing of data and channel state information (CSI) between the RUs to ensure that different cell-edge users can be assigned within the same cell rather than different cells [32, 33]. On the other hand, in these cells, different users may require different transmission performance characteristics e.g. signal bit rate and system power budget, therefore, to satisfy each user's particular need in a cost-effective manner, it is greatly advantageous to implement transceivers in the RUs that have flexible and versatile design architectures capable of dynamically accommodating different system performance requirements while avoiding any expensive and complicated DSP components.

1.2 Major Achievements of the Dissertation Research

Aimed at addressing all the bottleneck technical challenges outlined above, the dissertation research work has been carried out to investigate the performance of OFDM-based signal transmission techniques over standard single-mode fibre (SSMF) IMDD PON systems. Here, it should be noted that each of these signal transmission techniques supports an energy-free extra information-bearing dimension to improve the signal transmission capacity, transceiver flexibility and cost-effectiveness. The major achievements are summarized below:

- **Subcarrier index-power modulated optical OFDM (OOFDM)** [34, 35].

  A subcarrier index-power (SIP) information-bearing dimension is introduced into conventional OOFDM by setting the subcarrier power level at either low or high according to the incoming data sequence in order to convey an extra information bit per subcarrier. As a result, a novel signal transmission technique termed subcarrier index-power modulated optical OFDM (SIPM-OOFDM) is proposed for the first time. Compared with conventional OFDM adopting similar signal modulation formats, this technique offers an increase of 17% in signal bit rate without increasing the minimum required OSNRs for achieving a specific bit error rate (BER). In terms of the transceiver architecture, SIPM-OOFDM still maintains the exact same transceiver design as conventional OFDM, except that SIPM-OOFDM introduces an extra DSP element in the transmitter and in the receiver. Although these extra DSP elements need additional logic resources, compared to the core DSP logic resource requirements, are, however, marginal and these additional elements can be easily switched on (when SIPM-OFDM is used) or off (when conventional OOFDM is used) depending on system performance requirements. This implies that SIPM-OOFDM can improve both the transceiver design flexibility and performance adaptability.

- **Subcarrier index-power modulated optical OFDM with superposition multiplexing** [36].

  As the usage efficiency of high power level subcarriers is not fully maximised in SIPM-OOFDM, a technique termed SIPM-OOFDM with superposition multiplexing (SIPM-OOFDM-SPM) is proposed by applying the superposition multiplexing (SPM) operation for high power subcarriers. SPM passively adds different signal modulation

format-encoded complex numbers and assigns the sum to a high power subcarrier. As a direct result, SIPM-OOFDM-SPM considerably increases the SIPM-OOFDM signal bit rate without increasing the signal modulation formats. Moreover, the introduction of the SPM operation adds another dimension that can dynamically vary in the encoded signal constellation map compared with SIPM-OOFDM, thus further improving the transceiver design flexibility and system performance adaptability.

- **Subcarrier index-power modulated optical OFDM with dual superposition multiplexing** [37, 38].

  To further enhance the power usage efficiency of both subcarrier power levels, an improved version of SIPM-OOFDM-SPM, termed SIPM-OOFDM with dual superposition multiplexing (SIPM-OOFDM-DSPM) is proposed, which not only inherits all the above-mentioned benefits associated with SIPM-OOFDM-SPM in terms of DSP and hardware system complexity, but also improves the signal bit rate by adopting even lower signal modulation formats.

- **Multilevel subcarrier index-power modulated optical OFDM** [39].

  All the above-mentioned techniques utilise just two subcarrier power levels. To further increase the number of information bits conveyed per subcarrier, multi-level SIPM-OOFDM (ML-SIPM-OOFDM) is proposed and investigated, in which the number of subcarrier power levels can be increased to a predefined multilevel (ML). In terms of transceiver design, ML could be applied easily in SIPM-OOFDM, SIPM-OOFDM-SPM and SIPM-OOFDM-DSPM as the ML-associated operating principles, their DSP implementation procedures and corresponding performance advantages are very similar for these transmission techniques.

- **Subcarrier index power modulated with subcarrier grouping optical OFDM** [40].

  In all the above outlined SIPM-based OOFDM signal transmission techniques, each individual subcarrier is regarded as a separate unit to carry extra information bits. To enable a group of subcarriers of various power levels to carry the extra information bits, SIPM-OOFDM with subcarrier grouping (SIPM-SG-OOFDM) is proposed,

where each symbol is divided into multiple subcarrier groups to bear extra user information bits in the subcarrier group (SG) information-bearing dimension. In addition, subcarrier grouping provides SIPM-SG-OOFDM with an additional capability of automatically detecting and subsequently correcting errors at the receiver without consuming any valuable transmission bandwidth. As a direct result, compared with SIPM-OOFDM, an increase in signal bit rate is obtainable together with an enhanced system power budget. This implies that subcarrier grouping can improve the SIPM-SG-OOFDM performance capacity, adaptability and flexibility. Moreover, the performances can also be further enhanced by combining the ML and SG operating principles in each SIPM-based OOFDM signal transmission technique, this considerably increases the information-carrying dimension.

As a first author, the above-mentioned work has resulted in the publication of four journal papers, two of them have been published in Journal of Lightwave Technology [34, 40], while the remaining two have been published in Optics Communication [38] and Photonics Journal [39]. In addition, one conference paper has also been presented at the Optical Fiber Conference in 2016 [34]. As a second author, two journal papers have been published in Journal of Lightwave Technology [36] and Photonics Journal [37].

1.3 Thesis Structure

This thesis consists of seven chapters. This chapter presents the targets and challenges facing future 5G networks to show the motivation behind the dissertation research. To provide an understanding of the work presented in this thesis, Chapter 2 presents the basic principles of OOFDM by describing each DSP block in detail. Chapter 2 explores the basic concepts involved in optical transceivers, which includes SSMF and IMDD OOFDM transmission systems. Chapter 2 also describes the fundamental concepts behind PONs and presents examples of current and advanced PON technologies.

Chapter 3: This chapter covers the SIPM-OOFDM technique where, by introducing the additional SIP dimension into OFDM, the high and low power subcarriers that convey an extra information bit are encoded with 8-phase shift keying (8-PSK) and quadrature-phase shift keying (QPSK) respectively according to an incoming data sequence. Full details of the

SIPM-OOFDM signal encoding/decoding procedure are presented. In addition, the transceiver architecture is also provided, based on which, numerical simulations are undertaken to identify the optimum transceiver parameters affecting the maximum achievable performance. Over cost-sensitive IMDD PON systems, the results show that compared with conventional OOFDM using the same modulation formats, SIPM-OOFDM offers a 17% increase in signal bit rate without increasing the OSNR and the transceiver DSP/architecture complexity as well as while preserving transmission performance tolerances to channel characteristics including chromatic dispersion and fiber nonlinearity.

Chapter 4: This chapter is divided into two parts; the first part addresses SIPM-OOFDM-SPM, an improved variant of the SIPM-OOFDM technique described in Chapter 3, whilst the second part addresses SIPM-OOFDM-DSPM, an improved variant of SIPM-OOFDM-SPM. In the first part, the SPM-based mapping and demapping procedures are discussed in detail. Following the optimization of key transceiver parameters affecting the SIPM-OOFDM-SPM performance over SSMF IMDD PON systems, numerical simulations shows a significant increase of 28.6% in signal bit rate compared with SIPM-OOFDM. Moreover, compared with the 32-PSK/QPSK-encoded SIPM-OOFDM technique capable of achieving the same signal bit rate as SIPM-OOFDM-SPM, the latter technique improves the system power budget and performance tolerance to both chromatic dispersion and fiber nonlinearity. In the second part, the SIPM-OOFDM-DSPM technique uses the SPM operation on both high and low power subcarriers. Based on the identified optimum transceiver parameters, the SIPM-OOFDM-DSPM performance characteristics are explored. Over SSMF IMDD PON systems, it is shown that compared to SIPM-OOFDM-SPM, SIPM-OOFDM-DSPM enables an 11% increase in signal bit rate compared with SIPM-OOFDM-SPM with the transceiver DSP/hardware complexity still preserved. Similar to SIPM-OOFDM-SPM, the improvements in system power budget and fiber performance tolerances are also achievable in SIPM-OOFDM-DSPM when compared with 32-PSK/8-PSK-encoded SIPM-OOFDM technique operating at the same signal bit rate.

Chapter 5: This chapter introduces ML-SIPM-OOFDM where four predefined subcarrier power levels are employed to enable each subcarrier to carry two extra information bits in the SIP information-carrying dimension. According to an incoming data sequence, the corresponding subcarrier is encoded using one of the following four signal modulation formats: binary phase shift keying (BPSK), QPSK, 8-PSK and 16-phase shift keying (16-

PSK). Extensive explorations of ML-SIPM-OOFDM transmission performance characteristics are undertaken, based on which, optimum key transceiver parameters are identified. Over SSMF IMDD PON systems, the results show that this technique enables a significant increase of 30% in signal bit rate compared with SIPM-OOFDM. Moreover, further 9% and 10% ML-SIPM-OOFDM signal bit rate enhancements are also feasible when use is made of adaptive bit loading and subcarrier count doubling, respectively.

Chapter 6: This chapter exploits the subcarrier-grouping scheme in order to introduce a technique termed SIPM-SG-OOFDM where a group of subcarriers convey the extra bits in the SG information-bearing dimension, i.e., each subcarrier group is specifically assigned with a predefined subcarrier power pattern according to an incoming data sequence. Full details of the grouping mapping/de-mapping procedures are discussed and theoretical analysis is provided to highlight the impact of subcarrier grouping on the overall system performance. In addition, extensive numerical simulations are computed to identify key grouping parameters affecting the maximum achievable signal bit rate. This chapter also proposes and explores an effective SG-associated automatic error detection and correction technique with zero-overhead and low DSP complexity at the receiver. As a direct result, an optimum trade-off among system performance characteristics such as signal bit rate and system power budget is achieved by simply varying the grouping parameters. In fact, numerical simulations show that SIPM-SG-OOFDM, offers an OSNR gain of approximately 1.0dB while simultaneously enabling an 11% improvement in signal bit rate compared to SIPM-OOFDM.

Finally, Chapter 7 summarizes the thesis and suggests future research work.

References:

[1] World Stats, Internet World Stats, *Miniwatts Marketing Group*, Nov. 2018.

[2] Number of smart phone users in the United States from 2010 to 2021 (in millions), *Statista*. Available on: https://www.statista.com/statistics/201182/forecastof-smartphone-users-in-the-us, Mar. 2017.

[3] T. S. Rappaport, W. Roh, and K. Cheun, "Wireless engineers long considered high frequencies worthless for cellular systems. They couldn't be more wrong," *IEEE Spectr*., vol. 51, no. 9, pp. 34–58, Sep. 2014.

[4] T. Nakamura *et al.*, ''5G Radio access: requirements, concept and experimental trials,'' *IEICE Trans. Commun.*, vol. E98-B, no. 8, pp.1397-1406, Aug. 2015.

[5] Akhil Gupta and Rakesh K. Jha, ''A survey of 5G network: architecture and emerging technologies,'' *IEEE Access.*, vol.3, pp. 1206-1232, Aug. 2015.

[6] M. Sun, H. Chen and B. Shu, ''Predict-then-Prefetch caching strategy to enhance QoE in 5G networks,'' *IEEE World Cong. on Ser. (SERVICES)*, Jul. 2018.

[7] M. Bennis, M. Debbah, and H. V. Poor, ''Ultra-reliable and low-latency wireless communication: tail, risk and scale,'' *Cornell Uni. Lib.*, (Early Access), available at: arXiv:1801.01270v2, Oct. 2018.

[8] W. Wang and Q. Zhang, ''Local cooperation architecture for self-healing femtocell networks,'' *IEEE Wirel. Commun.*, vol. 21, no. 2, pp. 42–49, 2014.

[9] V. Jungnickel *et al.*, ''The role of small cells, coordinated multipoint, and massive MIMO in 5G,'' *IEEE Commun. Mag.*, vol. 52, no. 5, pp.44–51, May 2014.

[10] J. G. Andrews *et al.*, "What will 5G be?," *IEEE J. Sel. Areas Commun.*, vol. 32, no. 6, pp. 1065–1082, Jun. 2014.

[11] Y. Morioka, ''LTE for mobile consumer devices", *ETSI Workshop on Machine to Machine Standardization*, 2011.

[12] A. Tzanakaki *et al.*, ''Wireless-optical network convergence: enabling the 5G architecture to support operational and end-user services,'' *IEEE Commun. Mag.*, vol. 55, no. 10, pp. 184–192, Oct. 2017.

[13] F. Tian, Z. Yan, X. Liang and P. Zhang, ''Trusted cooperation among virtual base stations in C-RAN,'' *IEEE Access*, vol. 6, pp. 57787 – 57801, Oct. 2018.

[14] H. Raza ''A brief survey of radio access network backhaul evolution: part I,'' *IEEE Commun. Mag.*, vol. 49, no. 6, pp. 164-171, Jun. 2011.

[15] C. Browning *et al.*, ‘‘5G wireless and wired convergence in a passive optical network using UF-OFDM and GFDM,’’ *IEEE Int. Conf. on Commun. Works. (ICC Workshops),* pp. 386 - 392, May 2017.

[16] X. Gong, L. Guo, and Q. Zhang, ‘‘Joint resource allocation and software-based Reconfiguration for energy-efficient OFDMA-PONs,’’ *J. Opt. Commun. Netw.,* vol. 10, no.8, pp. C75-C85, Aug. 2018.

[17] G. Berardinelli et al., ‘‘On the potential of OFDM enhancements as 5G waveforms,’’ *Veh. Tech. Conf. (VTC Spring),* pp. 1-5, May 2014.

[18] F. Li, J. Yu, Z. Cao, J. Zhang, M. Chen, and X. Li, “Experimental demonstration of four-channel WDM 560 Gbit/s 128QAM-DMT using IM/DD for 2-km optical interconnect,” *J. Lightw. Technol.*, vol. 35, no. 4, pp. 941– 948, Feb. 2017.

[19] J. Zhou *et al.*, “256-QAM interleaved single carrier FDM for shortreach optical interconnects,” *IEEE Photon. Technol. Lett.*, vol. 29, no. 21, pp. 1796–1799, Nov. 2017.

[20] A. Hazareena and B. A. Mustafa, ‘‘A Survey: On the Waveforms for 5G,’’ *Int. Conf. on Elect., Commun. and Aero. Tech. (ICECA),* Mar. 2018.

[21] C. Li *et al.*, “Phase noise cancelled polarization-insensitive all-optical wavelength conversion of 557-Gb/s PDM-OFDM signal using coherent dual-pump,” *J. Lightw. Technol.*, vol. 33, no. 13, pp. 2848–2854, Jul. 2015.

[22] A. Triana, D. Pastor, and M. Varón, ‘‘Code division multiplexing applied to FBG sensing networks: FBG sensors designed as discrete prolate spheroidal sequences (DPSS-FBG sensors),’’ *J. Lightw. Technol.*, vol. 35, no. 14, pp. 2880– 2886, Jul. 2017.

[23] H. Li *et al.*, “Digital code-division multiplexing channel aggregation for mobile fronthaul architecture with low complexity,” *IEEE Photon. J.*, vol. 10, no. 2, Apr. 2018.

[24] P. Khodashenas et al., “Comparison of spectral and spatial super-channel allocation schemes for SDM networks,” *J. Lightw. Technol.*, vol. 34, no. 11, pp. 2710–2716, Jun. 2016.

[25] N. Hua *et al.*, “Capex benefit analysis of space division multiplexing (SDM) optical networks,” *14th Int. Conf. on Opt. Commun. and Net. (ICOCN),* Aug. 2015.

[26] J. G. Andrews, “Seven ways that HetNets are a cellular paradigm shift,” *IEEE Commun. Mag.*, vol. 51, no. 3, pp. 136–144, Mar. 2013.

[27] S. M. Abd El-atty and Z. M. Gharsseldien, “On performance of HetNet with coexisting small cell technology,” in *Proc. IEEE Conf. Wireless Mobile Netw.*, pp. 1–8, 2013.

[28] J. G. Andrews, H. Claussen, M. Dohler, S. Rangan, and M. C. Reed, "Femtocells: past, present, and future," *Jour. on Sel. Areas in Comm.*, vol. 30, no. 3, pp. 497–508, Apr. 2012.

[29] C. X. Wang *et al.*, ''Cellular architecture and key technologies for 5G wireless communication networks,'' *IEEE Commun. Mag.*, pp.122-130, Feb. 2014.

[30] M. Agiwal, A. Roy, and N. Saxena, ''Next generation 5G wireless networks: a comprehensive survey,'' *IEEE Comm. Sur. & Tut.*, vol.18, no.3, pp.1617-1655, Aug. 2016.

[31] C. Bockelmann *et al.*, ''Massive machine-type communications in 5G: physical and MAC-layer solutions,'' *IEEE Commun. Mag.*, vol. 54, no. 9, pp. 59 – 65, Sep. 2016.

[32] E. Hossain, M. Rasti, H. Tabassum, and A. Abdelnasser, ''Evolution toward 5G multi-tier cellular wireless networks: an interference management perspective,'' *IEEE Wireless Commun.*, vol. 21, no. 3, pp. 118-127, Jun. 2014.

[33] C, Choi, L. Scalia, T. Biermann and S. Mizuta, ''Coordinated multipoint multiuser-MIMO transmissions over backhaul-constrained mobile access networks,'' *IEEE Inter. Symp. on Personal, Indoor and Mobile Radio Commun. Conf.*, Sep. 2011.

[34] F. Halabi, L. Chen, S. Parre, S. Barthomeuf, R. P. Giddings, C. Aupetit-Berthelemot and J. M. Tang, "Subcarrier index-power modulated optical OFDM and its performance in IMDD PON systems," *J. Lightw. Technol.*, vol. 34, no. 9, pp. 2228–2234, May 2016.

[35] F. Halabi, L. Chen, S. Parre, S. Barthomeuf, R. P. Giddings, C. Aupetit-Berthelemot and J. M. Tang, "Subcarrier index-power modulated optical OFDM (SIPM-OOFDM) for IMDD PON systems,'' *Proc. Optical Fibre Communication (OFC) Conference*, Th3C.1, pp.1-3, Mar. 2016.

[36] L. Chen, F. Halabi, R. P. Giddings, and J. M. Tang, "Subcarrier index-power modulated optical OFDM with superposition multiplexing for IMDD transmission systems," *J. Lightw. Technol.*, vol. 34, no. 9, pp. 2228–2234, Oct. 2016.

[37] L. Chen, F. Halabi, J. Zhang, R. P. Giddings, and J. M. Tang, "Subcarrier index-power modulated-optical OFDM with dual superposition multiplexing for directly modulated DFB-based IMDD PON systems," *IEEE Photon. J.*, vol. 10, no. 6, Dec. 2018.

[38] F. Halabi, L. Chen, R. P. Giddings, A. Hamié, Y. Dumas, P. Freyssinet, C. Aupetit-Berthelemot and J. M. Tang, ''Subcarrier index-power modulated optical OFDM with dual superposition multiplexing for IMDD PON systems'', *Optics Commun.*, vol. 433, pp. 190-194, Oct. 2018.

[39] F. Halabi, L. Chen, R. P. Giddings, A. Hamié, and J. M. Tang, "Multilevel subcarrier index-power modulated optical OFDM with adaptive bit loading for IMDD PON systems," *IEEE Photon. J.*, vol. 8, no. 6, Art. No. 7907114, Dec. 2016.

[40] F. Halabi, L. Chen, R. P. Giddings, A. Hamié, and J. M. Tang, "Subcarrier grouping-enabled improvement in transmission performance of subcarrier index-power modulated optical OFDM for IM/DD PON systems," *J. Lightw. Technol.*, vol. 36, no. 20, pp. 4792–4798, Oct. 2018.

2. Fundamental Concept

2.1 Introduction

This chapter covers the fundamentals of OFDM and its applications in optical transmission systems. The chapter starts with a brief history of OFDM, and then major DSP components that form an OFDM transceiver are described in detail. After that, the principles of adaptively modulated OFDM techniques are provided. Moreover, the subcarrier index modulated OFDM principle is extensively covered in this chapter as it is the basis of the dissertation research.

In addition, to provide an in-depth understanding of the work undertaken in this thesis, optical transceivers, fiber channel characteristics (including both linear and nonlinear effects) and the OOFDM IMDD transmission systems are also described in detail. Finally, the last section of this chapter covers the fundamental concepts associated with passive optical networks (PONs).

2.2 History of OFDM

OFDM was firstly proposed by R.W. Chang in the mid-60s [1] in order to achieve a highly efficient usage of the transmission bandwidth by partially overlapping individual subcarriers, but without causing inter-channel interference (ICI) and inter-symbol interference (ISI), under the condition they are all mutually orthogonal, i.e., a precise mathematical relationship between the subcarrier frequencies has to be satisfied as detailed in the following section. To maintain the orthogonality, not only set of mixers and filters were needed but also each subcarrier required an individual stable oscillator that was constantly maintained in an extreme stable manner. As a result, the early OFDM transceivers were highly complex and therefore not feasible from a technical or economic perspective for wide deployment and so initially OFDM was limited to military applications for many years.

In 1971, the use of the inverse discrete Fourier transform (IDFT) was proposed by Weinsten and Elbert [2] to maintain the subcarrier orthogonality. This was a key step in making OFDM a more realistic proposition. Moreover, full digital implementations could be built around special-purpose hardware performing the fast Fourier transform (FFT) and inverse fast Fourier transform (IFFT), which are the efficient implementations of the discrete Fourier transform (DFT) and IDFT, respectively. Recent advances in DSP technology make high-speed, large-size IFFT/FFT chips commercially affordable. Furthermore, to improve the OFDM's effectiveness in reducing the ISI and ICI effects, Peled and Ruiz introduced the concept of cyclic prefix (CP) in 1983 [3]. As such, in the 1980s, OFDM was studied for high-speed modems, digital mobile communications and high density recording. In the 1990s, OFDM was exploited for wideband data communication over copper pairs in digital subscriber lines (DSLs), very-high-speed digital subscriber lines (VDSLs), digital audio broadcasting (DAB), digital video broadcasting (DVB), and high-definition television (HDTV) terrestrial broadcasting [4, 5]. In 2000s, a remarkable number of wireless standards adopted OFDM as a signal modulation technique such as wireless local area networks (LANs) i.e., WiFi, wireless metropolitan area networks (MANs) i.e., WiMAX as well as in 4G LTE mobile networks [7].

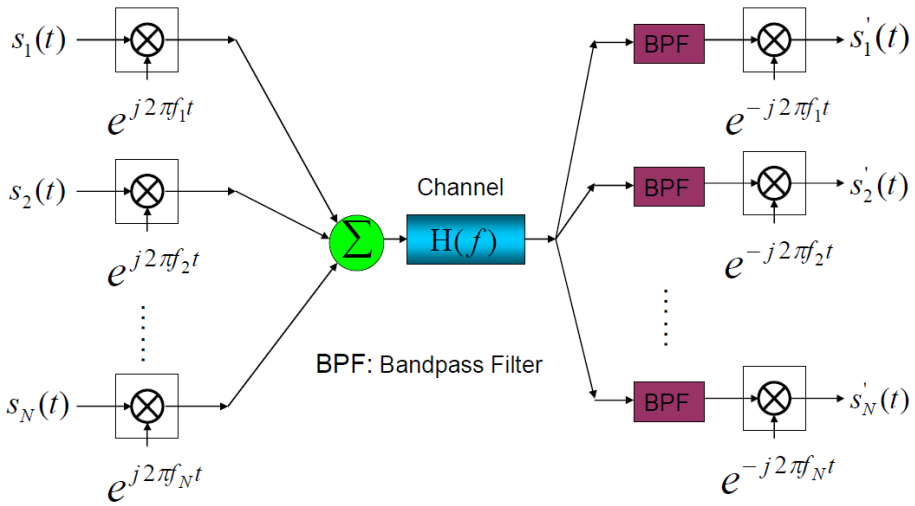

Fig. 2.1. Diagram for a generic FDM system

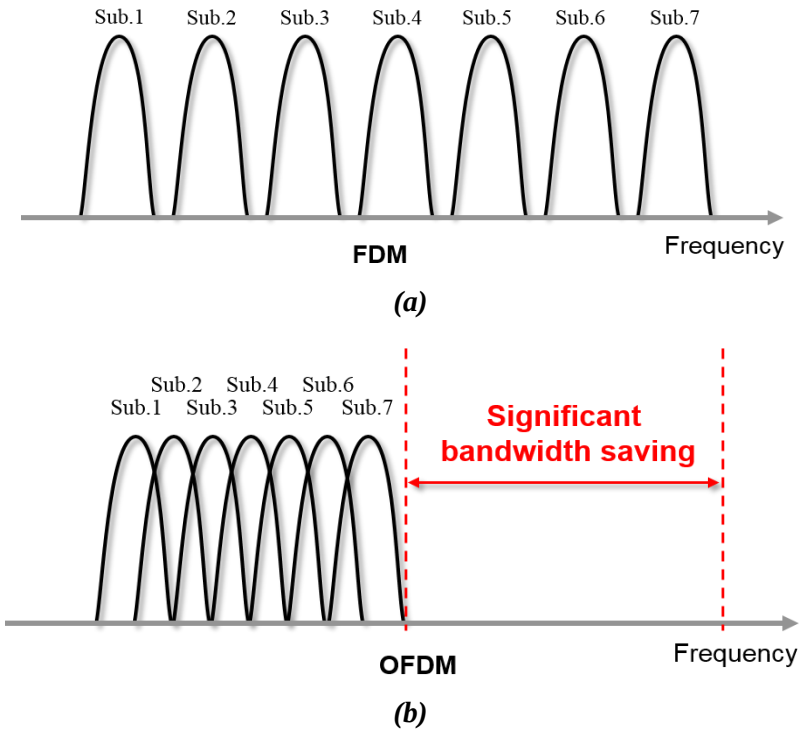

Fig. 2.2. Spectrum of (a) FDM and (b) OFDM

Following the significant success of OFDM in wireless systems, the emergence of OFDM in optical communication system started in 2005 [8]. Since then, optical OFDM (OOFDM) has been widely used in the optical communication community leading to extensive simulation and experimental demonstrations of OOFDM transmission systems for a wide range of application scenarios. Furthermore, as discussed in Chapter 1, OFDM is considered as a promising signal modulation technique for future 5G networks seamlessly converging legacy optical and wireless networks.

2.3 OFDM Fundamentals

2.3.1 OFDM Basic Concepts

As OFDM is a special type of the frequency division multiplexing (FDM) technique, descriptions of FDM are thus first provided. The basic idea of FDM is to transmit multiple signals simultaneously over a wideband channel by modulating each signal onto a dedicated subcarrier and multiplexing the modulated subcarriers, as shown in Fig. 2.1. More

specifically, the FDM transmitter uses an oscillator array operating at different radio frequencies (RFs) with a sufficiently wide inter-channel guard between two adjacent subcarrier frequencies, as illustrated in Fig. 2.2(a). Each subcarrier is modulated separately by a classical modulation format such as *M*-ary Quadrature Amplitude Modulation (QAM) or PSK. In the receiver, each of these subcarriers are filtered by a bandpass filter (BPF) and demodulated with an identical RF frequency by an oscillator.

Compared with FDM, OFDM precisely chooses the inter-subcarrier RF frequency spacing such that all RF frequencies are harmonically related and thus ensuring orthogonality between the subcarriers. The orthogonality allows spectral overlap between them but without interference, this result in significant enhancement in spectral efficiency compared to FDM, as shown in Fig. 2.2 (b).

To explain the principle of orthogonality between OFDM subcarriers, the *k*-th subcarrier in the *n*-th OFDM symbol can be written as:

$$s_{k,n(t)} = X_{k,n} e^{j2\pi f_k t} \prod(t - nT_s) \tag{2.1}$$

where

$$X_{k,n} = A_{k,n} e^{j\Theta_{k,n}} \tag{2.2}$$

and

$$\prod(t) = \begin{cases} 1, & 0 \le t \le T_s \\ 0, & otherwise \end{cases} \tag{2.3}$$

In Eq. (2.2), $A_{k,n}$ and $\Theta_{k,n}$ are the amplitude and phase of the encoded data $X_{k,n}$, respectively. In Eq. (2.3), T_s is the OFDM symbol period and $\prod(t)$ has a rectangular pulse shape of unity magnitude over the time duration of T_s which indicates that each subcarrier' spectrum has a *sinc* shape as described later on. To achieve subcarrier orthogonality, the subcarrier frequencies are arranged to satisfy the following condition:

$$f_k = f_c + \frac{k}{T_s} \qquad k=0,1,2,\ldots, N_s - 1 \tag{2.4}$$

where N_s is the total number of subcarriers, f_c is the central frequency, f_k is the frequency of the *k*-th subcarrier. Here, it should also be noted the phase of each subcarrier has to be constant before modulation. In order to examine the subcarriers' orthogonality, a correlation between any two subcarriers within the *n*-th symbol period is given by:

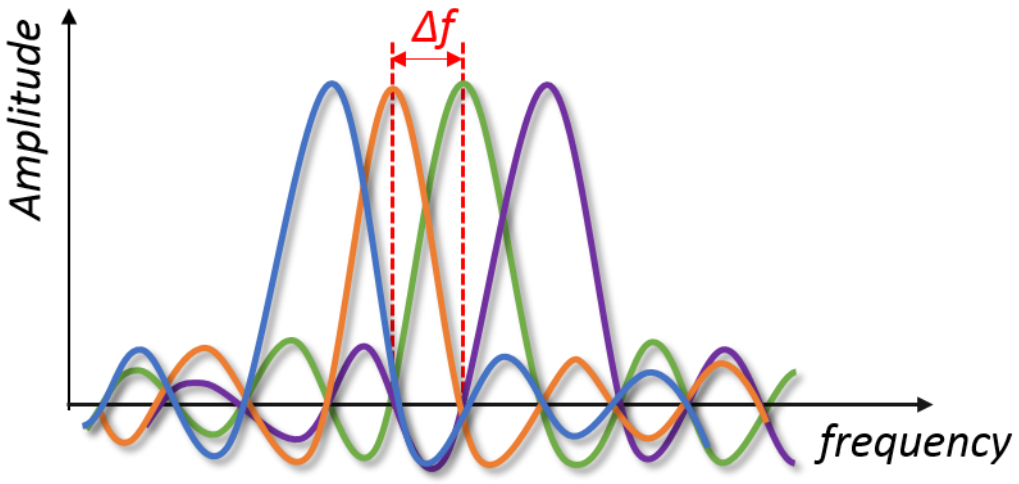

Fig. 2.3. OFDM signal spectrum

$$\frac{1}{T_s}\int_{(n-1)T_s}^{nT_s} s_{k,n(t)}\; s^*_{l,n(t)}\, dt \tag{2.5}$$

Using Eq. (2.1)-Eq.(2.4), Eq. (2.5) can be further expressed as:

$$\frac{1}{T_s}\int_{(n-1)T_s}^{nT_s} X_{k,n(t)}\; X^*_{l,n(t)} e^{j2\pi(f_k - f_l)t}\, dt = \begin{cases} = 0, & k \neq l \\ \neq 0, & k = l \end{cases} \tag{2.6}$$

Eq. (2.6) confirms that mutual orthogonality between subcarriers is achieved when Eq.(2.4) is met. The orthogonality principle means that when an OFDM symbol containing multiple subcarriers, is correlated with a single complex valued, reference subcarrier with a fixed frequency, only the subcarrier at the same frequency will contribute to a non-zero correlation output while all other subcarriers at different frequencies result in zero-valued correlation outputs. The correlation output thus reveals the amplitude and phase of the subcarrier at the correlated frequency.

The orthogonality principle is also illustrated in Fig.2.3 where a subcarrier frequency difference, Δf, is considered. It is shown that each subcarrier has a spectrum with a zero value at the center frequencies of other subcarriers' spectrums as such for ideal cases no ICI occurs between different subcarriers even when their spectrums are overlapping.

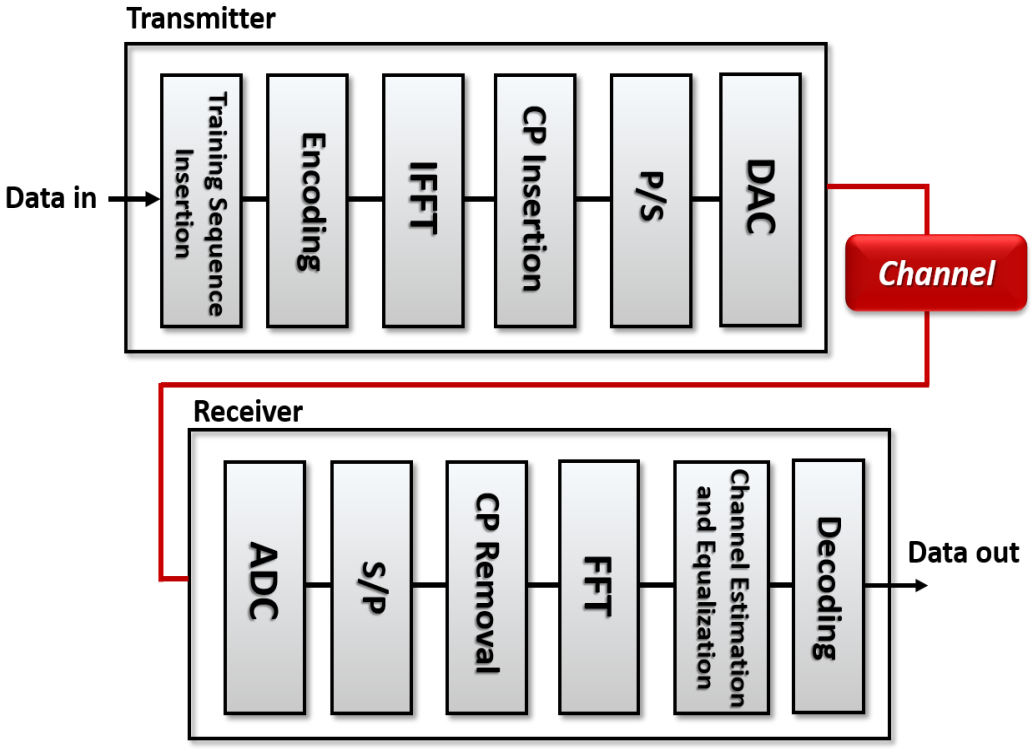

Fig. 2.4. Block diagram of an OFDM transmission system

2.3.2 OFDM Transceivers

This section explores the architecture behind a representative OFDM transceiver, which is illustrated in Fig.2.4. In the transmitter, the major DSP functions consists of training sequence insertion, encoder, IFFT, CP insertion, parallel-to-serial (P/S) converter and a digital-to-analogue converter (DAC). After the analogue signal is transmitted through the transmission channel, the signal is converted back to the digital domain through an analogue-to-digital converter (ADC) in the receiver, where the digital signal is processed by the following DSP functions such as, serial-to-parallel (S/P) converter, CP removal, FFT, channel estimation equalization and finally the data is recovered by the decoder.

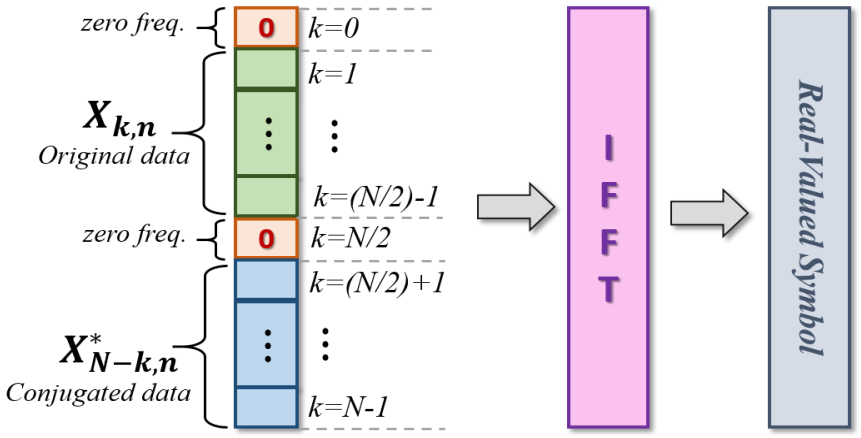

Fig. 2.6. Generation of real-valued OFDM symbol

2.3.3 IFFT/FFT

As the work presented in this thesis is based on IMDD transmission systems, the output of the IFFT has to be real-valued [4]. To achieve such a requirement, the N point IFFT inputs are arranged to satisfy the Hermitian symmetry [9] as illustrated in Fig.2.6. In this figure, $X_{k,n}$ is the encoded complex data defined in Eq.(2.2) (k=N-1,…,(N/2)+1, N/2, (N/2)-1,…,0). Its conjugate is denoted as $X^*_{k,n}$ where $X_{-k,n} = X^*_{k,n}$. As shown in Fig.2.6, such symmetry also requires X_0=$X_{N/2}$=0 and those zero frequency subcarriers cannot transmit any data. This implies that the total number of data-carrying subcarriers are N_s=$(N/2)-1$.

Following the Hermitian arrangement, the resulting time-domain n-th OFDM symbol waveform within [$(n-1)\,T_s$, nT_s], can be written as:

$$s_n(t) = \frac{1}{Ns}\sum_{k=0}^{Ns-1} X_{k,n}\, e^{j2\pi t f_k} \tag{2.7}$$

When $s_n(t)$ is sampled at a speed of $f_S = N_s/T_s$, then the m-th sample within [$(n-1)\,T_s$, nT_s], can be expressed as:

$$s_n(m) = \frac{1}{Ns}\sum_{k=0}^{Ns-1} X_{k,n}\, e^{j2\pi f_k \frac{mT_S}{Ns}} = \frac{1}{Ns}\sum_{k=0}^{Ns-1} X_{k,n}\, e^{j\frac{2\pi mk}{Ns}} \tag{2.8}$$

where m=0, 1, 2, …, N_s-1. It is interesting to note that if Eq. (2.1) is rewritten to consider a single OFDM symbol, it is equivalent to Eq. (2.8) which means that IFFT can be used in the transmitter to maintain orthogonality between different subcarriers and, similarly, FFT can be

used in the receiver to select any individual subcarrier. The output discrete frequency domain complex numbers of the FFT, Y_k, can be expressed as:

$$Y_k = \sum_{i=0}^{Ns-1} y_i \, e^{j\frac{-2\pi}{Ns}ki} \qquad k = 0,1,2 \ldots Ns-1 \tag{2.9}$$

where y_i is the sampled time domain signal at the input of the FFT with all y_i samples originating from the same OFDM symbol. Y_k is the frequency domain sample for the *k*-th subcarrier at the output of the FFT. It should also be noted that only the positive frequency bins are needed as the negative frequency bins contain the same data.

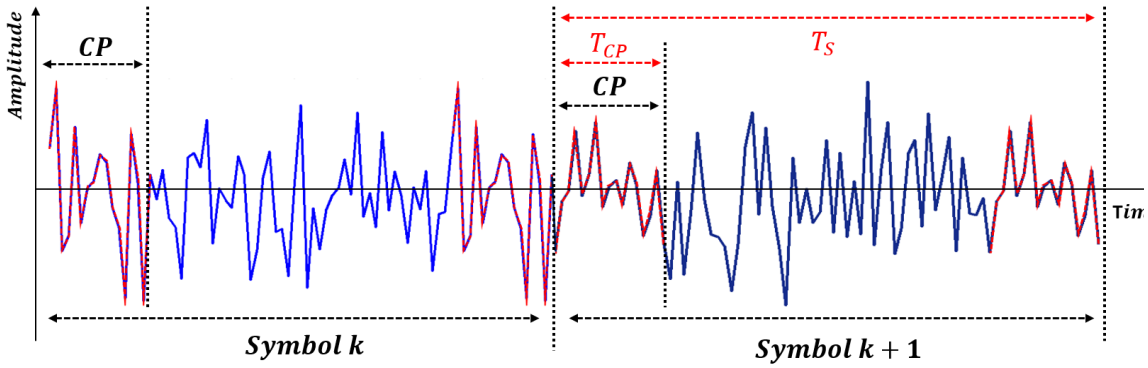

Fig. 2.7. OFDM symbols with cyclic prefix

2.3.4 Cyclic Prefix

OFDM is highly tolerant to signal dispersion, which causes signal spread and ISI, and the interference is localized mainly at the edges of the OFDM symbols. Therefore, to reduce the effect of ISI, in the transmitter, a CP is employed by copying some samples from the end of an OFDM symbol and placing them at the beginning of the same symbol. After transmission, the distorted CP is removed in the receiver, thus the OFDM symbol carrying useful information can be recovered without significant interference between adjacent symbols. In addition to the ISI reduction, CP is also employed to reduce ICI. Here, it should be noted that the IFFT process used to maintain the subcarrier orthogonality described in the previous section is not ideal. This is because, at the output of the IFFT, no periodic structure exists. Therefore, the utilization of CP partially produces a quasi-periodically extended time domain OFDM symbol, this leads to improved orthogonality between subcarriers within the symbol.

As an example of the CP insertion procedure, Fig.2.7 is presented which shows that the original samples, N_{SP}, are increased by an amount of N_{CP} samples hence the new OFDM symbol length is $N_{SP}+N_{CP}$. Therefore, if the time duration of CP is T_{CP} then the new symbol time duration is T_S and the duration of the OFDM symbol carrying real user information is $T_S - T_{CP}$. The CP parameter used throughout this thesis is defined as:

$$\eta = \frac{T_{CP}}{T_S - T_{CP}} \tag{2.10}$$

From the above description, it is clear that, if a CP time duration is smaller than the maximum dispersion-induced time delay, the imperfectly compensated dispersion effect limits considerably the maximum achievable OFDM transmission performance. On the other hand, if the CP is longer than the maximum dispersion-induced time delay, the dispersion effect is localized within the CP region only. However, for a fixed signal sampling speed, the CP wastes the transmitted signal power, giving rise to a degraded effective signal SNR. Furthermore, an excessive length of CP also prevents the full utilization of available system bandwidth. Adaptive CPs [10] can be used to maximize the CP's advantages and simultaneously minimize its disadvantages.

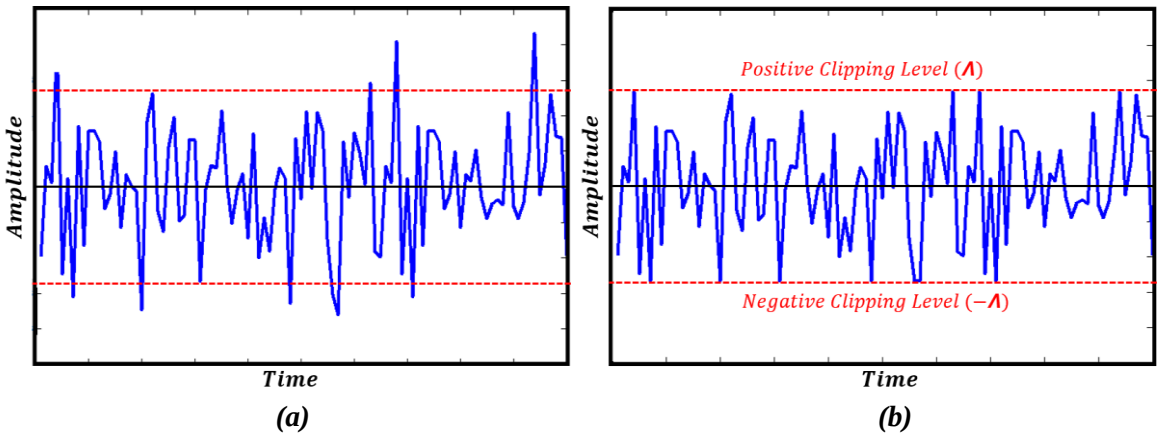

Fig. 2.8. (a) OFDM signal with high PAPR prior clipping and (b) the resulted clipped OFDM signal

2.3.5 DAC/ADC

As an OFDM signal consists of independently modulated subcarriers, these subcarriers can give a high peak-to-average power ratio (PAPR) when added up coherently. An example of an OFDM signal is shown in Fig. 2.8(a).

As explained later in this section, a high PAPR requires a wide dynamic operation range of components involved in the transmitter and receiver, thus inducing large quantization noise for fixed quantization bits. Therefore, in the DAC/ADC, clipping is applied to the OFDM signal to reduce its PAPR. For a given clipping level of $\pm\Lambda$, and assuming $X(t)$is real, the clipped signal is given by:

$$X_{clip}(t)=\begin{cases} X(t), & -\Lambda \le X(t) \le \Lambda \\ \Lambda, & X(t) > \Lambda \\ -\Lambda, & X(t) < -\Lambda \end{cases} \tag{2.11}$$

The clipping ratio ξ is defined as $\xi=\Lambda^2/Pm$ with Pm being the average signal power [9]. As an example, the impact of clipping on an OFDM signal is shown in Fig.2.8 where the same OFDM signal is generated before (Fig.2.8(a)) and after the clipping process (Fig.2.8(b)).

The clipped signal is then linearly quantized into a set of equally distributed quantization levels within the entire range of [-Λ, Λ]. The quantisation process can be described as follows:

$$Q(X_q) = \sum_{i=-\frac{L}{2}+1}^{\frac{L}{2}} \frac{X_i+X_{i-1}}{2} g(X_q, X_i, X_{i-1}) \tag{2.12}$$

where X_i and X_{i-1} represent the *i*-th and (*i*-1)-th quantization threshold value. *L* represents the quantization levels given by $L=2^b$ where *b* is the number of quantization bits. g is the rectangular function defined as:

$$g\,(X, X_1, X_2)\begin{cases} 1, & X_1 \le X < X_2 \\ 0, & otherwise \end{cases} \tag{2.13}$$

From the above analysis, is it easy to understand the following physical mechanism behind the clipping ratio and the quantization bits; when the clipping ratio is increased, the dynamic range (-Λ, Λ) is increased as well, on one hand, the clipping-induced distortion is decreased, on the other hand, for a fixed quantization bits, strong quantization noise occurs since the difference between the quantization levels increases, i.e., the signal is stretched. In practice, these two effects always co-exist. Therefore, for a given transmission system, an optimum clipping ratio exists which ensures that the quantization noise is minimized.

2.3.6 Training Sequence-based Equalization

The frequency response of a practical transmission channel introduces some variations to the subcarrier's amplitude and phase. To overcome such subcarrier distortion, channel equalization, located directly after FFT, is used. Such procedure can be achieved by inserting a random training sequence (TS) within the user data in the transmitter. Specifically speaking, after inserting the first TS at the beginning of the OFDM signal, the following TSs are periodically inserted after each *n* symbols. In the receiver, the estimated system frequency response of the *k*-subcarrier can be expressed as

$$\alpha_{s,k} = \frac{Y_{s,k}}{X_{s,k}} \tag{2.14}$$

where $X_{s,k}$ and $Y_{s,k}$ are the corresponding transmitted and received TSs respectively of the *k*-th subcarrier and $\alpha_{s,k}$ is also termed as the equalization coefficient. The equalization procedure corrects the received data of the *k*-subcarrier, y_k, by dividing it by its corresponding equalization coefficient:

$$y'_k = \frac{y_k}{\alpha_{s,k}} \tag{2.15}$$

where y'_k is the equalized complex data. To further reduce the effects of channel noise, the estimated system frequency response can be averaged over many TSs as long as the channel is considered to be static over the averaging period. It should be mentioned that this is one-tap equalization as each subcarrier is multiplied by a single complex coefficient.

2.4 Adaptively Modulated OFDM

A key advantage associated with OFDM is its capability of using the available channel spectra in an effective manner. This is achieved by applying adaptive loading algorithms (ALAs) such as adaptive power loading (APL) and adaptive bit loading (ABL), i.e., adaptive allocation of bit and/or power on each individual subcarrier. Such adaptive allocations require the knowledge of the system frequency response of each subcarrier, which can be easily obtained by using the corresponding TSs described in the previous section. For a specific application scenario, through negotiations between the transmitter and the receiver, each ALA can thus be applied according to the total channel BER_T and each individual subcarrier BER. The total channel BER_T is defined as

$$BER_T = \frac{1}{N_S - 1} \sum_{k=1}^{N_S - 1} BER_k \tag{2.16}$$

where BER_k is the BER corresponding to the *k*-th subcarrier. *Ns* is the total number of data-carrying subcarriers within an OFDM symbol [11]. In addition, subcarriers suffering a very low SNR may be dropped completely (set to zero) in order to maintain a BER_T of 1.0×10^{-3}.

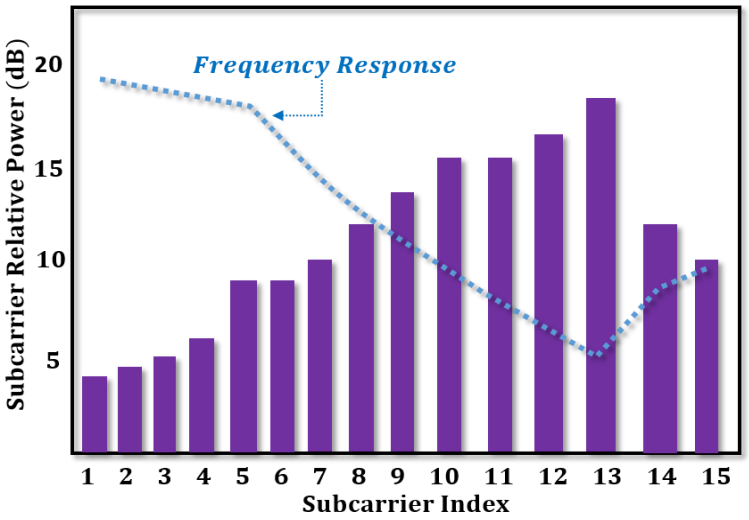

Fig. 2.9. Adaptive power loading technique

In APL, according the channel frequency response, the power of each individual subcarrier within an OFDM symbol varies. Generally speaking, higher (lower) power is allocated to a subcarrier with low (high) SNR, with the total electrical signal power kept fixed, to ensure that the individual subcarrier BERs detected in the receiver are almost uniformly distributed among all the subcarriers and that the corresponding total channel BER_T is $\leq 1.0\times10^{-3}$. Fig.2.9 shows an example of the use of such technique where the assigned subcarrier powers in the transmitter compensates the estimated system frequency response occurring for an OFDM transmission system [12]. In ABL, according the channel frequency response, the signal modulation format taken on each individual subcarrier within an OFDM symbol varies. Generally speaking, a high (low) signal modulation format is used on a subcarrier experiencing a high (low) SNR [13]. The modulation formats may vary from quadrature binary PSK (QPSK) to 256-QAM. As an example of this ALA, Fig.2.10 is illustrated.

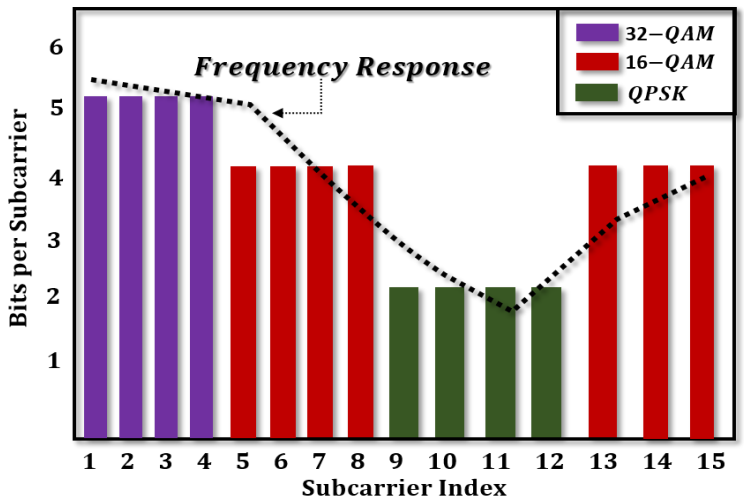

Fig. 2.10. Adaptive bit loading technique

Based on the above description, depending on the transmission system requirements, these ALAs are utilized to maximize the signal bit rate for a given BER and a fixed power constraint, or to minimize the BER for a given signal bit rate in order to increase the system power budget. Specifically speaking, it is easy to understand that, for power budget-limited transmission systems, APL are preferred whilst for bandwidth-hungry transmission systems with sufficiently large power budgets, ABL are preferred.

It is worth mentioning that these two techniques can be combined together resulting in adaptive bit and power loading (BPL) where both the electrical power and signal modulation format taken on each individual subcarrier are adjusted independently [11]. Although this ALA enhances the system flexibility and transmission performance, such enhancement is at the expense of increasing the system complexity [12, 13].

In this thesis, APL and ABL are utilized in Chapter 3 and Chapter 5 respectively, where it is shown that these ALAs improve not only the flexibility and performance robustness of OFDM transmission systems but also overall transmission performance.

2.5 Subcarrier Index Modulation

This section provides an insight into some variants of the OFDM transmission technique based on subcarrier index modulation (SIM). Three fundamental SIM techniques are described including SIM-OFDM, enhanced SIM-OFDM (ESIM-OFDM) and OFDM with

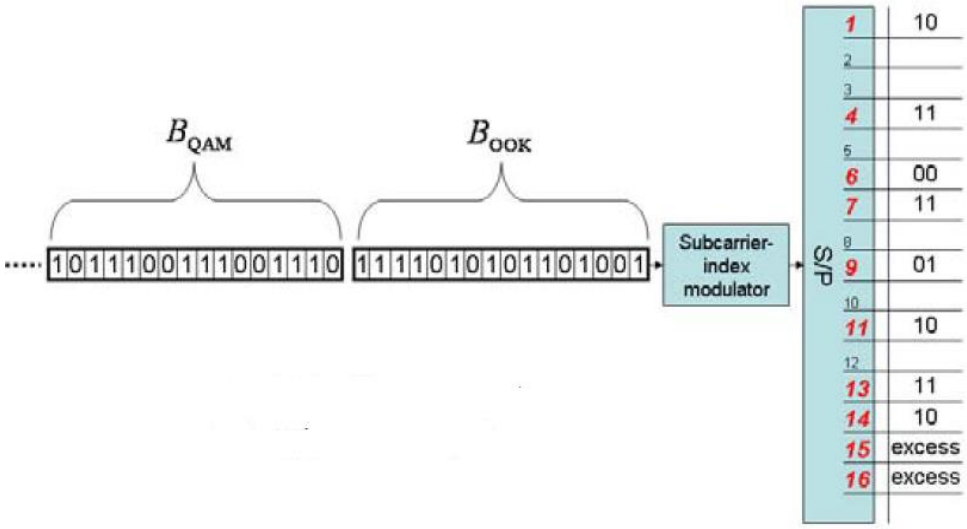

Fig. 2.11. SIM-OFDM encoding procedure [14]

index modulation (OFDM-IM). These techniques have rapidly gained huge attention and interest in the communication R&D community and have led to the emergence of numerous SIM-based OFDM variants.

2.5.1 Subcarrier Index Modulated OFDM

To reduce the multipath propagation-induced fast channel spectral variation effect associated with wireless transmission systems, SIM-OFDM has been proposed in 2009, where an additional information-carrying dimension is introduced into conventional OFDM [14].

The main concept of SIM-OFDM is illustrated in Fig.2.11, in which, the incoming bit stream is divided into blocks of bits, each having a length of $N(1+\frac{log_2 M}{2})$ with N being the number of subcarriers, and M being the constellation size of the respective M-QAM modulation format. Each of these blocks consists of two parts: the first N bits of the block form a sub-block, referred to as B_{OOK}, and the remaining $N\frac{log_2 M}{2}$ bits form a second sub-block, referred to as B_{QAM}. The operating principle of this technique can be summarized below: Before transmission, the B_{OOK} sub-block is inspected in order to detect which bit (1 or 0) has the most occurrences, in other words, "majority bit-value". Each bit in B_{OOK} is mapped a subcarrier by activating or deactivating the subcarrier. To maximize B_{QAM}, all the subcarriers associated with the subset of the majority bit value (ones in Fig.2.11) are activated and subsequently modulated utilizing the second bit stream B_{QAM}, while the remaining subcarriers are deactivated.

Based on the above analysis, it can be understood that in SIM-OFDM the subcarrier index is utilized as an extra dimension to carry user information i.e., a specific subcarrier is activated or deactivated according to an incoming data sequence, thus the resulting on and off subcarrier pattern within an OFDM symbol also bears user information. Compared to conventional OFDM, SIM-OFDM improves the system BER performance due to the subcarrier power reallocation, i.e., the power originally allocated to inactive subcarriers is equally redistributed among the active ones. Therefore, when the total signal power is fixed, the power allocated to each active subcarrier is increased, thus resulting in a better BER performance.

At the receiver, to reconstruct the sub-block B_{OOK}, use is made of an on-off keying (OOK) detector to determine the power status of each individual subcarrier. In this process, when a subcarrier power is above (below) a certain threshold, the subcarrier is marked as active (inactive), based on this pattern the sub-block B_{OOK} is reconstructed and subsequently the active subcarriers are demodulated according to the respective M-QAM modulation format adopted, and finally, this leads to the recovery of the B_{QAM} sub-block.

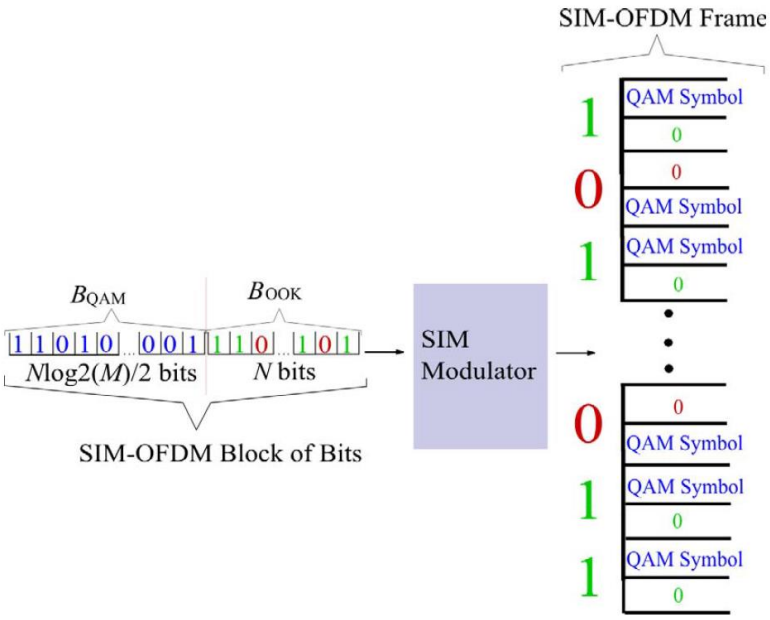

Fig. 2.12. ESIM-OFDM Encoding Procedure [15]

From the above description, it is clear that, an incorrect detection of a subcarrier power status not only leads to incorrect detection of the bits it encodes, but also, it misplaces all subsequent bits in the B_{QAM} sub-block giving rise to strong error propagation.

2.5.2 Enhanced SIM-OFDM

To address the error propagation effect associated with SIM-OFDM, ESIM-OFDM was proposed in [15]. In this technique, a slight modification is made to the way active subcarriers are encoded. As shown in Fig.2.12, instead of each bit in B_{OOK} being conveyed using the power status of a single subcarrier, it is conveyed using the power status of two consecutive subcarriers: whenever a ‘‘1’’ is encountered in B_{OOK}, the first subcarrier of a pair is set as active and the second one as inactive. On the other hand, a ‘‘0’’ in B_{OOK} implies that the first subcarrier of a pair is set as inactive and the second one as active. In each pair, it is certain that just one of the two subcarriers is active.

The above description indicates that those bits in B_{QAM} can no longer be misplaced due to a wrong detection of the previous subcarrier power status. As a direct result, ESIM-OFDM offers a significant error propagation reduction compared to SIM-OFDM. This encoding procedure also indicates that there is no longer a need to define a majority-bit value in the B_{OOK} sub-block, and the total number of active carriers is always the same *(N/2)*. The major downside of this modified scheme compared with the original one is the slightly reduced spectral efficiency, because ESIM-OFDM suffers the loss of half of the subcarrier-index-carried bits.

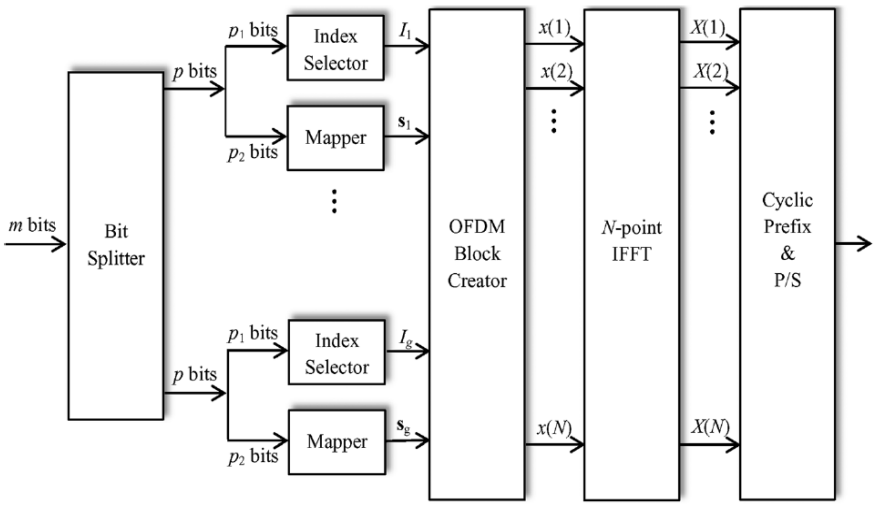

Fig. 2.13. OFDM-IM Encoding Procedure [16]

Table 2.1. A Look-up Table Example for $p_1=2$, $n=4$ and $k=2$

Index bits	Indices	Subblocks
$[0,0]$	$[1,2]$	$[S_{i_1}, S_{i_2}, 0, 0]$
$[0,1]$	$[2,3]$	$[0, S_{i_1}, S_{i_2}, 0]$
$[1,0]$	$[3,4]$	$[0, 0, S_{i_1}, S_{i_2}]$
$[1,1]$	$[1,4]$	$[S_{i_1}, 0, 0, S_{i_2}]$

2.5.3 OFDM with Index Modulation

To overcome the spectral efficiency shortage of ESIM-OFDM, OFDM-IM was proposed in [16] where subcarriers are split into OFDM sub-blocks and the sub-block size is no longer constrained to only two as in ESIM-OFDM. In fact, as shown in Fig.2.13, the incoming m information bits are firstly split into g groups each containing p bits, i.e., $m=pg$. Each group of p-bits is of length n, where $n=N/g$. For each sub-block, k out of n available subcarriers are activated, where $k \leq n$, while the remaining subcarriers are deactivated. To do so, the incoming p bits are divided into two parts as seen in Fig.2.14. The first part has p_1 bits and second part has p_2 bits, i.e., $p=p_1 + p_2$. The p_1 bits are fed to the index selector and depend on the number of activated subcarriers within a set of n subcarriers such that, $p_1 = \lfloor log_2(C_n^k) \rfloor$ where $\lfloor . \rfloor$ denotes the floor function. Whilst, $p_2 = klog_2(M)$, represent the bits of the g-th OFDM sub-block fed through the mapper block to be mapped to the k signal constellation symbols. As a direct result, the total number of bits that can be transmitted by a single block of OFDM-IM scheme is $B = (p_1 + p_2)g$.

The above encoding procedure implies that a simple look-up table is needed in the transmitter to map the incoming information bits to subcarrier indices. As an example, Table 2.1 is presented in which S_{i1} and S_{i2} are arbitrary user data. It is seen that for each OFDM sub-block, the indices of the modulated subcarriers are determined by the two index bits, with the bit streams [0,0], [0,1], [1,0] and [1,1] corresponding to the index patterns [1,2], [2,3], [3,4] and [1,4], respectively. At the receiver, a maximum likelihood (ML) detector based on a log-likelihood ratio (LLR) is employed to determine the most likely active subcarriers. Based on this mapping/demapping procedure, unlike the ESIM-OFDM in which the number of active subcarriers is fixed, OFDM-IM provides an optimum trade-off between complexity and spectral efficiency by simply altering the number of active subcarriers [16] for a given application scenario.

It should be noted, in particular, that, all three above-outlined signal transmission techniques almost halve the achievable signal bit rate and spectral efficiency, in comparison with conventional OFDM encoded using identical signal modulation formats since nearly half of those subcarriers are deactivated.

2.6 Optical Transmission Systems

Having described the basic concept behind the OFDM transceivers, the next step is to discuss optical OFDM transceivers. Firstly this section provides a general description of optical fibers and optical transceivers. Secondly, key fiber transmission effects such as fiber loss, chromatic dispersion (CD) and fiber nonlinearity are described in detail. In addition, to describe optical OFDM (OOFDM) IMDD transmission systems, intensity modulator and photodetector are presented in this section.

2.6.1 Fundamentals of Optical Fibers

2.6.1.1 Optical Fiber Transmission

The role of optical fibers in optical transmission systems is to transport optical signals from a transmitter to a receiver. Generally speaking, an optical fiber consists of a cylindrical core of silica glass surrounded by a cladding whose refractive index is lower than that of the core. The optical fiber can be commonly classified into two categories including multi-mode fibers (MMFs) and single mode fibers (SMFs). A MMF has a large core diameter (~50-62.5μm) which enables multiple light modes to propagate. In MMFs, different modes propagate at different speeds, this result in mode delay. Such dispersive effect is called modal dispersion which narrows the transmission system bandwidth and limits the maximum length of transmission distance. As a result, MMFs are often installed in LANs. On the other hand, SMF have a smaller core diameter (~8-10.5μm) and it is typically designed to operate at 1310nm and 1550nm wavelength. Compared with a MMF, light can only propagate in one mode thus eliminating modal dispersion, however, the SMF still suffers from the dispersive effect caused by chromatic dispersion as discussed in the following section. In terms of fiber cost, SMFs are relatively cheaper than MMFs, but MMF-based transmission systems are considerably cheaper than those based on SMFs. [17].

2.6.1.2 Chromatic Dispersion

Chromatic dispersion is caused by frequency dependence of the refractive index of an optical fiber. As a result, different spectral components of an optical signal travel at slightly different group velocities for a SMF of length L and the resulting time delay ΔT, which is by

$$\Delta T = LD\Delta\lambda \tag{2.17}$$

where D is the dispersion parameter and expressed in units of ps/(km·nm). Δλ is the signal bandwidth in *nm*. In practice, D, is expressed as

$$D = -\frac{2\pi c}{\lambda^2}\beta_2 \tag{2.18}$$

where β_2 is the Group-Velocity Dispersion (GVD) parameter, c is the velocity of light in vacuum and λ is the central wavelength. D is wavelength dependent and for standard SMF (SSMF), D is zero near 1310nm and around 17 ps/(km·nm) at 1550nm, as shown in Fig.2.15.

The chromatic dispersion-induced time delay brings about ISI in the received signal and thus imposes limitations for maximum achievable performance of optical communication systems. In OOFDM transmission systems, the chromatic dispersion-induced ISI can be compensated by using CP and by channel equalization which automatically compensates linear effects. CP and channel equalization are discussed in Section 2.3.4 and Section 2.3.6 respectively.

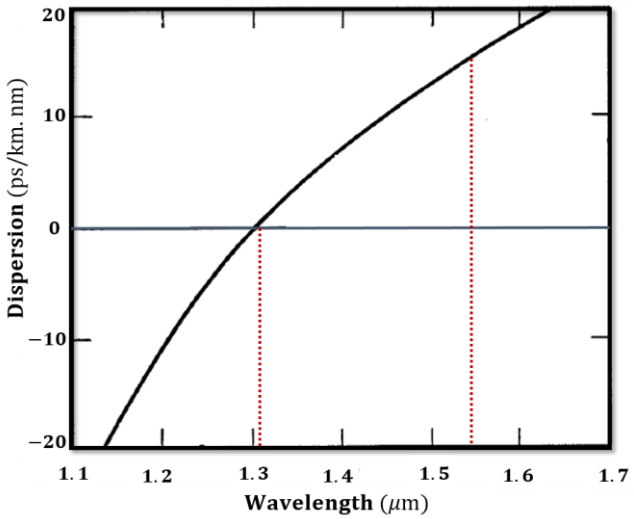

Fig. 2.15. Dispersion versus wavelength for SSMF

2.6.1.3 Fiber Loss

When transmitted through the SMFs, the signal power is attenuated due to fiber loss. The fiber loss can be described by

$$P_{out} = P_{in}10^{\frac{-\alpha L}{10}} \tag{2.19}$$

where α is the attenuation coefficient and expressed in units of dB/km, P_{in} is the power launched at the input end of a fiber with length L and P_{out} is the power at the output end of the fiber. Several factors contribute to overall losses and the two most important factors are material absorption and Rayleigh scattering. The detailed descriptions of these factors can be found in [18].

2.6.1.4 Fiber Nonlinearity

Under an intense electromagnetic field, the response of optical fiber to light becomes nonlinear. In general, the origin of such nonlinear response is related to the random motion of bound electrons under the influence of an applied field. As a result, fiber nonlinearities affect both power and phase of optical signals propagating through the SSMF.

The fiber nonlinear effects are generally divided into two types. The first type involves energy exchange from the optical field to the medium by inelastic scattering. Such scattering effects include stimulated Brillouin scattering (SBS) and stimulated Raman scattering (SRS). In both SBS and SRS, the frequency of the scattering light is shifted downward and its intensity grows exponentially once the launch power exceeds a certain threshold, which is usually ≈30dBm for SRS and ≈10dBm for SBS [18]. In this thesis, the optical launch powers employed in all simulations are well below such values so the impact of SBS and SRS is negligible. As such, this section focuses on the second type of fiber nonlinearities, which is related to the fact that, at high intensities, the refractive index of silica increases with the intensity of the propagating optical signal. The three most important effects are self-phase modulation, cross-phase modulation (XPM) and four-wave mixing (FWM).

Self-Phase Modulation

SPM refers to the self-induced phase shift experienced by an optical field [18]. Due to the optical intensity dependence of refractive index in an optical fiber, the nonlinear phase shift

Φ_{NL} imposed on the optical field is proportional to the optical intensity which can be expressed as:

$$\Phi_{NL} = n_2 k_0 L |E|^2 \tag{2.20}$$

where n_2 is the nonlinear refractive coefficient, throughout the thesis, is referred to as the Kerr coefficient. $k_0 = 2\pi/\lambda$ and λ is the carrier wavelength and $|E|^2$ is the optical intensity inside the fiber. The self-phase modulation affects the pulse shape and often leads to additional pulse broadening.

Cross-Phase Modulation

XPM refers to the nonlinear phase change of an optical field induced by a co-propagating field at a different wavelength. Its origin can be understood by noting that when two optical fields, E_1 and E_2 at frequencies ω_1 and ω_2 respectively, propagate simultaneously inside the fiber. The induced nonlinear phase change for the field at ω_1 is then given by:

$$\Phi_{NL} = n_2 k_0 L(|E_1|^2 + 2|E_2|^2) \tag{2.21}$$

It can be found from Eq.(2.20) and (2.21) that, for optical fields with identical power, the contribution of XPM to the nonlinear phase shift is twice that of self-phase modulation for the case of co-polarized channels. Similar to self-phase modulation, XPM also causes a greater temporal broadening as signal propagates along the fiber due to the effect of CD.

Four-Wave Mixing

When three optical fields with carrier frequency ω_1, ω_2 and ω_3 respectively co-propagate simultaneously inside the fiber, a fourth optical field is generated whose frequency is related to the others by:

$$\omega_4 = \omega_1 \pm \omega_2 \pm \omega_3 \tag{2.22}$$

FWM occurs only when phase-matching condition between the propagating signals is achieved, that is, for energy to flow effectively from one frequency to another, this condition must remain satisfied.

FWM often occur in WDM systems where the multiple channel wavelengths are equally spaced resulting in crosstalk between different frequency channels. The effects of FWM become more severe with decreased channel spacing such as in Dense WDM (DWDM)

systems and/or at high signal power levels. FWM is dependent on the channel spacing thus one efficient way to suppress this effect is to use uneven WDM channel spacing.

For the scenarios considered in this thesis, the influences of self-phase modulation, XPM and FWM are not significant because the transmission distance is often short and the optical launch power is low.

2.6.2 Photodetector

In the receiver, the transmitted optical signal is detected by a photodetector, which converts the incident optical power P_{in} into an electrical current.The generated photocurrent, I_p, is given by:

$$I_p = RP_{in} \tag{2.23}$$

where R (in A/W) is the photodetector responsivity. In practice, two fundamental noise mechanisms associated with the photodetector exists: shot noise and thermal noise, which lead to fluctuations in the current even when the incident optical signal has a constant power [18]. In optical transmission systems, the commonly used photodetectors are *p-i-n* and avalanche photodiode (APD). Throughout this thesis a *p-i-n* is considered. Both shot and thermal noise associated with *p-i-n* photodetectors are analysed below.

Shot noise arises from the statistical nature of the generation of photo-electrons when an optical signal is incident on a photodetector. The noise variance is proportional to the photocurrent, which is given by [18]

$$\sigma_S^2 = 2qI_p\Delta f \tag{2.24}$$

where q is the charge of electron and Δf is the receiver bandwidth.

Thermal noise, however, is due to another mechanism detailed as follows: at a finite temperature, electrons move randomly in any conductor; random thermal motion of electrons manifests as a fluctuating current and adds such fluctuation to the photocurrent. The noise variance is given by [18]

$$\sigma_T^2 = \frac{4Tk_B}{R_L}\Delta f \tag{2.25}$$

where k_B is the Boltzmann constant with a value of 1.38×10^{-23} J/K, T is the absolute temperature and R_L is the load resistor.

If I_s and I_t are used to express the current fluctuation induced by shot noise and thermal noise respectively, the total current resulted from the photodetector expressed in Eq. (2.23) is modified:

$$I = I_p + I_s + I_t \tag{2.26}$$

Both I_s and I_t are independent random processes with Gaussian statistics [18]. Eq.(2.26) clearly indicates that the noise lowers the received SNR and thus worsens the BERs in the receiver.

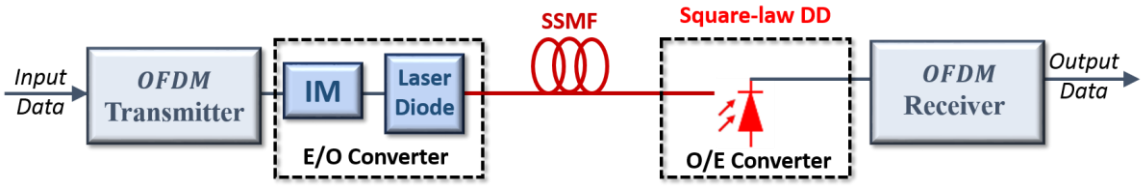

Fig. 2.16. IMDD OOFDM transmission system

2.6.3 IMDD OOFDM Transmission Systems

In the IMDD OOFDM transmission systems, the electrical-to-optical (E/O) block converts the electrical OFDM signal to an optical signal by intensity-modulation (IM), whilst, the optical-to-electrical (O/E) block converts the optical OFDM to an electrical signal through a direct-detection (DD) process.

Fig.2.16 describes the IMDD OOFDM transmission system. In the transmitter, the electrical driving current of the OFDM signal, *s(t)*, is given by:

$$i(t) = I_{dc} + s(t) \tag{2.27}$$

where I_{dc} is the added DC bias to ensure that the driving current is non-negative. In the E/O, assuming an ideal intensity modulation, the optical intensity modulator generates an optical power $p(t) = i(t)$. Then the optical field, $E(t)$, can be expressed as

$$E(t) = \sqrt{p(t)} = \sqrt{I_{dc} + s(t)}e^{j\phi t} \tag{2.28}$$

where ϕ is the phase of the diode laser which serves as an optical source.

After the SSMF transmission, the detected optical signal undergoes direct detection by a square-law PIN photodetector in the receiver and is given by:

$$y(t) = | (\sqrt{I_{dc} + s(t)}e^{j\phi t}) \otimes h(t) + w(t) |^2 \quad (2.29)$$

where $h(t)$ and $w(t)$ are the channel impulse response and channel noise respectively. By using Taylor series expansion on the square root term in Eq.(2.29) and ignoring the channel noise for simplicity, the detected signal is expressed as:

$$\begin{aligned} y(t) = [\ (\sqrt{I_{dc}} + \left(\frac{s_{(t)}}{2\sqrt{I_{dc}}}\right) - \left(\frac{s^2_{(t)}}{8I^{3/2}_{dc}}\right) + \cdots) e^{j\phi t} \otimes h(t)\ ] \\ \times [(\sqrt{I_{dc}} + \left(\frac{s_{(t)}}{2\sqrt{I_{dc}}}\right) - \left(\frac{s^2_{(t)}}{8I^{3/2}_{dc}}\right) + \cdots)\ e^{j\phi t} \otimes h(t)]^* \quad (2.30) \\ = I_{dc} + \frac{s_{(t)} \otimes (h_{(t)} + h^*_{(t)})}{2} - \frac{s^2_{(t)} \otimes (h_{(t)} + h^*_{(t)})}{8I_{dc}} + \cdots \end{aligned}$$

In the above equation, the first term on the right hand side is the DC component whilst the second term represents the OFDM signal required for recovery. The following terms represent the unwanted subcarrier intermixing products resulted from the square-law detection procedure. After the O/E converter, the electrical signal is fed into the OFDM receiver where the transmitted OFDM signal, *s(t)*, is then recovered using the receiver functions described in Section 2.3.2.

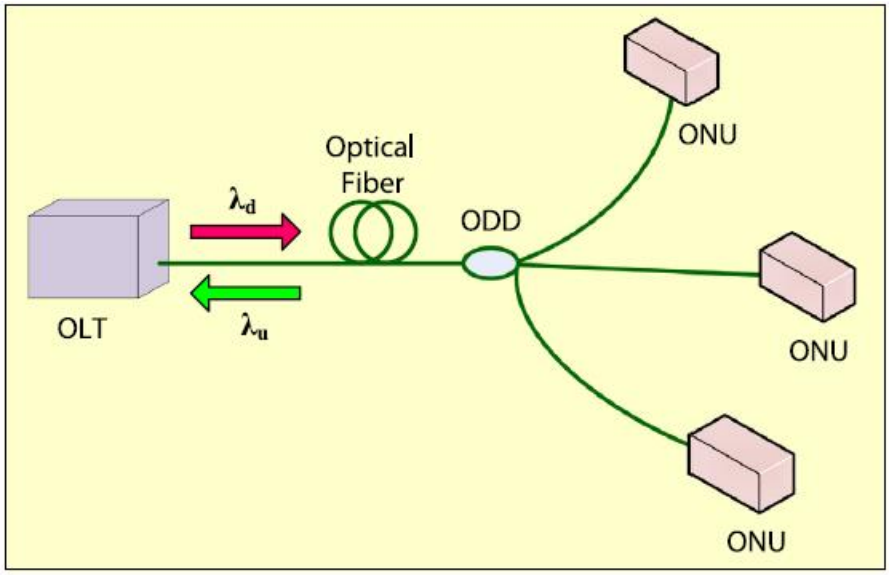

Fig. 2.17. General architecture of PON [19]

2.7 Passive Optical Networks

2.7.1 Basic Concept of PON

Optical access networks have evolved to achieve high signal transmission capacity and good scalability in terms of link range and number of users.

The general architecture of PON is shown in Fig. 2.16. A PON basically comprises an optical line terminal (OLT) at the central office (CO), an optical fiber, an optical distribution node (ODD), and multiple optical network units (ONUs) close to users' premises. The OLT assigns the downlink wavelength (λ_d), modulates the downstream data on this wavelength and then propagates it into the optical fiber. The ODD (or remote node (RN)) de-multiplexes the downstream data to multiple ONUs and also multiplexes the upstream traffic from the ONUs to the optical fiber. The ONUs receive the downstream traffic from the RN and generate the upstream traffic to the optical link on the uplink wavelength (λ_u) [19].

There are two traditional types of PONs: time division multiplexing-PON (TDM-PON) and WDM-PON. In addition, orthogonal frequency division multiplexing-PON (OFDM-PON) has also been widely researched as a future PON candidate technology.

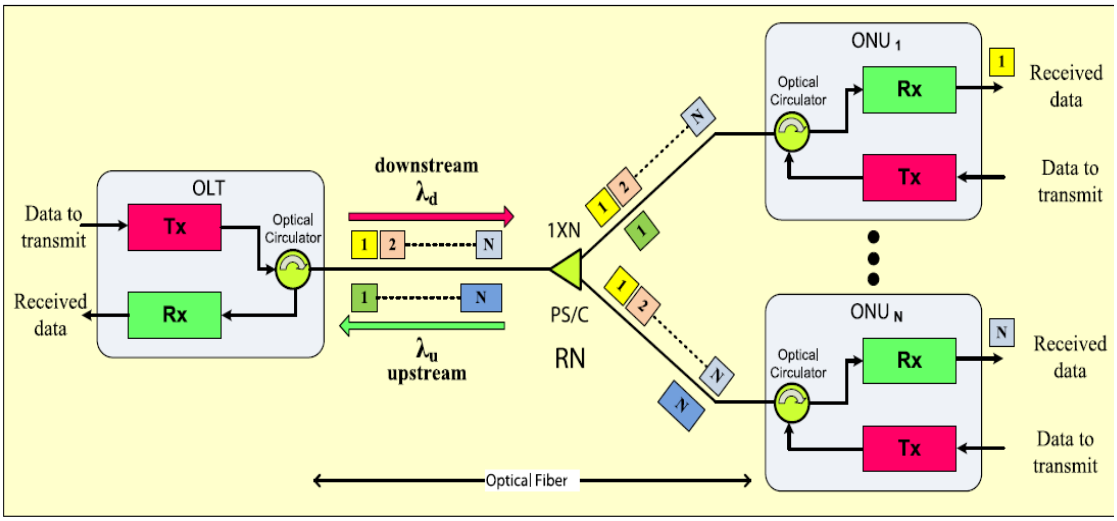

Fig. 2.18. Network architecture of TDM PON [19]

2.7.2 TDM-PON

The architecture of TDM-PON is shown in Fig.2.18. The OLT dedicates timeslots to *N* subscribers (ONU_1, ONU_2, …,ONU_N). A 1×*N* passive optical power splitter/combiner (PS/C)

is used to distribute the optical signal to/from multiple ONUs. For bidirectional TDM-PONs, optical circulators are used to separate the upstream and downstream signals at the CO and the ONUs. One downlink wavelength (λ_d) is used to transport the downstream data from OLT to ONUs. The downstream data is broadcast to all the connected ONUs. Each ONU selects the stream slot allocated to it and discards the slots directed to other ONUs. Another uplink wavelength (λ_u) transports the upstream data from ONUs to OLT. As there is only one receiver in the OLT and a single feeder fibre, ONUs take turns to send their data in a TDM schedule. Moreover, when an ONU is not sending data, it has to turn off its laser to avoid interference with other ONUs' upstream transmission. As a result, the use of burst mode ONU transmitters is critical in TDM-PONs.

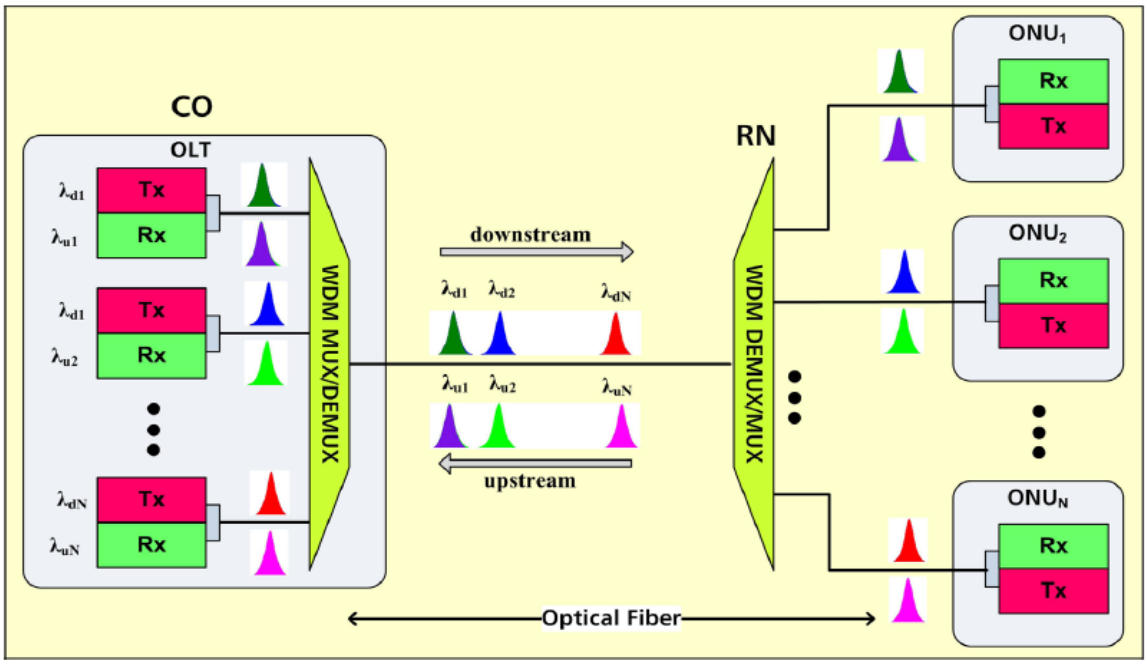

Fig. 2.19. Network architecture of WDM-PON [19]

2.7.3 WDM-PON

It is widely agreed that PONs based on pure TDM cannot cope with the requirements of future networks with a large aggregated bandwidth and a high power budget. A promising solution to address this challenge is to adopt WDM-PONs. The WDM-PON also provides excellent scalability and flexibility because it can support multiple wavelengths over the same fiber infrastructure as detailed below. The WDM-PON also has good protocol transparency and security [21].

The architecture of a WDM-PON is shown in Fig.2.19 where a wavelength division multiplexer/demultiplexer (WDM MUX/DEMUX) is used at the OLT and the RN. The WDM-PON is designed to appoint *N* separate wavelength channels from the CO to the ONUs in the downstream direction called downlink wavelengths (λ_{d1}; λ_{d2};…; λ_{dN}). At the CO, a WDM MUX/DEMUX is used to multiplex the downstream data before transmission. At the RN, the WDM MUX/DEMUX distributes the downstream optical signals to the dedicated ONU (ONU_1, ONU_2… ONU_N) according to the downlink wavelengths. In the upstream direction, the uplink wavelengths (λ_{u1}; λ_{u2};…; λ_{uN}) pass from the ONUs to the OLT. At the RN, WDM MUX/DEMUX combines the upstream data to send them along the optical fiber to the OLT. At the CO, a WDM MUX/DEMUX is also used demultiplex the ONU signals.

Although WDM-PON assigns a dedicated wavelength for each user to exploit the full bandwidth, OLT has to allocate *N* wavelengths for *N* ONUs, and each of which requires a tunable laser resulting in high-cost transmission systems [22].

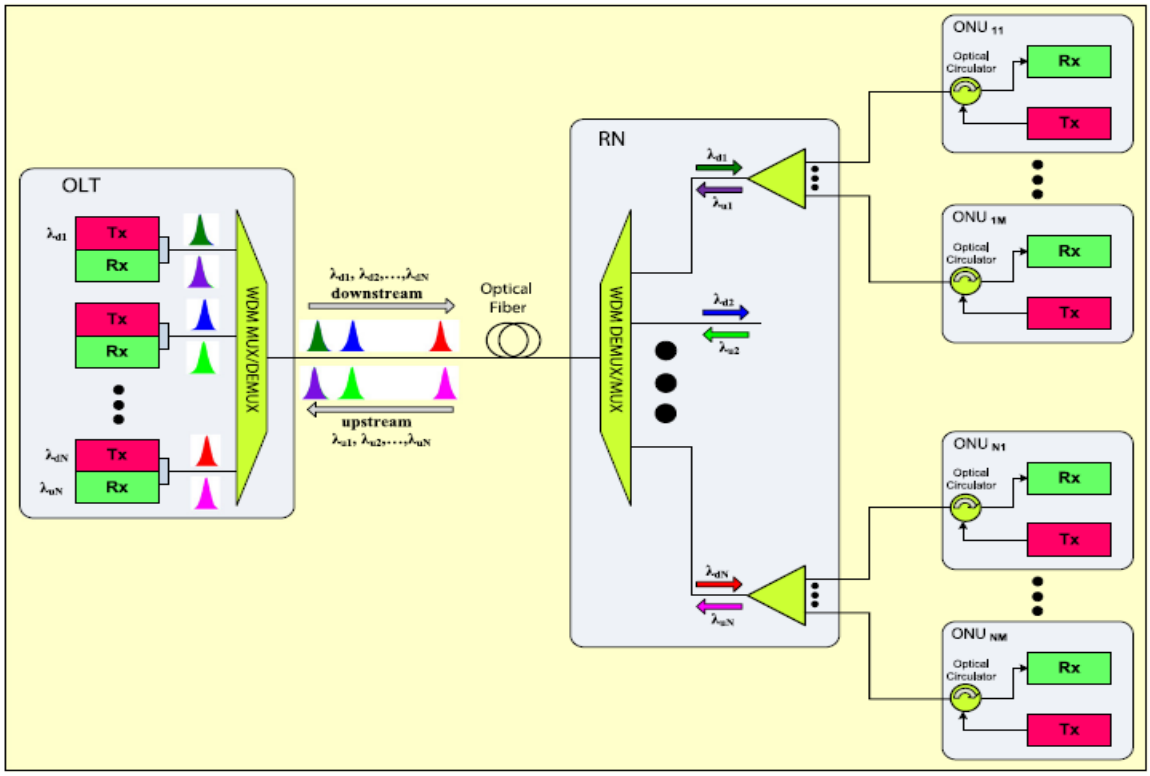

Fig. 2.20. Network architecture of the WDM/TDM PON [19]

In practice, a WDM-PON can also be combined with a TDM-PON to increase ONU count, transmission distance and system scalability. A hybrid WDM/TDM-PON is a PON in which more than one wavelength is used in each direction for communications between an OLT and a number of ONUs and each wavelength is shared among several ONUs by using the TDM technique as illustrated in Fig.2.20. The WDM/TDM-PON possesses a number of advantages over both WDM and TDM such as the ability to decrease costs by sharing wavelengths between users. In addition, with the increased number of customers enabled by the WDM/TDM-PON, the number of COs can also be reduced leading to considerable power and maintenance cost savings [23].

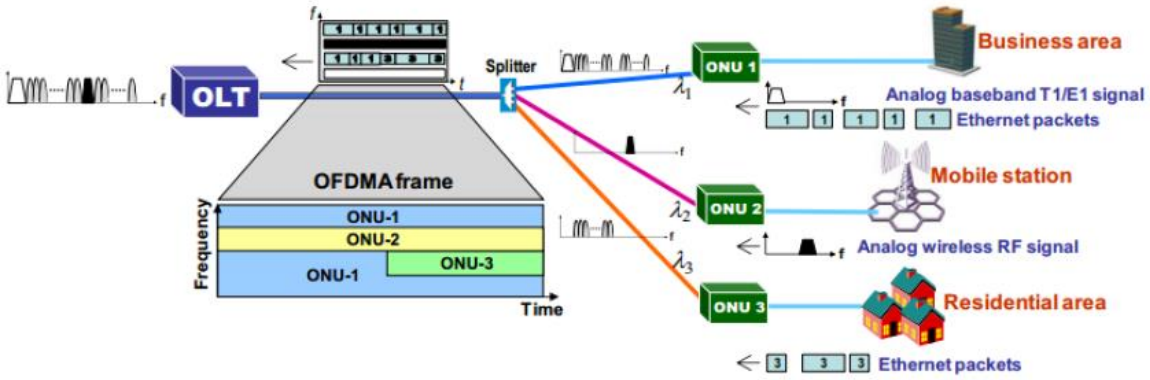

Fig. 2.21. Network architecture of OOFDM-PON [24]

2.7.4 Optical OFDM-PONs

In optical OFDM-PONs, different OFDM subcarriers are dynamically assigned to different customers/services in different TDM timeslots [24]. Fig.2.21 shows typical network architecture and multiple access strategy of optical OFDM-PONs. For downstream traffic, different services per ONU share the same laser and the downstream wavelength. The downstream signal is broadcast to all ONUs by using an optical splitter. Each ONU recovers its signal from its allocated subcarriers and timeslots. For upstream traffic, each ONU maps its data to its allocated subcarriers, sets all the other subcarriers to zero and generate electrical OFDM symbols. The signals are then converted to optical signals with optical intensity modulators such as directly modulated lasers (DMLs) for transmission over the fibre. The OOFDM symbols from multiple ONUs will be combined at the optical coupler (OC) in the RN, and detected by a single photodetector at the OLT receiver. To avoid collisions in the

upstream, synchronisation is highly critical. ONUs must be timeslot synchronized so that the OFDM symbols are aligned correctly at the OLT [25].

Compared to conventional TDM-PON technologies, the optical OFDM-PONs has a number of salient advantages such as high spectral efficiency, high chromatic dispersion tolerance, excellent system scalability and fine granularity bandwidth control [26, 27].

References

[1] R. W. Chang, “Synthesis of band-limited orthogonal signals for multi-channel data transmission,” *Bell System Technical Journal*, vol. 46, pp. 1775-1796, 1966.

[2] S. B. Weinstein and P. M. Ebert, “Data transmission by frequency-division multiplexing using the discrete Fourier transform,” *IEEE Tans. Commun. Technol.*, vol. 19, no.5, pp.628-634, Oct. 1971.

[3] A. Peled and A. Ruiz, “Frequency domain data transmission using reduced computational complexity algorithms,” *IEEE Proc. ICASSP 80*, Denver, CO, USA, vol. III, pp. 964-967, 1980.

[4] Hirosaki, B., ‘‘A 19.2 kbits voice band data modem based on orthogonality multiplexed QAM Techniques,’’ *Proc. of IEEE ICC’85*, pp. 21.1.1-5, 1985.

[5] R. Prasad, ‘‘OFDM for wireless communications systems,*’’Artech House*, Aug. 2004.

[6] B. J. Dixon, R. D. Pollard, and S. Iezekiel, “Orthogonal frequency-division multiplexing in wireless communication systems with multimode fiber feeds,” *IEEE Transactions on Microwave Theory and Techniques*, vol. 49, no.8, pp. 1404-1409, Aug. 2001.

[7] S. Sun *et. al*., ‘‘Overlay cognitive radio OFDM system for 4G cellular networks,’’ *IEEE Wireless Communications*, vol.20, no.2, Apr. 2013.

[8] N. E. Jolley, H. Kee, R. Rickard, J. Tang, and K. Cordina, “Generation and propagation of a 1550 nm 10 Gb/s optical orthogonal frequency division multiplexed signal over 1000 m of multimode fibre using a directly modulated DFB,” *OFC/NFOEC,* (OSA), Paper OFP3, 2005.

[9] J. M. Tang, P. M. Lane, and K. A. Shore, “High-speed transmission of adaptively modulated optical OFDM signals over multimode fibers using directly modulated DFBs,” *J. Lightw. Technol.*, vol. 24, no. 1, pp. 429–441, Jan. 2006.

[10] X. Sun, X. Zheng, Y. Yin, and Z. Zhuang ‘‘Dual-band optical orthogonal frequency division multiplexing with adaptive cyclic prefix,’’ *APCA Int. Conf. on Control and Soft Computing (CONTROLO),* Jun. 2018.

[11] X. Q. Jin, J. L. Wei, R. P. Giddings, T. Quinlan, S. Walker, and J. M. Tang, “Experimental demonstrations and extensive comparisons of end-to-end-time optical

OFDM transceivers with adaptive bit and/or power loading," *IEEE Photon. J.*, vol. 3, no. 3, pp. 500–511, Jun. 2011.

[12] E. Giacoumidis, A. Kavatzikidis, A. Tsokanos, J. M. Tang, and I. Tomkos, ''Adaptive loading algorithms for IMDD optical OFDM PON systems using directly modulated lasers,'' *Opt. Commun. Netw.*, vol. 4, no. 10, pp. 769–778, Oct. 2012.

[13] X. Q. Jin, J. L. Wei, R. P. Giddings, T. Quinlan, S. Walker, and J. M. Tang, ''Experimental demonstrations and extensive comparisons of end-to-end real-time optical OFDM transceivers with adaptive bit and/or power loading,'' *IEEE Photon. J.*, vol. 3, no. 3, pp. 500-511, Jun. 2011.

[14] R. Abu-alhiga and H. Haas, "Subcarrier-index modulation OFDM," in *Proc. IEEE Int. Sym. Personal, Indoor Mobile Radio Commun.*, pp. 177–181, Sep. 2009.

[15] D. Tsonev, S. Sinanovic, and H. Haas, "Enhanced subcarrier index modulation (SIM) OFDM," in *Proc. IEEE GLOBECOM Workshops*, pp. 728–732, Dec. 2011.

[16] E. Başar *et al.*, "Orthogonal frequency division multiplexing with index modulation," *IEEE Trans. Signal Process.*, vol. 61, no. 22, pp. 5536–5549, Nov. 2013.

[17] S. Hawkin, Communication Systems, 4th ed., NJ, USA: *Wiley*, 2001.

[18] G. P. Agrawal, Fibre-Optic Communication Systems, 2nd ed. Hoboken, NJ, USA: *Wiley*, 1997.

[19] R.Q. Shaddad *et al.*, ''A survey on access technologies for broadband optical and wireless networks'', *Optics Commun.*, vol. 41, pp. 459-472, May. 2014.

[20] L. G. Kazovsky, W. Shaw, D. Gutierrez, N. Cheng, and S. W. Wong, "Next-generation optical access networks," *J. Lightw. Technol.*, vol. 25, no. 11, pp. 3428-3442, Nov. 2007.

[21] J. Sie-Wook *et. al.*, ''Long-reach transmission experiment of a wavelength division multiplexed-passive optical networks transmitter based on reflective semiconductor optical amplifiers'', *Opt. Eng.*, vol. 51, no. 1, Jan. 2012

[22] F. Carvalho and A. Cartaxo, ''Multisignal OFDM-based hybrid optical-wireless WDM LR-PON with colorless ONU,'' *IEEE Photonics Tech. Lett.*, vol. 27, no. 11, pp. 1193-1196, Jun. 2015.

[23] K. Kondepu, L. Valcarenghi, P. Castoldi, "Reconfiguration Triggering Optimization in TWDM PONs with Fluctuating Load," in *Optical Fiber Communication Conference (OFC)*, Anaheim, 2016, paper W2A.67.

[24] X. Gong, L. Guo, and Q. Zhang, ‘‘Joint resource allocation and software-based Reconfiguration for energy-efficient OFDMA-PONs,’’ *J. Opt. Commun. Netw.*, vol.10, no.8, pp. C75-C85. Aug. 2018.

[25] IEEE Standard 802.3, Carrier sense multiple access with collision detection (CSMA/CD) access method and physical layer specifications, 2005 Edition.

[26] R. P. Giddings and J. M. Tang, ‘‘Experimental demonstration and optimisation of a synchronous clock recovery technique for realtime end-to-end optical OFDM transmission at 11.25Gb/s over 25km SSMF,’’ *Opt. Exp.*, vol. 19. No.3, pp. 2831-2845, Jan 2011.

[27] X. Q. Jin and J. M. Tang, “Experimental investigations of wavelength spacing and colorlessness of RSOA-based ONUs in real-time optical OFDMA PONs,” *J. Lightw. Technol*., vol. 30, no. 16, pp. 2603-2609, Aug. 2015.

3. Subcarrier Index-Power Modulated OOFDM

3.1 Introduction

Having described the motivation behind employing OFDM for future access networks in Section 1.1, and inspired by the subcarrier index modulation (SIM) approach [1-3] discussed in Section 2.5, this chapter presents a novel signal transmission technique called subcarrier index-power modulated optical OFDM (SIPM-OOFDM) [4, 5] for use in cost-sensitive IMDD PON systems. In SIPM-OOFDM, the combined subcarrier index and subcarrier power acts as an extra information-carrying dimension, here referred to as subcarrier index-power (SIP) information bearing dimension, i.e., a specific subcarrier is set at a low or high power according to an incoming data sequence. Hence, the resulting high and low subcarrier power levels within an OFDM symbol enables not only extra information bits to be conveyed but also all the subcarriers to be activated all the time. Therefore, compared with both conventional OFDM and previously discussed SIM-OFDM-based techniques, SIPM-OOFDM enables a significant increase in signal bit rate without increasing the signal modulation formats and without compromising the minimum required OSNR for achieving a specific BER. In addition, SIPM-OOFDM offers improved transceiver design flexibility and system performance adaptability since it maintains the exact hardware design of conventional OOFDM. The only difference is that additional encoding/decoding DSP elements have been digitally introduced that avoid any complicated and sophisticated algorithms.

This chapter explores the proposed SIPM-OOFDM technique in terms of the following three important aspects: 1) Fundamental operating principles. 2) Optimizations of key transceiver parameters affecting the maximum achievable SIPM-OOFDM transmission performances. 3) Explorations of practically obtainable SIPM-OOFDM transmission performances when simple signal modulation formats such as quadrature phase shift keying (QPSK) and eight-phase shift keying (8-PSK) are considered for low and high power subcarriers, respectively. Moreover, compared to conventional OOFDM, similar SIPM-OOFDM tolerances to both fibre chromatic dispersion and Kerr-related fibre nonlinearity are confirmed in this chapter.

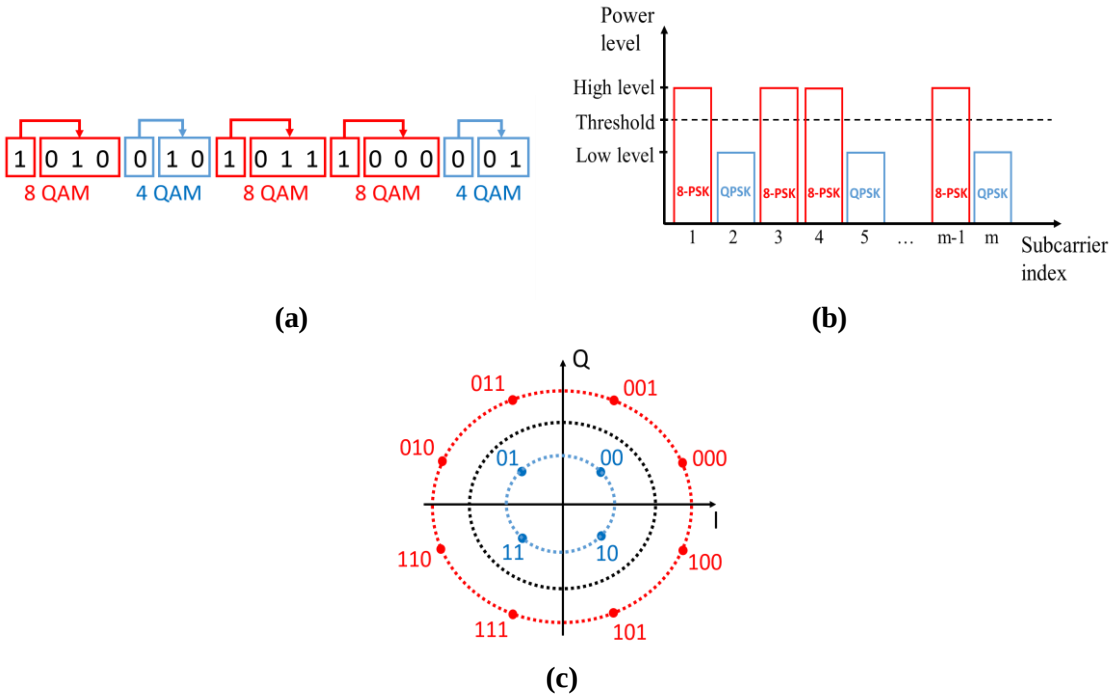

Fig.3.1. (a) SIPM-OOFDM encoding process. (b) Schematic diagram showing how a subcarrier of a specific power level is encoded using QPSK and 8-PSK. A subcarrier power threshold is represented using a line that lies between these two distinct QPSK and 8-PSK-encoded subcarrier power levels. (c) Overall QPSK- and 8-PSK-encoded SIPM-OOFDM constellations.

3.2 Operating Principle

In general, the operating principle of the proposed SIPM-OOFDM technique is similar to conventional OOFDM [6], except that the SIPM-OOFDM transmitter (receiver) data-encoding (decoding) DSP functions are modified as explained below in detail. In addition, new DSP functions for detecting the subcarrier power status and calculating the subcarrier power threshold are also introduced prior to equalization in the receiver. To encode an incoming pseudo-random binary sequence (PRBS) in the transmitter, as illustrated in Fig. 3.1(a), when a ‘‘1(0)’’ bit is encountered, the corresponding subcarrier power is set high (low) as shown in Fig.3.1(b), and the following 3(2) bits of the PRBS data sequence are then encoded using 8-PSK (QPSK). The resulting overall SIPM-OOFDM constellations are presented in Fig.3.1(c). After 8-PSK (QPSK)-encoding, the resulting complex number is finally assigned to the subcarrier. Such a data-encoding procedure ensures that all the subcarriers are always active, and equally important, setting each individual subcarrier at a specific power level enables each subcarrier to carry an extra information bit.

As seen in Fig.3.1(c), the overall QPSK/8-PSK-encoded SIPM-OOFDM signal constellation is very similar to a conventional 16-QAM-encoded OOFDM signal constellation with its four corner points being removed. The similar minimum Euclidian distances between these two constellations lead to some transmission performance similarities between these two signals over various transmission systems. However, as each individual SIPM-OOFDM subcarrier is encoded (decoded) separately in the transmitter (receiver) utilizing a single modulation format at a time, SIPM-OOFDM is thus expected to have stronger immunity to various transmission system-induced noise in comparison with 16-QAM-encoded OOFDM. The aforementioned performance behaviours are confirmed in Section 3.4.

To decode the received signal in the receiver, the subcarrier power detection and threshold decision DSP functions located between the FFT and channel estimation and equalization first calculate the optimum power threshold for the subcarrier, by making use of a training sequence that is periodically inserted into the user data sequence in the transmitter. The subcarrier power threshold, $P_{threshold}$ is defined as:

$$P_{threshold} = \frac{P_{8\text{-}PSK} + P_{QPSK}}{2} \tag{3.1}$$

where $P_{8\text{-}PSK}$ and P_{QPSK} are the received powers of the same subcarrier encoded using 8-PSK and QPSK, respectively. The threshold obtained for each subcarrier of the same frequency, is averaged over time, and utilized to recover the information bit carried in the SIP

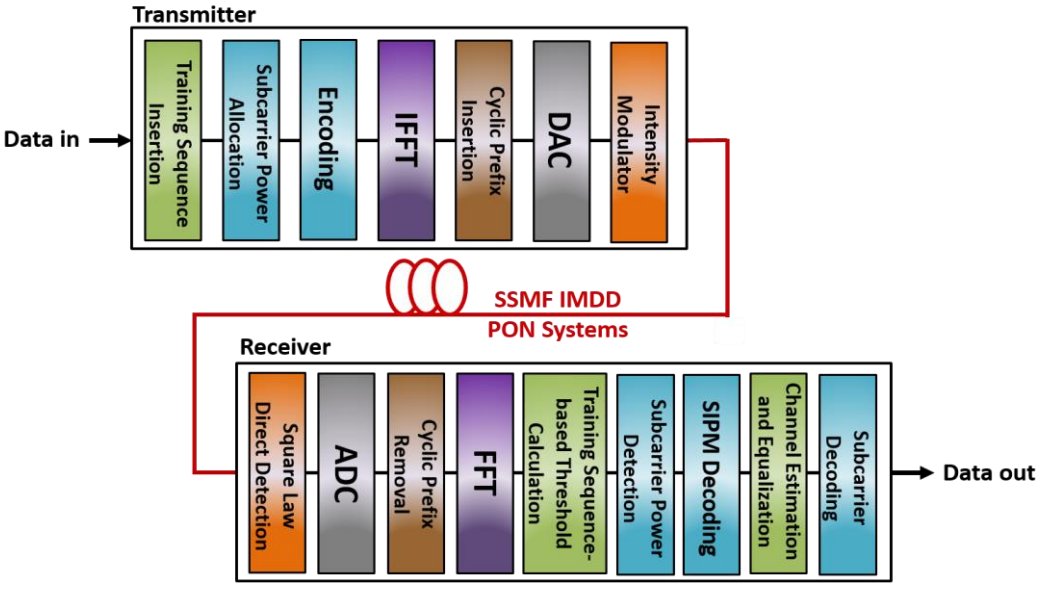

Fig.3.2. Schematic setup diagram of the considered SIPM-OOFDM IMDD PON transmission system

information-bearing dimension. In addition, the subcarrier power threshold is also employed to subsequently determine the signal modulation format taken on the subcarrier. After the subcarrier power decision is made, use is made of the same received training sequence to perform channel estimation and equalization before decoding the information bits taken on the subcarriers [7].

From the above description, it is easy to understand the following four aspects: a) SIPM-OOFDM does not require complicated and bandwidth-hungry transceiver negotiations to recover the information associated with the extra SIP dimension. b) For a representative system frequency response with a typical roll-off, the optimum subcarrier power threshold varies considerably with subcarrier index. c) For a given transmission system, there exists an optimum subcarrier power ratio between the 8-PSK-encoded subcarrier and the QPSK-encoded subcarrier of the same frequency. Such power ratio is independent of subcarrier index. Finally, d) similar to conventional OOFDM, both adaptive subcarrier power loading and standard OOFDM symbol synchronization [7] are still applicable and effective for SIPM-OOFDM.

3.3 Transceiver Parameter Optimization

The objective of this section is to identify the optimum SIPM-OOFDM transceiver parameters to maximize the transmission performance of the SIPM-OOFDM IMDD PON transmission system illustrated in Fig.3.2. As shown in this figure, the considered SIPM-OOFDM transceiver architecture is similar to that corresponding to conventional OOFDM [6, 7]. The signal generation procedure consists of the following major DSP functions: PRBS data generation, training sequence insertion, SIPM encoding, adaptive power loading, arrangement of all information-bearing subcarriers to satisfy the Hermitian symmetry with respect to their conjugate counterparts to ensure the generation of real-valued OFDM symbols after performing the IFFT, signal clipping, sample quantization and addition of cyclic prefix to each symbol. The corresponding receiver DSP functions includes: detection of the training sequence, cyclic prefix removal, FFT for generating complex-valued frequency domain subcarriers utilizing the received real-valued time domain symbols, subcarrier power detection, subcarrier power threshold calculation, demodulation of the information carried by the extra subcarrier index-power dimension, channel estimation and

equalization, demodulation of data-carrying subcarriers, and analysis of individual subcarrier BERs and overall channel BERs.

The widely adopted split-step Fourier method is used to model the propagation of optical signals over a SSMF. It is well known that for a sufficiently small fibre step length, this treatment yields an accurate approximation to the real fibre transmission effects. In simulations, the effects of linear loss, chromatic dispersion, and Kerr effect-induced optical power dependence of the refractive index are included [8].

To highlight the SIPM-OOFDM transmission performance over the IMDD PON systems, in the transmitter an ideal intensity modulator is adopted, which produces an optical field output signal, $S_O(t)$, having a waveform governed by:

$$S_O(t) = \sqrt{S_e(t)} \tag{3.2}$$

where $S_e(t)$ is the electrical driving current of the SIPM-OFDM signal with an optimum DC bias current being added. In the receiver, a PIN with a receiver sensitivity of -19dBm is also employed. Both shot noise and thermal noise are considered, which are simulated utilizing the procedures discussed previously in Section 2.6.2.

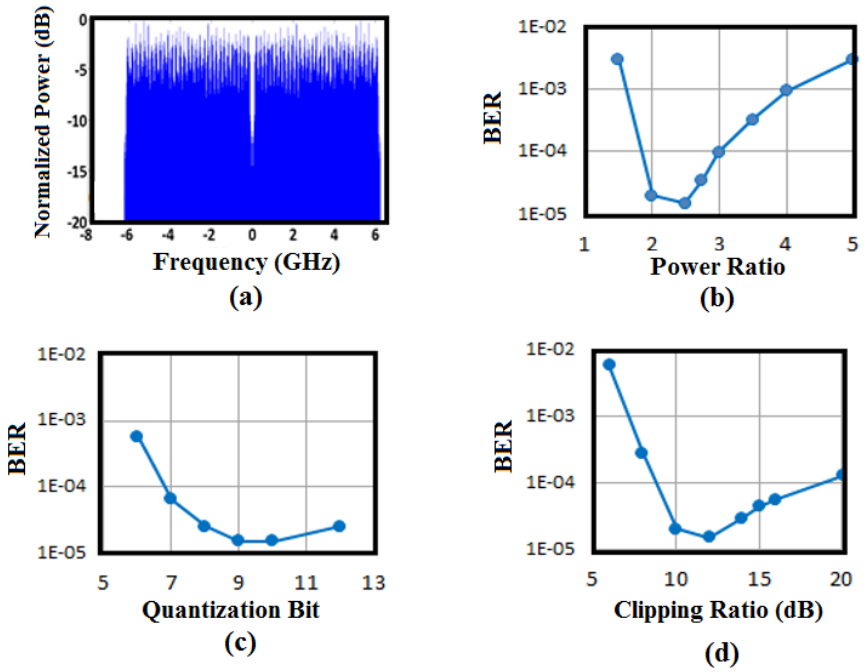

Fig.3.3. Overall BER performance against major transceiver parameters over 25km SSMF IMDD transmission systems when the optical launch power is fixed at -10dBm. (a) Representative spectrum of an electrical SIPM-OOFDM. (b) Overall BER versus power threshold. (c) Overall BER versus quantization bit. (d) Overall BER versus clipping ratio.

Over a 25km SSMF IMDD system with an optical launch power of -10dBm, numerical simulations are first undertaken to identify optimum SIPM-OOFDM transceiver parameters including clipping ratio, quantization bits and power ratio between the 8-PSK-encoded high power subcarrier and the QPSK-encoded low power subcarrier of the same frequency. In addition, a representative spectrum of an electrical SIPM-OOFDM signal prior to driving the ideal intensity modulator is also given in Fig.3.3(a). As a 12.5GS/s digital-to-analogue convertor (DAC)/analogue-to-digital convertor (ADC) is employed, the signal spectral bandwidth is thus 6.25GHz, and the subcarrier frequency spacing is approximately 195MHz. The simulated results are shown in Fig. 3.3(b), (c), and (d). In obtaining Fig.3.3(b), the power ratio is varied whilst the quantization bits and the clipping ratio are fixed at 9 bits and 12dB, respectively. In obtaining Fig.3.3(c), the quantization bits are varied, whilst the clipping ratio and power ratio are fixed at 12dB and 2.5, respectively. Finally, in obtaining Fig.3.3(d), the clipping ratio is varied whilst 9 quantization bits and a 2.5 power ratio are considered. The power ratio dependent BER performance is shown in Fig.3.3(b). When the power ratio is very low, QPSK and 8-PSK constellation points are too close to detect. This causes a high BER to occur. However, when the power ratio is very high, the 8-PSK constellation points are largely separated from the QPSK constellation points, this reduces the QPSK constellation sizes because the total electrical signal power is fixed. This causes a BER increase with increasing power ratio. As a direct result, as clearly seen in Fig.3.3(b), an optimum power ratio of 2.5 produces the lowest overall channel BER as the minimum Euclidian distance between two arbitrary points within each constellation are maximized.

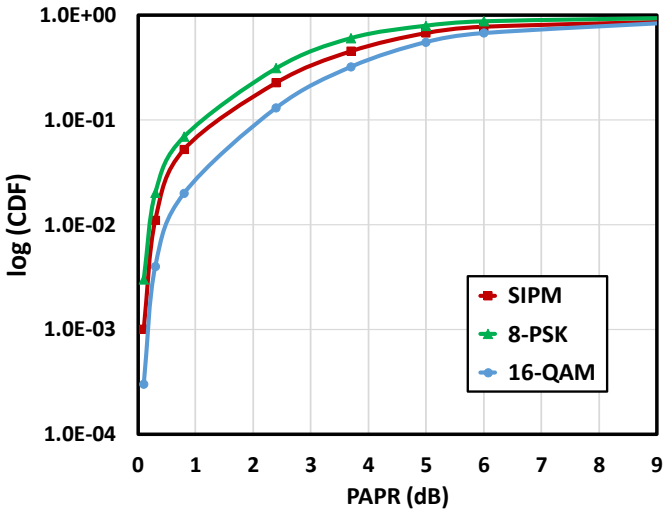

Fig.3.4. Cumulative distribution functions for SIPM-OOFDM and conventional OFDM using 8-PSK and 16-QAM

Table 3.1. *Transceiver and Transmission System Parameters*

Parameter	Value
Total number of IFFT/FFT points	64
Data-carrying subcarriers	31
Modulation formats for SIPM-OOFDM	QPSK or 8-PSK
PRBS data sequence length	400,000 bits
Cyclic prefix	25%
DAC & ADC sample rate	12.5GS/s
DAC & ADC bit resolution	9 bits
Clipping ratio	12 dB
Subcarrier power level ratio	2.5
PIN detector sensitivity	-19 dBm*
PIN responsivity	0.8 A/W
Effective noise bandwidth	6.25GHz
Q parameter	6
Boltzmann constant	1.38×10^{-23} J/K
Shot noise contribution	33%
Thermal noise contribution	66%
Fiber length	25km
SSMF dispersion parameter at 1550 nm	16 ps/(nm.km)
SSMF dispersion slope at 1550 nm	0.07 ps/nm/nm/km
Linear fiber attenuation	0.2 dB/km
Kerr coefficient	2.35×10^{-20} m²/W

*Corresponding to 10Gb/s non-return-to-zero data at a BER of 1.0×10^{-9}

Table 3.2. *Signal Bit Rate Comparisons*

Modulation Format	Signal Bit Rate (Gb/s)
QPSK	11.87
8-PSK	17.80
SIPM	20.77
16-QAM	23.73

It is seen in Fig.3.3(c) that a low quantization bit increases the quantization noise effect, thus leading to an increase in BER. Beyond the quantization bits of 9, the BER performance reaches its lowest value and remains at that value as expected. Similar to Fig.3.3(c), in Fig.3.3(d), a low clipping ratio leads to a high overall channel BER since the signal waveform is significantly clipped. The BER reaches its lowest value for a clipping ratio of 12dB, beyond which the BER increases with increasing clipping ratio because of the increased quantization noise effect. Furthermore, as shown in Fig.3.4, compared to both 8-PSK-encoded OFDM and 16-QAM-encoded OFDM cumulative distribution function (CDF) curves, SIPM-OOFDM' CDF curve exhibit an almost identical performance in terms of peak-to-average power ratio (PAPR). This indicates that the proposed technique does not alter the conventional OFDM tolerance in terms of PAPR.

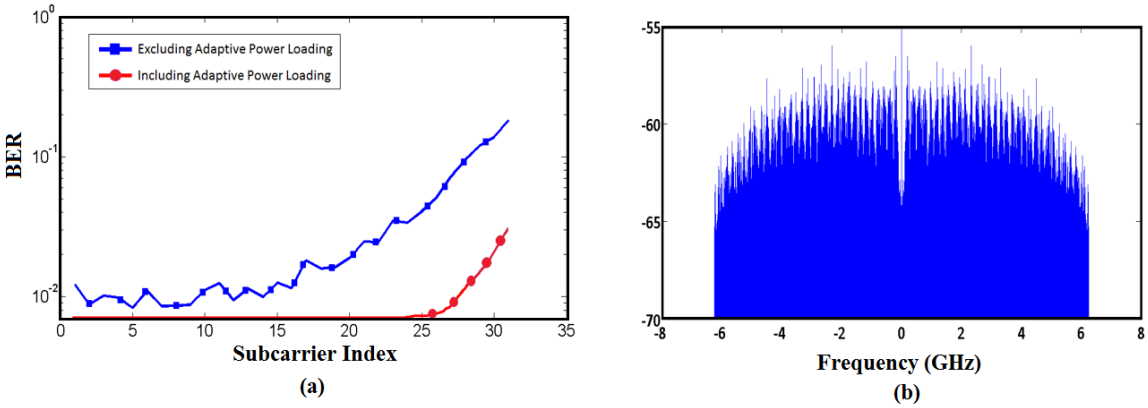

Fig.3.5. (a) SIPM-OOFDM subcarrier BER versus subcarrier index for including and excluding APL. (b) Optical SIPM-OOFDM signal spectrum excluding APL. In simulating (a) and (b), an 80km SSMF IMDD transmission system is considered and the optical launched power is fixed at -10dBm.

The major transceiver and transmission system parameters adopted in this chapter are listed in Table 3.1, where the 12dB signal clipping ratio, the DAC/ADC resolution of 9 bits and the 2.5 power ratio are also presented. Unless stated explicitly in the corresponding text, these parameters are adopted throughout this chapter. As seen in Table 3.2, these adopted transceiver and system parameters give rise to a SIPM-OOFDM signal bit rate of 20.77Gb/s, which significantly exceeds the 8-PSK-encoded OOFDM signal bit rate by approximately 17%, and almost doubles the signal bit rate of the 8-PSK-encoded SIM-OFDM (ESIM-OFDM and OFDM-IM) signal. This confirms the SIPM-OOFDM's ability of outperforming conventional SIM-OFDM, ESIM-OFDM, OFDM-IM and OOFDM.

Finally, it is also worth mentioning that, similar to conventional OOFDM, the utilization of APL in SIPM-OOFDM is also very effective in combating the channel fading effect associated with the IMDD transmission system, as presented in Fig.3.5(a). In obtaining this figure, an 80km SSMF IMDD transmission system is considered. As seen from the optical signal spectrum in Fig.3.5(b) after transmitting over the transmission conditions of Fig.3.5(b), the channel fading effect introduces a high transmission loss to a high frequency subcarrier. This brings about a reduced OSNR and subsequently a high BER for a high frequency subcarrier when APL is excluded. Whilst the adoption of APL enables the power of each individual subcarrier to be adaptively varied in the transmitter, i.e., a higher (lower) power is allocated to a higher (lower) frequency subcarrier with the total electrical signal power kept consistent. The APL-enabled excellent compensation of the channel fading effect not only considerably enhances the BER performances for the high frequency subcarriers but also simultaneously maintains the low frequency subcarrier BERs below an acceptable value. As a

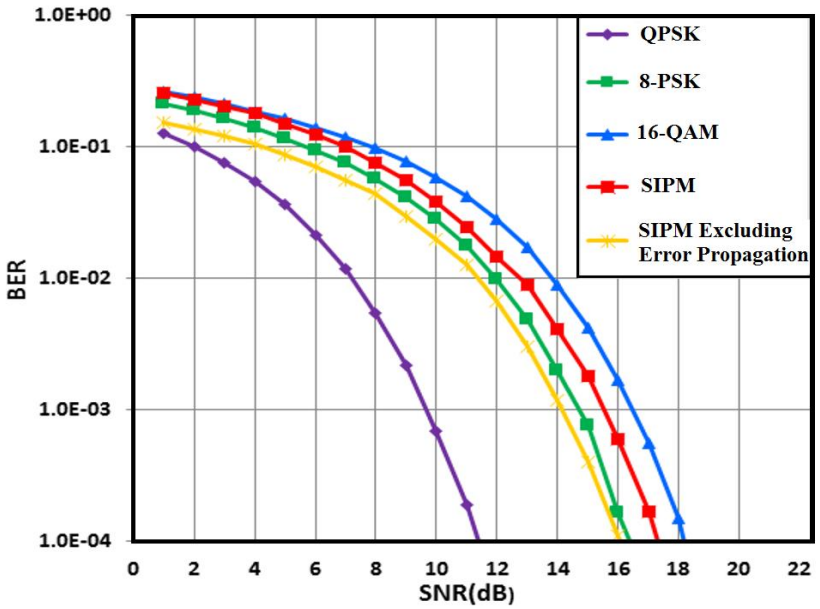

Fig.3.6. Overall channel BER versus electrical signal SNR over AWGN channels for conventional OFDM using QPSK, 8-PSK and 16-QAM, and SIPM-OOFDM for the cases of including and excluding the subcarrier-power error propagation.

direct result, the overall BER performance of the transmission system is considerably improved, as seen in Fig.3.5(a).

3.4 Transmission Performance

In this section, detailed numerical simulations are undertaken to investigate SIPM-OOFDM transmission performances over both additive white Gaussian noise (AWGN) channels and SSMF IMDD PON systems. In addition, performance comparisons between SIPM-OOFDM and conventional OOFDM using various signal modulation formats are also made to demonstrate the unique advantages associated with SIPM-OOFDM.

3.4.1 Performance over AWGN Channels

The impacts of subcarrier index-power modulation on minimum required electrical signal SNR over AWGN channels for achieving a specific BER are presented in Fig.3.6, where the BER performance comparisons are made between QPSK/8-PSK-encoded SIPM-OOFDM and conventional OFDM using QPSK, 8-PSK and 16-QAM. Fig.3.6 shows that SIPM-OOFDM has a BER developing trend very similar to 8-PSK-encoded conventional OFDM, and that, for achieving a BER of 1.0×10^{-3}, there exists a small SNR difference of

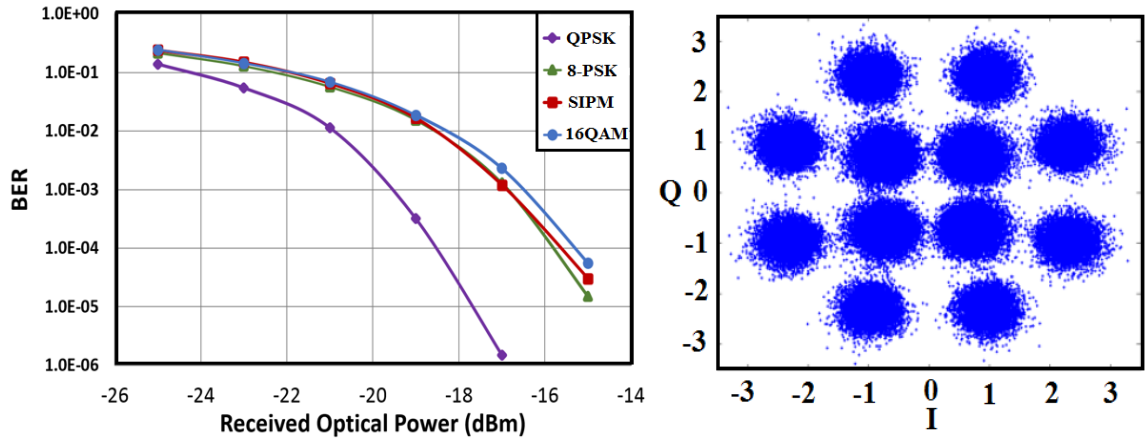

Fig.3.7. (a) Overall channel BER versus received optical power after transmitting through 25km SSMF IMDD PON systems for SIPM-OOFDM and conventional OOFDM using QPSK, 8-PSK and 16-QAM. (b) SIPM-OOFDM constellation.

approximately 0.9dB between SIPM-OOFDM and 8-PSK-encoded OFDM. This occurs mainly because of the combined effects of the SIPM-induced SNR gain and error propagation induced by wrong subcarrier power detections.

To distinguish the impact of the error propagation effect on the BER performance, a BER curve obtained by excluding the error propagation effect is also illustrated in Fig.3.6, in computing this curve, signal modulation formats taken on the subcarriers are first compared between the transmitter and receiver. A difference in signal modulation format indicates the occurrence of an error during subcarrier-power detection. When such error occurs, the corresponding bit conveyed by the extra subcarrier index-power dimension is removed, and also a random bit is added (removed) when a lower (higher) signal modulation format is detected in the receiver compared to the transmitter. It is shown in Fig.3.6 that, in comparison to conventional 8-PSK OFDM at a BER of 1.0×10^{-3}, the error propagation effect introduces an approximately 1.5dB SNR penalty, which is, however, offset by a 0.6dB SNR gain induced by SIPM, thus giving rise to an overall SNR penalty of 0.9dB. In addition, Fig.3.6 implies that the introduction of the extra SIP information-bearing dimension into OOFDM does not considerably compromise the signal SNR for AWGN channels.

3.4.2 Performance over SSMF IMDD PON Systems

In this subsection, we investigate the BER performance of 20.77Gb/s SIPM-OOFDM transmissions over 25km SSMF IMDD PON systems, the simulated results are shown in

Fig.3.7(a), where BER performances are also plotted for 17.8Gb/s 8-PSK OOFDM signals, 23.73Gb/s 16-QAM OOFDM signals and 11.87Gb/s QPSK OOFDM signals. In obtaining Fig.3.7(a), adaptive subcarrier power loading is applied and an optical power launched into the SSMF transmission system is fixed at -10dBm. As expected from Fig.3.6, Fig.3.7(a) shows that SIPM-OOFDM has an almost identical BER performance compared to 8-PSK OOFDM. This indicates that the extra information-bearing dimension-introduced 17% increase in signal bit rate does not alter the BER performance. Under the same transmission conditions of Fig.3.7(a), Fig3.7(b) illustrates representative SIPM-OOFDM constellations obtained after equalization at a BER of 1.0×10^{-3}.

From the discussions made in Fig.3.1(c), it is easy to understand that the minimum Euclidian distances for 8-PSK and squared 16-QAM constellations are similar. As a direct result, small differences in the BER curves occur between 8-PSK OOFDM and 16-QAM OOFDM, as seen in Fig.3.7. In addition, similar BER curves for SIPM-OOFDM and 16-QAM OOFDM are also observed in Fig.3.7. This, however, does not imply that 16-QAM OOFDM is preferable to SIPM-OOFDM because of the following three reasons: a) as presented in Fig.3.6, compared to 16-QAM OOFDM, SIPM-OOFDM introduces an approximately 2.4dB SNR gain at a BER of 1.0×10^{-3} when the error propagation effect is excluded. This indicates that SIPM-OOFDM can considerably improve the system power budget if the employed simple functions, for both subcarrier power detection and threshold calculation, are substituted by advanced ones. b) In SIPM-OOFDM, the subcarrier powers vary quickly from symbol to symbol. Based on discussions undertaken in wireless signal transmission systems in terms of utilizing SIM-OFDM to reduce the fast channel spectral variation effect [9-11], it is envisaged that SIPM may offer an effective approach in reducing modal noise associated with MMF transmission systems. Finally, c) the thrust of the chapter is to propose a novel technique utilizing the subcarrier index and power as an extra information-carrying dimension for OOFDM.

In addition to the present case where each individual subcarrier is just capable of carrying one extra information bit, the proposed technique can also be further extended by allocating multiple power levels to each individual subcarrier. Such extension results in not only each subcarrier conveying more extra information bits (>1), but also, multiple high signal modulation formats to be used simultaneously, thus significantly improved SIPM-OOFDM

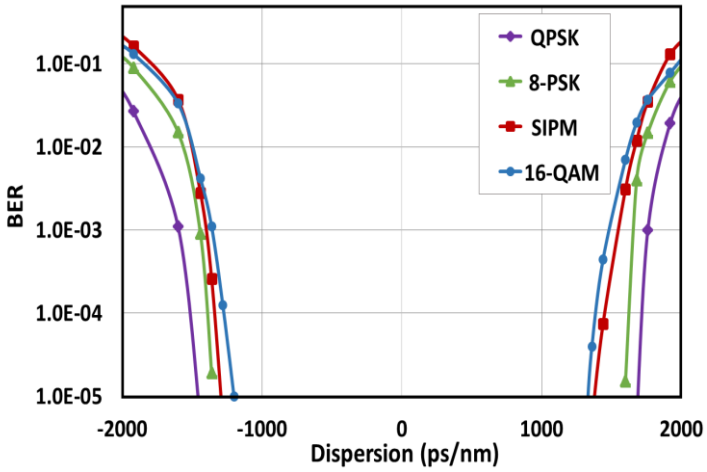

Fig.3.8. SIPM-OOFDM chromatic dispersion tolerance

signal bit rates are feasible. This approach is extensively explored in Chapter 5 in terms of signal transmission capacity and spectral efficiency.

3.4.3 Chromatic Dispersion Tolerance

Fig.3.8 demonstrates the fibre chromatic dispersion impact on the SIPM-OOFDM BER performance over SSMF IMDD PON systems. In simulating Fig.3.8, the Kerr-related fibre non-linearity and linear attenuation are disabled, and the optimum optical launch power is fixed at 5dBm. The adopted fibre dispersion parameters are -16 ps/(nm.km) and 16 ps/(nm.km) for the negative dispersion region and the positive dispersion region, respectively, whilst the transmission distance varies from 10km to 150km in each of the aforementioned regions. In addition, adaptive subcarrier power loading is also applied for all the cases considered. As expected, it is shown in Fig.3.8 that compared to conventional OOFDM using various signal modulation formats; SIPM-OOFDM does not considerably degrade the system tolerance to fibre chromatic dispersion since all these BER curves behave in a similar fashion.

3.4.4 Kerr-Related Fiber Nonlinearities Tolerance

The Kerr-related fibre nonlinearity impact on the SIPM-OOFDM transmission performance is investigated in Fig.3.9, where the transmission distance is fixed at 25km with all the fibre linear and Kerr-related non-linear effects being present. Once again, adaptive subcarrier

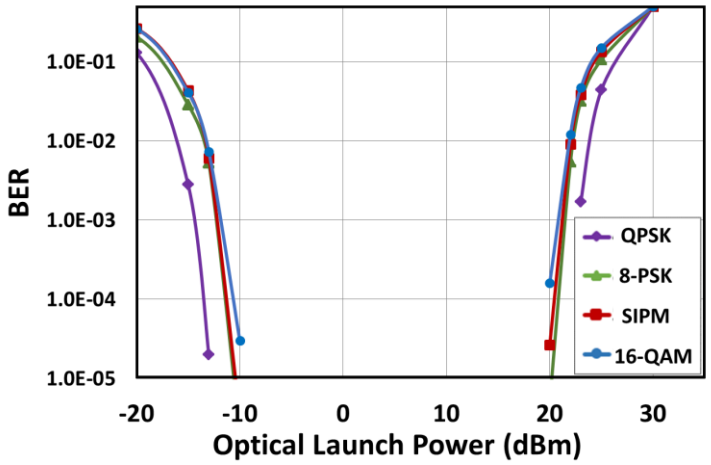

Fig.3.9. SIPM-OOFDM Kerr-related fibre nonlinearity tolerance

power loading is applied in the numerical simulations. It is shown in Fig.3.9 that for achieving a BER of 1.0×10^{-3}, almost identical optical launch power variation dynamic ranges of approximately 32dB are observed for both SIPM-OOFDM and conventional OOFDM using various signal modulation formats. This indicates that, compared to conventional OOFDM, SIPM-OOFDM does not degrade the system tolerance to Kerr-related fibre nonlinearity.

3.5 Conclusion

In this chapter, SIPM-OOFDM with an extra SIP information-bearing dimension has been proposed and investigated for the first time. Over SSMF IMDD PON systems, extensive numerical simulations have been undertaken of the SIPM-OOFDM performance characteristics to identify optimum values of key transceiver parameters affecting the maximum achievable SIPM-OOFDM performance, and to explore practically obtainable maximum transmission performances when QPSK (8-PSK) is considered for a low (high) power subcarrier. Results have shown that, compared to both conventional OOFDM and SIM-based OFDM techniques, SIPM-OOFDM offers an approximately 17% signal bit rate improvement over 25km SSMF IMDD PON systems without compromising minimum required OSNRs for achieving a specific BER and dispersion/nonlinearity tolerances as well as without increasing the transceiver DSP/architecture complexity.

References:

[1] R. Abu-alhiga and H. Haas, "Subcarrier-index modulation OFDM," *Proc. IEEE Int. Sym. Personal, Indoor Mobile Radio Commun.*, pp. 177–181, Sep. 2009.

[2] D. Tsonev, S. Sinanovic, and H. Haas, "Enhanced subcarrier index modulation (SIM) OFDM," *Proc. IEEE GLOBECOM Workshops*, pp. 728–732, Dec. 2011.

[3] E. Başar *et al.*, "Orthogonal frequency division multiplexing with index modulation," *IEEE Trans. Signal Process.*, vol. 61, no. 22, pp. 5536–5549, Nov. 2013.

[4] F. Halabi, L. Chen, S. Parre, S. Barthomeuf, R. P. Giddings, C. Aupetit-Berthelemot and J. M. Tang, "Subcarrier index-power modulated optical OFDM and its performance in IMDD PON systems," *J. Lightw. Technol.*, vol. 34, no. 9, pp. 2228–2234, May 2016.

[5] F. Halabi, L. Chen, S. Parre, S. Barthomeuf, R. P. Giddings, C. Aupetit-Berthelemot and J. M. Tang, "Subcarrier index-power modulated optical OFDM (SIPM-OOFDM) for IMDD PON systems,'' in *Proc. Optical Fibre Communication (OFC) Conference,* Th3C.1, pp.1-3, Mar. 2016.

[6] J. M. Tang, P. M. Lane, and K. A. Shore, "High-speed transmission of adaptively modulated optical OFDM signals over multimode fibers using directly modulated DFBs," *J. Lightw. Technol.*, vol.24, no.1, pp. 429–441, Jan. 2006.

[7] R. Giddings, ''Real-time digital signal processing for OFDM-base future optical access networks,'' *J. Lightw. Technol*., vol. 32, no.4, p.553, Feb. 2014.

[8] G. P. Agrawal, Fibre-Optic Communication Systems, 2nd ed. Hoboken, NJ, USA: *Wiley*, 1997.

[9] Y. Zhou, Y. Liu, and L. Guo, ''A novel polarization division multiplexing system employing polar-OFDM with subcarriers interlaced,'' *Int. Conf. on Opt. Commun. and Netw.*, pp. 1–3, Jul. 2015.

[10] T. Mori, T. Sakamoto, M. Wada, T. Yamamoto, and F. Yamamoto, ''Few-mode fibers supporting more than two LP modes for mode-division multiplexed transmission with MIMO DSP,'' *J. Lightw. Technol.*, vol.32, no.14, pp. 2468–2479, Jul. 2014.

[11] G. C. Papen and G. M. Murphy, "Modal noise in multimode fibres under restricted launch conditions," *J. Lightw. Technol*., vol. 17, no.5, pp. 817–822, May 1999.

4. SIPM-OOFDM with Superposition Multiplexing

4.1 Introduction

To improve the signal power usage efficiency of high level subcarriers in SIPM-OOFDM, this chapter introduces, for the first time, superposition multiplexing (SPM) in radio access networks [1] into SIPM-OOFDM leading to the proposition of a novel transmission technique, referred to as SIPM-OOFDM with SPM (SIPM-OOFDM-SPM) [2]. Compared to SIPM-OOFDM, for a high power subcarrier, SPM is employed to passively add two 8-PSK- and QPSK-encoded complex numbers, and the resulting sum is assigned to the high power subcarrier. Whilst for a low power subcarrier, similar to SIPM-OOFDM, only a single QPSK-encoded complex number is assigned to the subcarrier. Clearly, SIPM-OOFDM-SPM enables a more effective usage of high power subcarriers. In the SIPM-OOFDM-SPM receiver, instead of utilizing a sophisticated decoding algorithm [3, 4], a simple DSP algorithm is presented in Section 4.2.1, which is sufficient to recover the information conveyed by SPM-based high power subcarriers. For IMDD PON systems, it is shown that SIPM-OOFDM-SPM enables a 28.6% signal bit rate improvement compared to SIPM-OOFDM using the same signal modulation formats. In addition, in comparison with 32-PSK/QPSK-encoded SIPM-OOFDM capable of offering a signal bit rate identical to (8-PSK+QPSK)/QPSK-encoded SIPM-OOFDM-SPM, the proposed technique reduces the minimum required signal OSNR for achieving a specific BER and simultaneously improves the system tolerance to both chromatic dispersion and Kerr-related fiber nonlinearity.

Based on both SIPM-OOFDM and SIPM-OOFDM-SPM, a very interesting open question can be raised, as to whether SPM can also be employed in both low and high power subcarriers to further improve the signal power usage efficiency and the signal bit rate. As a direct result, an improved variant of SIPM-OOFDM-SPM known as SIPM-OOFDM with dual superposition multiplexing (SIPM-OOFDM-DSPM) is also proposed in this chapter [5, 6]. Compared with SIPM-OOFDM-SPM, the SIPM-OOFDM-DSPM encoding procedure on high power subcarriers remains unchanged, whereas SPM is applied on low power subcarriers as well by assigning the sum of BPSK- and QPSK-encoded complex numbers. Therefore, compared with both SIPM-OOFDM and SIPM-OOFDM-SPM, using similar signal modulation formats, the proposed technique enables an additional 43% and 11% increase in signal bit rate respectively with the transceiver DSP/hardware complexity still

preserved. Similar to SIPM-OOFDM-SPM, SIPM-OOFDM-DSPM also enhances the system power budget and simultaneously improves the system tolerance to both chromatic dispersion and Kerr-related fiber nonlinearity, compared with 32-PSK/8-PSK SIPM-OOFDM operating at the same signal bit rate. As these two techniques are technically very similar, this chapter is divided into two sections. Section 4.2 (Section 4.3) explores the SIPM-OOFDM-SPM (SIPM-OOFDM-DSPM) technique in terms of operating principle, identification of optimum transceiver design parameters and overall transmission performance over SSMF IMDD PON systems.

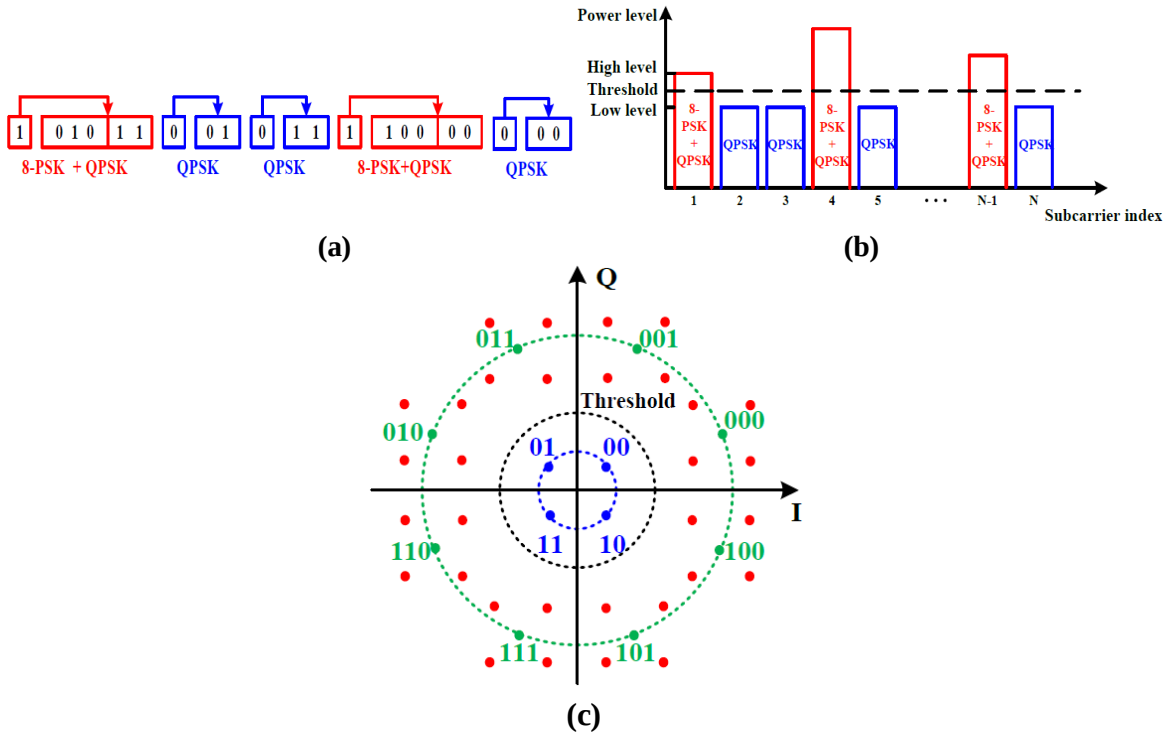

Fig.4.1. Bit allocations in the SIP dimension and corresponding bit-encoding for both low and high power subcarriers in the conventional subcarrier-information-carrying dimension, (b) Subcarrier power allocations and 8-PSK- and QPSK-encoding-based SPM operation for high power subcarriers, and (c) overall SIPM-OOFDM-SPM constellations for high and low power subcarriers.

4.2 SIPM-OOFDM-SPM

4.2.1 Operating Principle

As illustrated in Fig.4.1, the SIPM-OOFDM-SPM operating principle is similar SIPM-OOFDM [7, 8], except that, modifications should be made to relevant transceiver DSP

functions that deal with bit allocation/recovery in both the SIP information-bearing dimension and the conventional subcarrier-information-carrying dimension.

Fig. 4.1(a) shows the SIPM-OOFDM-SPM transmitter DSP procedures of how to allocate an information bit in the SIP dimension and how to subsequently encode information bits in the conventional subcarrier-information-carrying dimension. As an example, for an incoming PRBS stream, when a "1" bit is encountered, firstly the corresponding subcarrier is set at a high power level, and then further 5 bits from the PRBS stream are truncated, of which the first 3 bits are encoded using 8-PSK, and the remaining 2 bits are encoded using QPSK. After that, these two 8-PSK- and QPSK-encoded complex numbers are passively added together. Such an addition operation is referred to as SPM. Finally the resulting complex number is assigned to the high power subcarrier, as seen in Fig.4.1(b). Whilst when a "0" bit is encountered, the corresponding subcarrier is taken at a low power level, and further 2 bits following the "0" bit of the PRBS stream are encoded using QPSK. The QPSK-encoded complex number is assigned to the low power subcarrier, as shown in Fig.4.1(a) and Fig.4.1(b).

From the above description, it is easy to understand the following two aspects: i) a high (low) power subcarrier is capable of conveying 6(3) information bits in total; and ii) for a high power subcarrier, 8-PSK- and QPSK-encoding-based SPM operation produces four information-carrying satellite constellation points surrounding each virtual 8-PSK constellation point, as shown in Fig.4.1(c). This gives rise to total 32 information-carrying satellite constellation points, each of which represents a specific combination of a virtual 8-PSK constellation point and a virtual QPSK constellation point. These two aspects imply that 8-PSK- and QPSK-encoded SIPM-OOFDM-SPM supports a signal bit rate identical to SIPM-OOFDM encoded using 32-PSK and QPSK. The low-order signal modulation formats employed in SIPM-OOFDM-SPM increase the minimum Euclidean distance, thus resulting in a number of performance advantages over 32-PSK/QPSK-encoded SIPM-OOFDM, as discussed in detail in Section 4.2.2.

In the receiver, after FFT and standard training sequence-based channel estimation and channel equalization, the subcarrier power threshold, $P_{threshold}$, which distinguishes the received power of each individual subcarrier between the low level and high level, can be calculated using the formula expressed below:

$$P_{threshold} = \frac{min(P_{8\text{-}PSK+QPSK}) + P_{QPSK}}{2} \quad (4.1)$$

where $P_{8\text{-}PSK+QPSK}$ and P_{QPSK} are the received high and low subcarrier powers after equalization, respectively. It can be seen in Fig.4.1(c) that, as a direct result of SPM operation, $P_{8\text{-}PSK+QPSK}$ varies slightly from subcarrier (symbol) to subcarrier (symbol). To sufficiently enlarge the difference between $P_{8\text{-}PSK+QPSK}$ and P_{QPSK}, minimum $P_{8\text{-}PSK+QPSK}$ values are thus considered in Eq.(4.1). In addition, to effectively reduce the impact of random noises on $P_{threshold}$, the subcarrier power threshold is averaged periodically over many different training sequences. If the received power level of an information-bearing subcarrier is above (below), $P_{threshold}$, a "1" ("0") information bit carried in the SIP dimension is thus recovered, and the information conveyed in the conventional subcarrier-information-carrying dimension can also be decoded using the approach presented below. It should also be noted that an incorrect subcarrier power decision causes errors to occur in both the SIP dimension and the conventional subcarrier-information-carrying dimension. Such errors, however, do not propagate across different subcarriers and symbols.

As the DSP process adopted for decoding low power subcarriers is identical to that used in SIPM-OOFDM [7, 8], here attention is thus focused on the high power subcarrier decoding process. For a high power subcarrier, the received complex value after equalization can be written as:

$$C_R^E = C_4^* + C_8^* + \Delta C_4 + \Delta C_8 \quad (4.2)$$

where C_4^* and C_8^* represent the ideal "to be recovered" constellation points for QPSK and 8-PSK, respectively. ΔC_4 and ΔC_8 represent the differences between their actual received constellation point and their ideal constellation point. ΔC_4 and ΔC_8 arise due to the following three physical mechanisms including channel noise, nonlinear coupling, and nonlinear channel frequency response. To recover the information carried by each high power subcarrier, 32 comparisons between C_R^E and all 32 possible combinations of ideal "to be recovered" C_{4i}^* (i=1,2,3,4) and ideal "to be recovered" C_{8j}^* (j=1,2,…,8) are made, of which the combination gives rise to a minimum $|\Delta C_4|^2 + |\Delta C_8|^2$ is used to recover the information conveyed by the high power subcarrier.

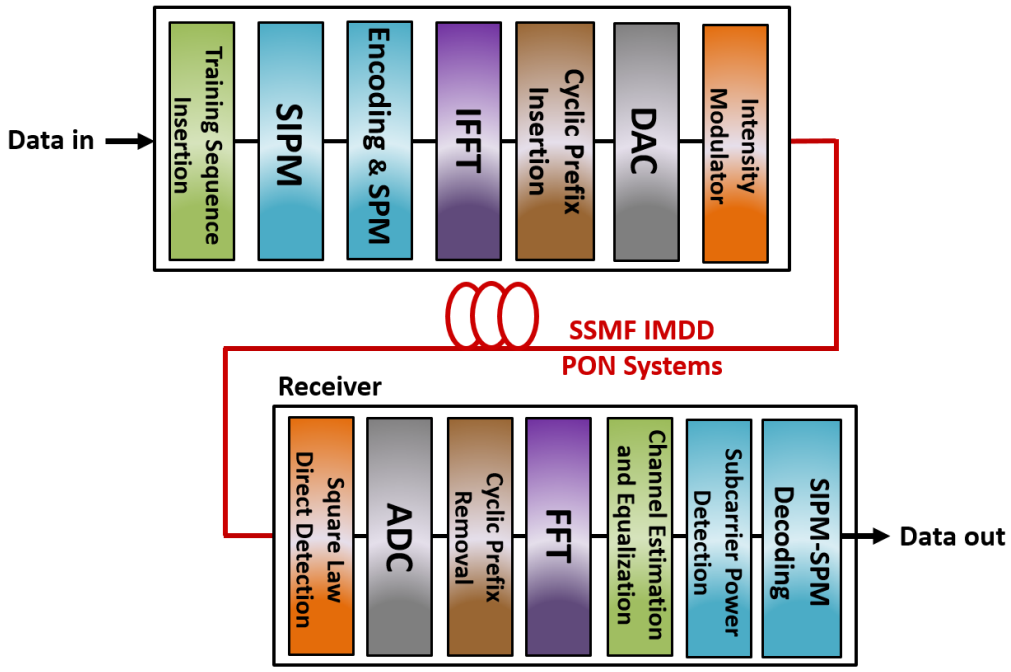

Fig.4.2. Schematic illustration of the SIPM-OOFDM-SPM transceiver architecture and the considered IMDD PON system.

By making use of the above-discussed SIPM-OOFDM-SPM operating principle, the relevant transceiver DSP architecture can be produced, which is schematically shown in Fig.4.2. Due to the DSP transceiver architecture similarity between SIPM-OOFDM-SPM, SIPM-OOFDM and conventional OOFDM [9], the general DSP procedures implemented in the SIPM-OOFDM-SPM are the same as SIPM-OOFDM except for the encoding and decoding DSP functions. Also similar to SIPM-OOFDM, an ideal intensity modulator, based on Eq. (3.2), is adopted in the transmitter. In addition, the SSMF simulation model based on the widely adopted split-step Fourier method is also used to model the propagation of an optical signal over IMDD PON systems where the effects of linear loss, chromatic dispersion and Kerr effect-induced optical power dependence of the refractive index are included [10].

4.2.2 Transceiver Parameter Optimization

Having discussed the general SIPM-OOFDM-SPM operating principle in the previous section, in this section, detailed numerical simulations are undertaken to identify optimum key transceiver design parameters. Throughout this chapter, the default transceiver parameters undertaken are listed in Table 4.1. Moreover, to clearly distinguish the advantages associated with the proposed technique, comparisons are always made between SIPM-OOFDM-SPM, 8-PSK/QPSK-encoded SIPM-OOFDM [7, 8] and 32-PSK/QPSK-encoded SIPM-OOFDM for all cases presented in both Section 4.2.2 and Section 4.2.3.

Table 4.1. *Transceiver and Transmission System Parameters*

Parameter	Value
Total number of IFFT/FFT points	64
Data-carrying subcarriers	31
Modulation formats for SIPM-OOFDM	QPSK or 8-PSK
PRBS data sequence length	400,000 bits
Cyclic prefix	25%
DAC & ADC sample rate	12.5GS/s
DAC & ADC bit resolution	9 bits
Clipping ratio	12 dB
PIN detector sensitivity	-19 dBm*
PIN responsivity	0.8 A/W
Fiber length	25km
SSMF dispersion parameter at 1550 nm	16 ps/(nm.km)
SSMF dispersion slope at 1550 nm	0.07 ps/nm/nm/km
Linear fiber attenuation	0.2 dB/km
Kerr coefficient	2.35×10^{-20} m²/W

*Corresponding to 10Gb/s non-return-to-zero data at a BER of 1.0×10^{-9}

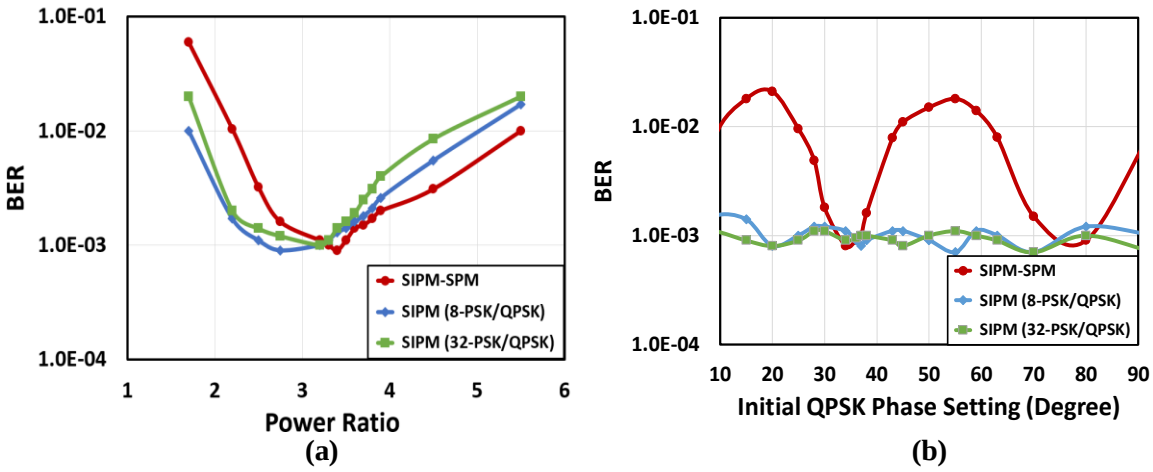

Fig.4.3. Optimum transceiver operation-parameter identifications for different transmission techniques. (a) Optimum power ratio. (b) Optimum initial QPSK phase setting with respect to 8-PSK. The AWGN channels are considered. The signal clipping ratio and quantization bits are fixed at 12dB and 9 bits, respectively.

Fig.4.3 explores the optimum transceiver operation parameters closely related to two salient features of the proposed technique, i.e., subcarrier index-power modulation (SIPM) and SPM operation. As the power ratio, which is defined as the ratio between the high power subcarrier and the low power subcarrier in the transmitter, plays a key role in the SIPM operation, Fig. 4.3(a) explores its impact on the transceiver BER performance to identify its optimum value. Whilst Fig. 4.3(b) reveals the optimum QPSK initial phase setting with respect to 8-PSK prior to the SPM operation. In obtaining Fig.4.3, AWGN channels are considered and the SNR values are fixed at 19dB. To highlight the impact of these inherent SIPM-OOFDM-SPM

features on the transceiver BER performance. The signal clipping ratio and DAC/ADC quantization bits are fixed at 12dB and 9 bits, respectively.

It is shown in Fig. 4.3(a) that SIPM-OOFDM-SPM has an optimum power ratio of 3.4, which is similar to those corresponding to other two transmission techniques. For power ratios lower than 3.4, the BER shoots up with decreasing power ratio, mainly resulting from the fast reduction in the minimum Euclidean distance of the SPM-generated 32-point constellation carried by the high power subcarriers. On the other hand, for power ratios larger than 3.4, the BER grows relatively slowly with increasing power ratio, this is because the fixed electrical power-induced slow reduction in the minimum Euclidean distance of the 4-points QPSK constellation carried by the low power subcarriers. It is easy to understand from Fig.4.1(c) that a phase rotation of QPSK with respect to 8-PSK alters the SPM-generated 32-point constellation and thus its minimum Euclidean distance. Such statement is verified in Fig.4.3 (b), where a periodic BER developing curve occurs for SIPM-OOFDM-SPM only, and the BER curves for the other two SPM-free transmission techniques remain almost constant. In Fig. 4.3(b), with respect to 8-PSK, an optimum initial QPSK phase setting of 34° is observed, corresponding to which the minimum Euclidean distance of the SPM-generated 32-point constellation is maximized. The observed difference of 45° between two consecutive optimum QPSK phase settings is determined by the phase difference between two consecutive 8-PSK constellation points. Fig.4.3(b) suggests that the SPM operation may offer a simple and effective approach of independently manipulating a feature of a signal constellation to satisfy a specific application without affecting the overall signal performance.

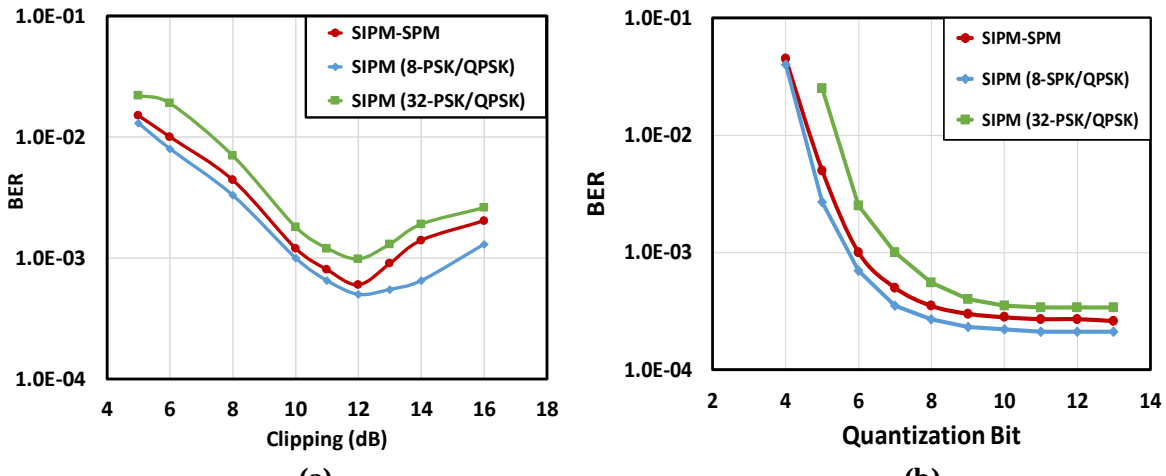

Fig.4.4. Overall BER performances against major DAC/ADC parameters over AWGN channels for three different transmission techniques. (a) BER versus clipping ratio where the quantization bits are fixed at 9. (b) BER versus quantization bit where the clipping ratio is fixed at 12dB.

To identify the optimum transceiver design parameters closely related to the most critical components, i.e., DACs/ADCs, Fig.4.4 is presented. The impacts of clipping ratio and quantization bit on the transceiver BER performance over AWGN channels are plotted in Fig. 4.4(a), with fixed quantization bits of 9, and in Fig. 4.4(b), with fixed clipping ratios of 12dB, respectively. In simulating Fig.4.4, use is also made of simulation parameters similar to those adopted in Fig.4.3. In particular, an SNR value of 19dB is considered and the optimum power ratio of 3.4 is taken along with an optimum initial QPSK phase setting of 34º. It can be seen in Fig. 4.4(a) that, for all the considered transmission techniques, their BERs reach the lowest values at clipping ratios of 12dB. For clipping ratios of lower than 12dB, the considerable BER growth with decreasing clipping ratio is due to strong clipping-induced serious distortions to signal waveforms. Whilst for clipping ratios beyond 12dB, the increase in BER is because of the enhanced quantization noise effect associated with increased dynamic ranges. Based on Fig.4.4(a), it is easy to understand the existence of minimum quantization bits of 9 for all transmission techniques in Fig. 4.4(b). It is shown in Fig. 4.4(b) that, for low quantization bits of <9, the BER increases quickly due to the low quantization bit-induced enhancement in the quantization noise effect. Whilst for quantization bits of >9, the quantization noise effect is almost negligible, thus giving rise to almost flattened BER developing trends in Fig.4.4(b).

4.2.3 Transmission Performance

The thrust of this section is to utilize the optimum transceiver parameters identified in Section 4.2.2 to explore achievable SIPM-OOFDM-SPM transmission performances over both AWGN and IMDD PON systems. For computing the performance characteristics of these three techniques, the same default parameters listed in Table 4.1 are also considered in this section.

Table 4.2. *Signal Bit Rate Comparisons*

Modulation Format	Signal Bit Rate (Gb/s)
SIPM (8-PSK/QPSK)	20.77
SIPM-SPM	26.71
SIPM (32-PSK/QPSK)	26.71

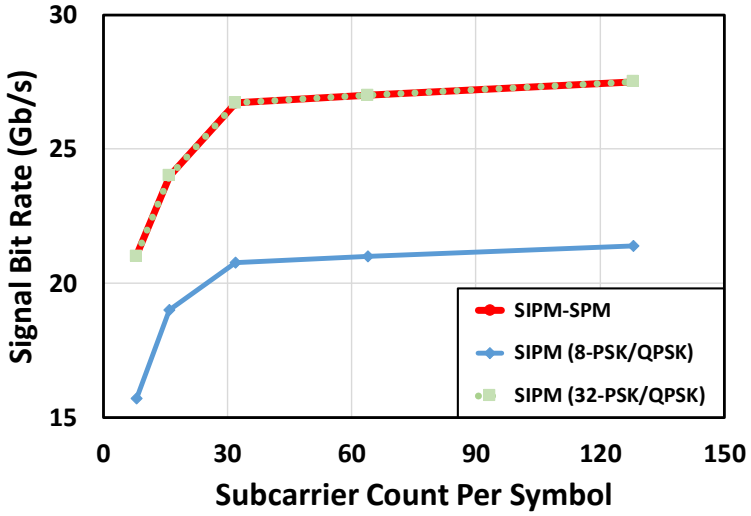

Fig.4.5. Subcarrier count-dependent signal bit rates for three transmission techniques considered. The AWGN channels are considered and the SNRs of all signals are fixed at 19dB.

4.2.3.1 Signal Bit Rate

The signal bit rates of SIPM-OOFDM-SPM, 8-PSK/QPSK-encoded SIPM-OOFDM and 32-PSK/QPSK-encoded SIPM-OOFDM are summarized in Table 4.2. It can be seen in this table that SIPM-OOFDM-SPM supports a signal bit rate of 26.71Gb/s, which exceeds 8-PSK/QPSK-encoded SIPM-OOFDM by 28.6%. Although 32-PSK/QPSK-encoded SIPM-OOFDM is capable of offering the same signal bit rate of 26.71Gb/s, it, however, suffers high OSNR and degraded tolerance to both chromatic dispersion and fiber nonlinearity, as analysed below in detail.

Based on the above-discussed SIPM-OOFDM-SPM operating principle, the SIPM-OOFDM-SPM signal bit rate, R_b, can be expressed as:

$$R_b = \frac{f_s[\rho_H(b_H+1)+\rho_L(b_L+1)]((N/2)-1)}{N(1+\sigma)} \tag{4.3}$$

where f_s is the DAC/ADC sampling rate, ρ_H and ρ_L ($\rho_H + \rho_L = 1$), are the occurrence probabilities of high and low power subcarriers within a symbol. b_H and b_L are the number of information bits carried by the high and low power subcarriers, respectively. N is the total number of subcarrier per symbol, and σ is the coefficient introduced to take into account signal bit rate reductions due to cyclic prefix and training sequence. Eq.(4.3) implies that the SIPM-OOFDM-SPM signal bit is subcarrier count-dependent.

The above analytical prediction is confirmed by numerically simulated results presented in Fig.4.5, where the signal bit rates of these three transmission techniques are plotted as a function of subcarrier count per symbol. Once again, in obtaining Fig.4.5, AWGN channels are considered and the SNRs of three corresponding signals are fixed at 19dB. Fig.4.5 shows the predicted subcarrier count-dependent behaviours, which become more pronounced when the total number of subcarriers is less than 64. In addition, an almost perfect signal bit rate overlap between SIPM-OOFDM-SPM and 32-PSK/QPSK-encoded SIPM-OOFDM is also observed in this figure, indicating that, instead of SPM, SIPM is the major physical mechanism underpinning such behaviour. It should be noted that the subcarrier count-dependent signal bit rate is in sharp contrast to conventional OOFDM.

4.2.3.2 Performance over AWGN Channels

The BER versus electrical SNR performances of the three considered transmission techniques over AWGN channels are presented in Fig.4.6. To explicitly distinguish the influence of the error propagation effect on signal SNR, an error propagation-free SIPM-OOFDM-SPM BER curve is also computed and subsequently plotted in Fig.4.6 by employing the error propagation removal approach described in the previous chapter. By comparing the BER curves between SIPM-OOFDM-SPM, 32-PSK/QPSK-encoded SIPM-OOFDM and error propagation-free SIPM-OOFDM-SPM it is very interesting to note that SPM gives rise to an approximately 3dB SNR gain at a BER of 1.0×10^{-3}, which is, however, offset by an

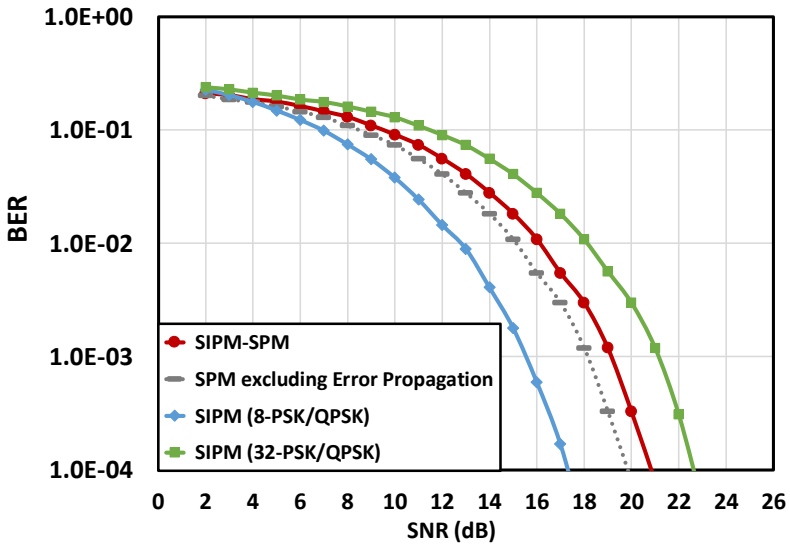

Fig.4.6. BER versus electrical SNR performances of three transmission techniques over AWGN channels. An error propagation-free SIPM-OOFDM-SPM BER curve is also shown.

proximately 1dB SNR penalty introduced by the error propagation effect, thus leading to an overall SNR gain of 2dB. The physical origin of the SNR gain is mainly due to the SPM-induced increase in the minimum Euclidean distance of the SPM-generated 32-point constellation. In addition, the 1dB error propagation-induced SNR penalty for SIPM-OOFDM-SPM is almost identical to that corresponding to 8-PSK/QPSK-encoded SIPM-OOFDM observed in the previous chapter at Section 3.4.1, this suggests that SPM does not contribute to the error propagation effect, and that the error propagation effect is independent of signal modulation formats taken on the subcarriers. This conclusion is valuable when more sophisticated SPM operations employing high-order signal modulation formats are applied to provide desired performances for specific application scenarios.

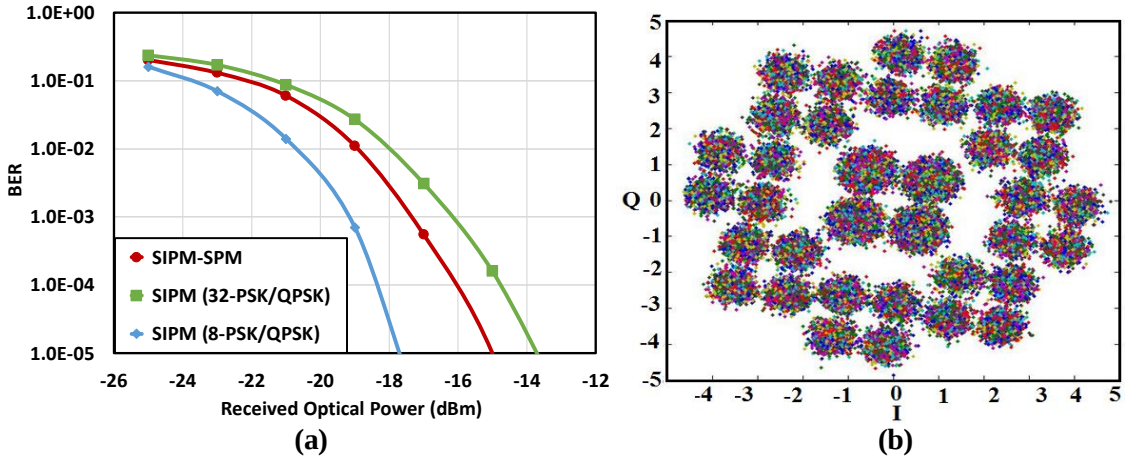

Fig.4.7. (a) BER as a function of received optical power of the three transmission techniques after transmitting through 25km SSMF IMDD PON. (b) SIPM-OOFDM-SPM Constellation.

4.2.3.3 Performance over SSMF IMDD PON Systems

The BER versus received optical power performances of the considered three transmission techniques are given in Fig.4.7(a) after transmitting through 25km SSMF IMDD PON systems. For all the cases, the optical launch powers are taken to be 5dBm. As expected from Fig.4.6, Fig.4.7(a) shows that SIPM-OOFDM-SPM can support 26.71Gb/s signal bit rates over 25km SSMF IMDD PON systems. On the contrary, when SIPM-OOFDM is applied, to achieve the same signal bit rate, high-order signal modulation formats such as 32-PSK/QPSK have to be adopted, which, however, cause an approximately 1dB optical power penalty at a BER of 1.0×10^{-3}, as seen in Fig.4.7(a). Such an optical power penalty agrees very well with the corresponding electrical SNR penalty observed in Fig.4.6. Given the fact that SSMF IMDD systems suffer from the channel fading effect, thus it is envisaged that a considerable improvement in SIPM-OOFDM-SPM transmission performance is achievable when use is

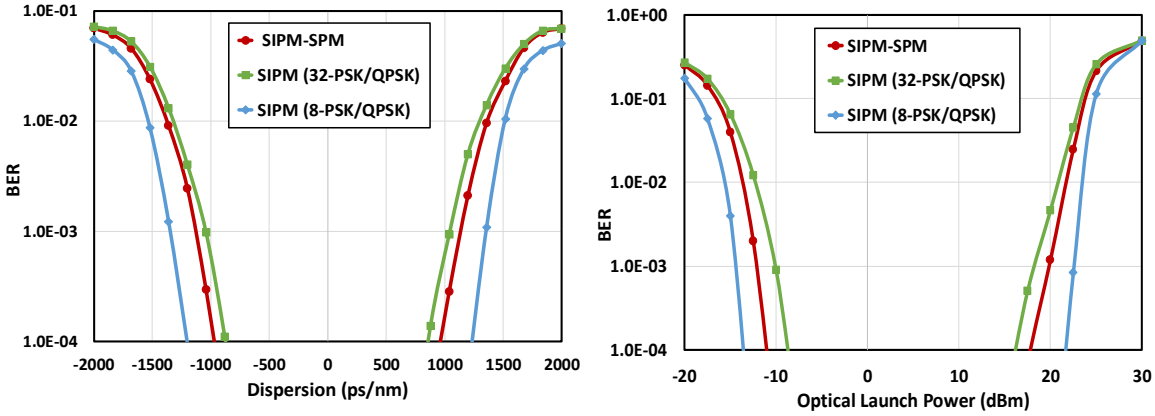

Fig.4.8. Performance tolerance of the three transmission techniques after transmitting through SSMF IMDD PON towards (a) chromatic dispersion and (b) fiber nonlinearity.

made of the well-known adaptive subcarrier power loading technique as discussed in Chapter 3 [7]. Under the same transmission conditions of Fig.4.7(a), Fig.4.7(b) illustrates representative SIPM-OOFDM-SPM constellations obtained after equalization at a BER of 1.0×10^{-3}.

The reduction in received optical power can be directly transferred to the optical link power budget improvement. Such improvement can also be utilized to improve the SIPM-OOFDM-SPM transmission tolerance to both chromatic dispersion and fiber nonlinearity associated with the IMDD PON systems. This is numerically verified in Fig.4.8(a) and Fig.4.8(b). In Fig.4.8(a), the BERs of these three considered transmission techniques are plotted as a function of chromatic dispersion of the IMDD PON systems. In simulating this figure, various SSMF lengths ranging from 10km to 125km are taken, and the optical launch powers are fixed at 5dBm. In addition, the Kerr-related fiber nonlinearity and fiber linear attenuation are disabled. The fiber dispersion parameters of -16.0ps/(km·nm) and 16.0ps/(km·nm) are used to represent the negative and positive chromatic dispersion regions, respectively. As shown in Fig.4.8(a), in comparison with the 26.71Gb/s 32-PSK/QPSK-encoded SIPM-OOFDM signal, an increase in dispersion tolerance range of approximately 130ps/nm at a BER of 1.0×10^{-3} is feasible for the SIPM-OOFDM-SPM signal operating at the same signal bit rate.

For the 26.71Gb/s SIPM-OOFDM-SPM signal, 20.77Gb/s 8-PSK/QPSK-encoded SIPM-OOFDM signal and 26.71Gb/s 32-PSK/QPSK-encoded SIPM-OOFDM signal, their performance tolerances to fiber nonlinearity of the 25km SSMF IMDD PON systems are explored in Fig.4.8(b). In this figure, the BERs of these signals are plotted as a function of optical launch power, by taking into account simulation parameters identical to Fig.4.7(a). Here all the fiber linear and nonlinear effects are present. As expected, Fig.4.8(b) shows that, compared to 32-PSK/QPSK-encoded SIPM-OOFDM, SIPM-OOFDM-SPM enhances the optical launch power dynamic range by approximately 3dB at a BER of 1.0×10^{-3}. This indicates that SIPM-OOFDM-SPM improves system performance tolerance to fiber nonlinearity.

4.3 SIPM-OOFDM-DSPM

Having extensively investigated the SIPM-OOFDM-SPM transmission technique, in this section attention is shifted towards SIPM-OOFDM-DSPM where detailed description and numerical simulations are provided to show the key differences and unique benefits of SIPM-OOFDM-DSPM over SIPM-OOFDM-SPM.

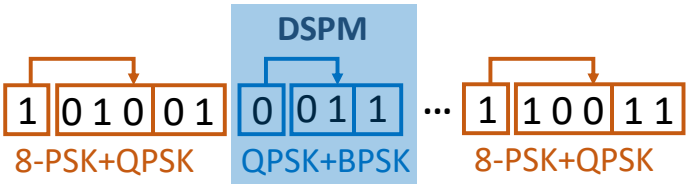

Fig.4.9. SIPM-OOFDM-DSPM data encoding in the transmitter

4.3.1 Operating Principle and Transceiver Architecture

In SIPM-OOFDM-DSPM, the encoding process is similar to SIPMOOFDM-SPM, where for an incoming PRBS, when a ‘‘1’’ bit is encountered, the SPM operation is applied and the corresponding subcarrier is set at a high power level, as illustrated in Fig.4.9, and the following 5 bits from the PRBS are truncated, of which 3 are encoded using 8-PSK and the remaining 2 bits are encoded using QPSK. Afterwards, these two 8-PSK- and QPSK-encoded complex numbers are added together. On the other hand, when a ‘‘0’’ bit is encountered, the

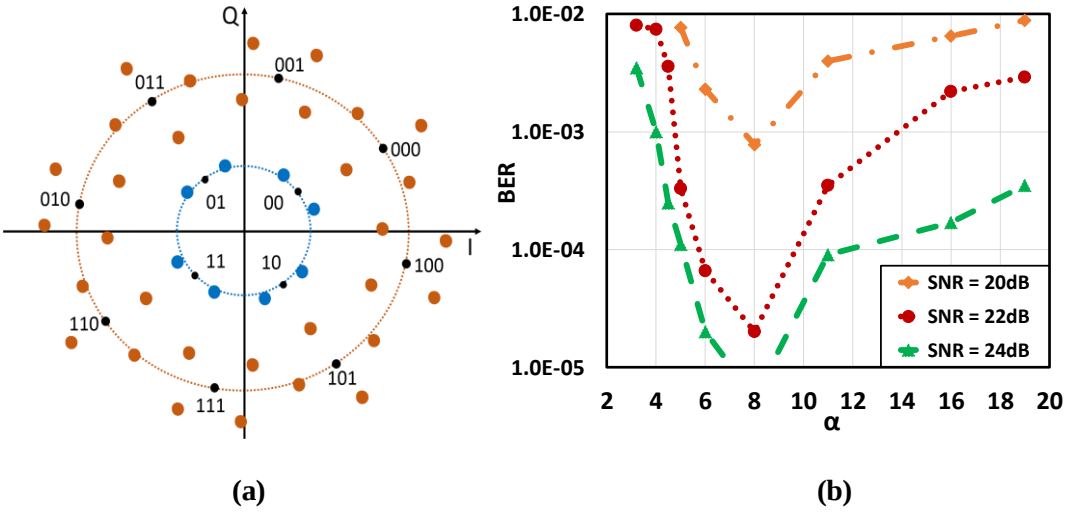

Fig.4.10. (a) Ideal SIPM-OOFDM-DSPM constellation. (b) Overall channel BER versus α over AWGN channels with the SNR values varying from 20dB to 24dB.

corresponding subcarrier is set at a low power level and the following 3 bits from the sequence are truncated, of which 2 bits are encoded using QPSK, and the remaining bit is encoded using BPSK. The SPM operation is then performed again by adding these two QPSK- and BPSK-encoded complex numbers together; the resulting sum is subsequently assigned to the low power subcarrier, as illustrated in Fig.4.9. The ideal SIPM-OOFDM-DSPM constellation is presented in Fig. 4.10(a) in which, for high (low) power subcarriers encoded using 8-PSK- (QPSK) and QPSK (BPSK), DSPM produces four (two) information-carrying satellite constellation points surrounding each virtual 8-PSK (QPSK) point as in SIPM-OOFDM-SPM. This gives rise to a total of 32 (8) information-carrying satellite constellation points for high (low) power subcarriers. This indicates that SIPM-OOFDM-DSPM uses low signal modulation formats including 8-PSK, QPSK and BPSK to achieve a signal bit rate identical to SIPM-OOFDM encoded using higher signal modulation formats such as 32-PSK and 8-PSK. It is worth mentioning that SIPM-OOFDM-DSPM can be implemented using any signal modulation formats with circular constellations.

It should be noted that since the QPSK modulation format is used on two subcarrier power levels, the optimum 34° QPSK (BPSK) initial phase setting with respect to 8-PSK (QPSK) described in Section 4.2.2 is still applicable in SIPM-OOFDM-DSPM for all subcarriers. Moreover, as illustrated in Fig. 4.10(a), a phase rotation of ±90° should be applied to the BPSK constellation points which are superposed with either the ‘01’ or ‘10’ encoded-QPSK point in order to maximize the difference between two subcarrier power levels. As a result,

the overall constellation for low power level subcarriers is very similar to 8-PSK, but this offers additional transmission performance advantages, as discussed later in Section 4.3.2. To optimize the SIPM-OOFDM-DSPM transceiver parameters, a parameter α is introduced, which represents the ratio between high subcarrier powers and low subcarrier powers. For a fixed total electrical signal power, Fig.4.10(b) is plotted to investigate the α-impact on the system BER performance. In simulating this figure, AWGN channels are considered with three SNR values varying from 20dB to 24dB. It is shown in Fig.4.10(b) that the lowest BER is obtainable when α is approximately 8, and that the optimum α value is SNR-independent. For α values lower than 8, the BER rises sharply, this results from the fast decrease in the subcarrier power difference between the high and low power subcarriers, whereas, when α exceeds 8, a relatively slow rise in BER is observed due to the reduction in the minimum Euclidean distance of the 8-point constellation taken on the low power subcarriers.

To decode the received signal in the receiver, the subcarrier power detection and threshold decision DSP functions detailed in Section 4.2.1 are still employable for this technique where, after the FFT and standard training sequence-based channel estimation and equalization, a threshold decision DSP function is introduced to differentiate between the received high and low power subcarriers. The subcarrier power threshold, $P_{threshold}$, is defined as

$$P_{threshold} = \frac{(P_{8\text{-}PSK+QPSK}) + (P_{QPSK+BPSK})}{2} \tag{4.4}$$

where $P_{8\text{-}PSK+QPSK}$ ($P_{QPSK+BPSK}$) is the lowest (highest) subcarrier power of the high (low) power subcarriers. In the SIPM-OOFDM-DSPM decoder, the decoding approach used in SIPM-OOFDM-SPM is also applicable here. As such, in order to recover the information carried by each high (low) power subcarrier, 32 (8) comparisons between the received complex value C_R^H (C_R^L) and all the possible 32 (8) ideal complex values C_{Ii}^H (i=1,2,...,32) (C_{Ij}^L (j=1,2,...,8)) are made. The received complex value which corresponds to the minimum of $|C_R^H - C_{Ii}^H|^2$ ($|C_R^L - C_{Ij}^L|^2$) is used to recover the information conveyed by the high (low) power subcarrier.

The SIPM-OOFDM-DSPM transceiver architecture and the IMDD PON transmission system considered in this section are illustrated in Fig.4.11. As seen in this figure, major DSP functions involved in the SIPM-OOFDM-DSPM transmitter are almost identical to those employed in SIPM-OOFDM-SPM. Based on the transceiver architecture and the above-

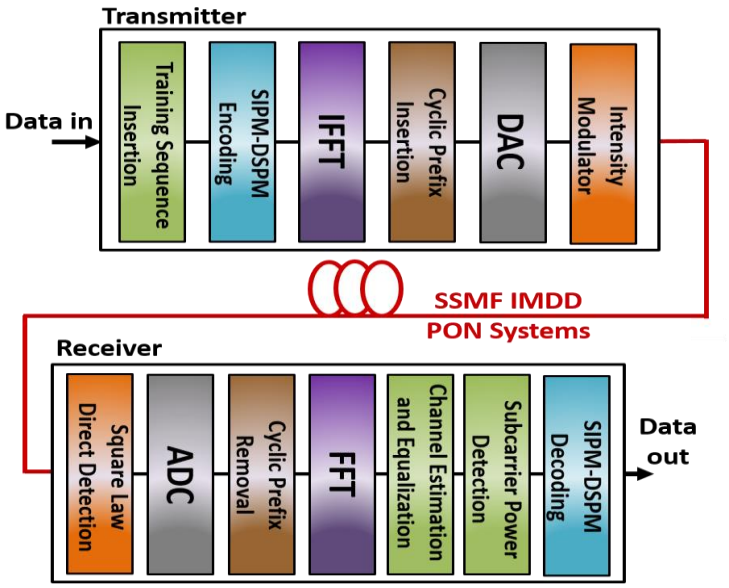

Fig.4.11. Schematic illustration of the SIPM-OOFDM-DSPM transceiver architecture and the considered IMDD PON system.

discussed SIPM-OOFDM-DSPM transceiver design principle, it is easy to understand the following unique features associated with the proposed SIPM-OOFDM-DSPM technique. These features are summarized below:

- High signal bit rate enabled by low signal modulation formats;
- Enhanced transceiver flexibility because DSP logic resources remain almost constant for various transmission techniques including SIPM-OOFDM, SIPM-OOFDM-SPM and SIPM-OOFDM-DSPM;
- Improved performance adaptability. For different transmission system requirements, simple DSP modifications result in dynamic variations in system transmission performance characteristics (signal bit rate and system power budget) to ensure that the optimum system performance is always delivered regardless of traffic/network status.
- Low DSP and hardware transceiver complexity. For specific transceiver architecture, an increase in signal bit rate does not require any significant increase in DSP complexity. In terms of hardware, the transceiver design identical to SIPM-OOFDM-SPM is still applicable here. On the other hand, in terms of DSP complexity, the same simple DSP functions used in the SIPM-OOFDM-SPM transmitter and receiver are also used in this technique.

Table 4.3. *Transceiver and Transmission System Parameters*

Parameter	Value
Total number of IFFT/FFT points	64
Data-carrying subcarriers	31
Modulation formats for SIPM-OOFDM	BPSK or QPSK or 8-PSK
PRBS data sequence length	400,000 bits
Cyclic prefix	25%
DAC & ADC sample rate	12.5GS/s
DAC & ADC bit resolution	9 bits
Clipping ratio	12 dB
PIN detector sensitivity	-19 dBm*
PIN responsivity	0.8 A/W
Fiber length	25km
SSMF dispersion parameter at 1550 nm	16 ps/(nm.km)
SSMF dispersion slope at 1550 nm	0.07 ps/nm/nm/km
Linear fiber attenuation	0.2 dB/km
Kerr coefficient	2.35×10^{-20} m²/W

*Corresponding to 10Gb/s non-return-to-zero data at a BER of 1.0×10^{-9}

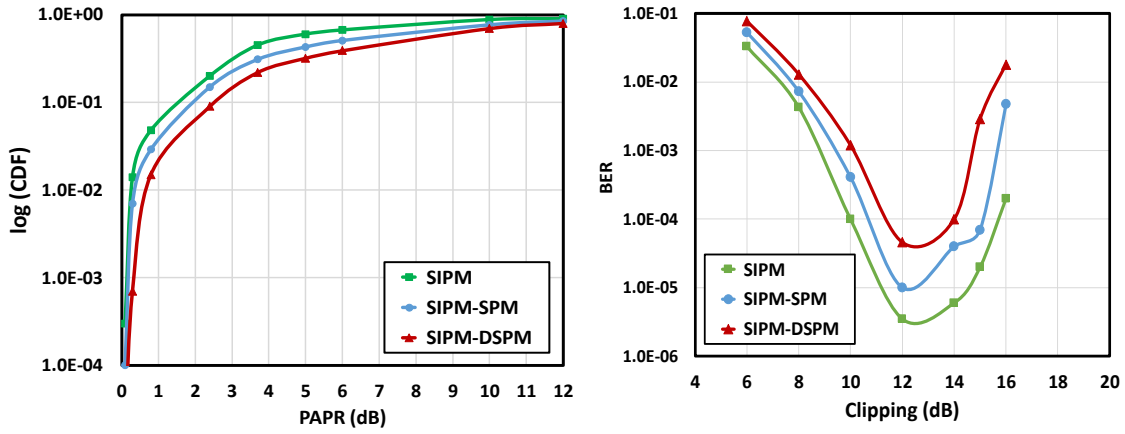

(a) **(b)**

Fig.4.12. (a) Cumulative distribution functions for SIPM-OOFDM, SIPM-OOFDM-SPM and SIPM-OOFDM-DSPM. (b) BER performance versus clipping ratio over AWGN channels with a SNR value fixed at 22dB.

4.3.2 Transmission Performance

Based on the SIPM-OOFDM-DSPM transceiver architecture shown in Fig.4.11, the optimum parameters identified in Section 4.3.1, and the operation parameters listed in Table 4.3, the transmission performance of the proposed technique is investigated in this subsection. Throughout this subsection, the optimum clipping ratio, quantization bits and DAC/ADC sampling rates are fixed at 12dB, 9 bits and 12.5GS/s, respectively. In particular, it is shown in Fig.4.12(a) that, compared to both SIPM-OOFDM and SIPM-OOFDM-SPM' CDF curves, SIPM-OOFDM-DSPM's CDF curve has an almost identical performance in terms of PAPR.

As a direct result, the same optimum clipping ratios between these three techniques are observed in Fig.4.12(b) where the optimum clipping ratios of 12dB give rise to minimum BERs. In calculating Fig.4.12(b), an AWGN channels with a SNR value of 22dB is considered.

Table 4.4. *Signal Bit Rate Comparisons*

Modulation Format	Signal Bit Rate (Gb/s)
SIPM-SPM	26.71
SIPM-DSPM	29.73
SIPM (32-PSK/8-PSK)	29.73

4.3.2.1 Signal Bit Rate

By making use of Eq.(4.3), the SIPM-OOFDM-DSPM signal bit rate can be easily computed and compared with other transmission techniques of similar nature, as summarized in Table 4.4. In this table, it is shown that the proposed technique gives rise to a signal bit rate of 29.73Gb/s, which outperforms (8-PSK+QPSK)/QPSK-encoded SIPM-OOFDM-SPM by 11%. Table 4.4 also indicates that SIPM-OOFDM-DSPM can provide the same signal bit rate of 29.73Gb/s, compared to 32-PSK/8-PSK-encoded SIPM-OOFDM where higher signal modulation formats are adopted. As a direct result, in comparison with 32-PSK/8-PSK-encoded SIPM-OOFDM, the SIPM-OOFDM-DSPM technique gives rise to a minimum received optical power and improved performance tolerance to both chromatic dispersion and

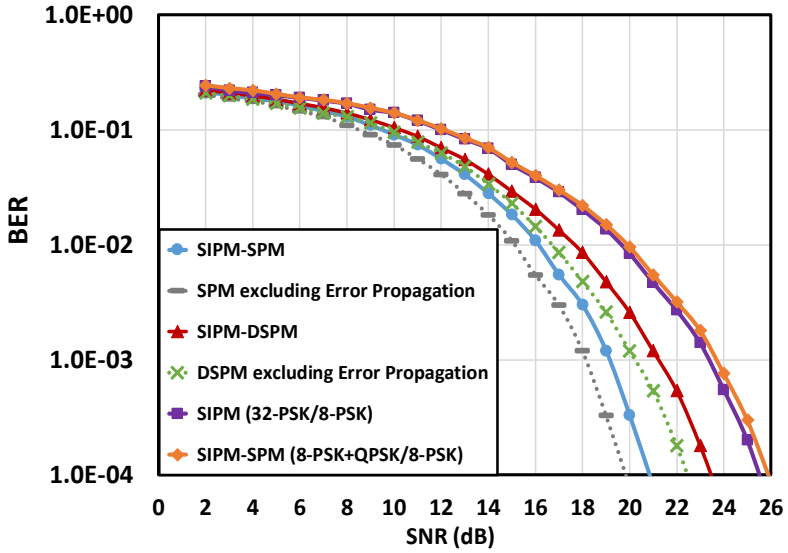

Fig.4.13. BER performance versus signal SNR over AWGN channels for various transmission techniques.

fiber nonlinearity, as discussed in the following subsections.

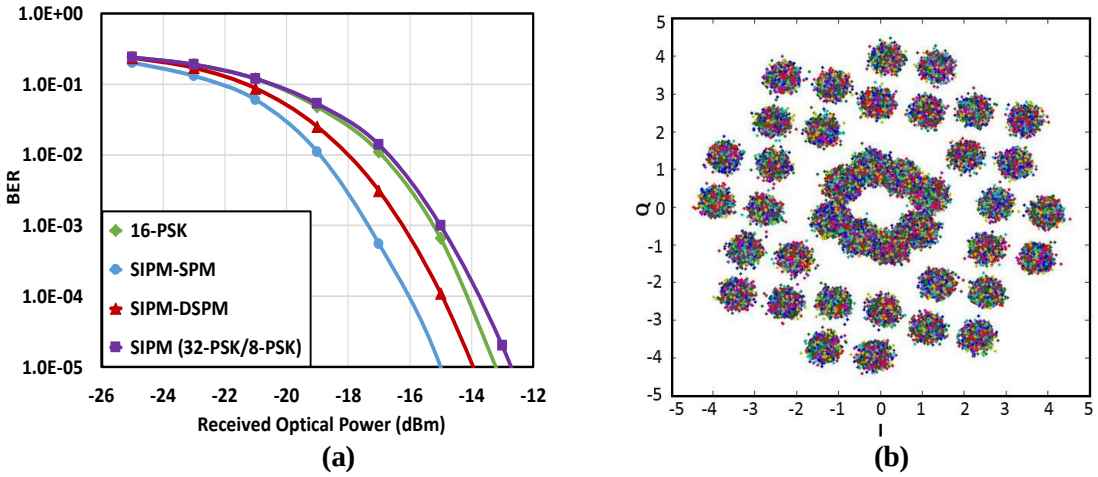

Fig.4.14. (a) Overall channel BER versus received optical power for various transmission techniques. (b) SIPM-OOFDM-DSPM constellation.

4.3.2.2 Performance over AWGN Channels

The impacts of DSPM on minimum required electrical SNR over AWGN channels are presented in Fig.4.13. It is shown that the 29.73Gb/s SIPM-OOFDM-DSPM signal introduces an SNR penalty of approximately 1.9dB at a BER of 1.0×10^{-3} in comparison with the 26.71Gb/s (8-PSK+QPSK)/QPSK-encoded SIPM-OOFDM-SPM signal. More importantly, the proposed technique offers almost 2.5dB gain at a BER of 1.0×10^{-3} when compared with both the 29.73Gb/s 32-PSK/8-PSK-encoded SIPM-OOFDM and (8-PSK+QPSK)/8-PSK-encoded SIPM-OOFDM-SPM signals. Such SNR gains confirm that the DSPM operation offers a considerable performance improvement compared with the use of only 8-PSK in low power subcarriers. The error propagation-free approach described in Section 3.4.1 is also applicable in this technique. As shown in Fig.4.13, when applying such an approach in SIPM-OOFDM-DSPM, the same impact resulting from excluding error propagation in SIPM-OOFDM-SPM is also observed here where an SNR gain of approximately 1.0dB is achieved. For fair performance comparisons, in the remaining parts of this section, error propagation is excluded in both SIPM-OOFDM-SPM and SIPM-OOFDM-DSPM.

4.3.2.3 Performance over SSMF IMDD PON Systems

Based on the same fiber transmission model used in Chapter 3, the 29.73Gb/s SIPM-OOFDM-DSPM transmission performances over 25km SSMF IMDD PON systems are investigated in this subsection.

In simulating Fig.4.14(a) an optical launch power of 5dBm is considered. In this figure, the BER performance comparison of the 29.73Gb/s SIPM-OOFDM-DSPM signal with both the 26.71Gb/s (8-PSK+QPSK)/QPSK-encoded SIPM-OOFDM-SPM signal and the 29.73Gb/s 32-PSK/8-PSK-encoded SIPM-OOFDM signal shows that there exists a 0.9dB power penalty and a 1.0dB received optical power gain respectively at a BER of 1.0×10^{-3}. In addition, when compared with a 23.73Gb/s 16-PSK-encoded conventional OOFDM signal, a 0.9dB received optical power gain is achieved at a BER of 1.0×10^{-3}. Under the same transmission conditions of Fig.4.14(a), the representative SIPM-OOFDM-SPM constellations obtained after equalization at a BER of 1.0×10^{-3} are illustrated in Fig.4.14(b). It is shown in this figure that the sizes of the inner constellation points are relatively larger than the outer constellation points. This is because the inner (outer) constellation points are associated with low (high) signal modulation formats. Assuming that each signal modulation format is encoded at an equal probability, thus the occurrence probability of a specific constellation point of the low signal modulation format is higher than that corresponding to the high signal modulation format.

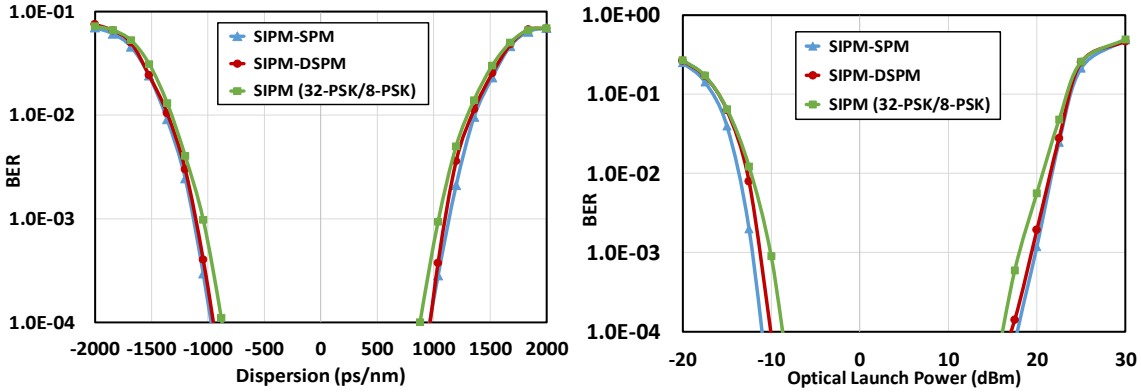

Fig.4.15. Performance tolerance of three transmission techniques after transmitting through SSMF IMDD PON systems (a) chromatic dispersion and (b) fiber nonlinearity.

At a specific BER, the reduction in received optical power means an improvement in system optical power budget, this results in an improved SIPM-OOFDM-DSPM performance tolerance to both chromatic dispersion and fiber nonlinearity for the considered IMDD PON systems. Such a statement is verified in Fig.4.15(a) and Fig.4.15(b). For the 29.73Gb/s 32-PSK/8-PSK-encoded SIPM-OOFDM, 29.73Gb/s SIPM-OOFDM-DSPM and 26.71Gb/s SIPM-OOFDM-SPM techniques, the BER against chromatic dispersion is explored in Fig.4.15(a). In simulating this figure, the same system conditions as those described in

Fig.4.8(a) (Section 4.2.2.3) are also adopted here. As expected, it is shown in Fig.4.15(a) that, the 29.73Gb/s SIPM-OOFDM-DSM signal improves the dispersion tolerance range by almost 75ps/nm at a BER of 1.0×10^{-3}, compared to the 32-PSK/8-PSK-encoded SIPM-OOFDM signal operating at the same signal bit rate. The physical origin of such an improvement is mainly due to the use of low signal modulation formats in low power subcarriers. As a direct result of the physical mechanism, it is also shown in 4.15(b) that, to achieve a BER of 1.0×10^{-3}, the proposed technique can improve the optical launch power dynamic range by 2dB compared to the 29.73Gb/s 32-PSK/8-PSK-encoded SIPM-OOFDM-SPM signal.

Table 4.5. *SIPM-OOFDM-DSPM Performance Comparisons*

Modulation Format	Signal Bit Rate (Gb/s)	Power Penalty (dB)
16-PSK-OOFDM	25% Increase	-1.7
SIPM-SPM	11% Increase	0.9
SIPM(32-PSK/8-PSK)	Identical	-1.8

The above discussions indicate that, for practical applications, the signal modulation format selection can be adaptive and flexible: for power budget-limited transmission systems, relatively low signal modulation formats are preferred to increase the system power budget. On the other hand, for bandwidth-hungry transmission systems with sufficiently large power budgets, relatively high signal modulation formats are preferred to maximise the signal bit rate. Furthermore, as seen in Table 4.5, the DSPM-introduced 11% increase in signal bit rate causes only 0.9dB changes to the system power budget for a specific BER. This table also shows that, in comparison with the 32-PSK/8-PSK-encoded SIPM-OOFDM technique capable of offering a signal bit rate identical to SIPM-OOFDM-DSPM, the proposed technique improves the system power budget by 1.8dB. Table 4.5 also shows that, in comparison with 16-PSK-encoded conventional OOFDM, a 25% increase in signal bit rate as well as a 1.7dB gain in system power budget is achieved.

4.4 Conclusion

This chapter has proposed and investigated two signal transmission techniques namely SIPM-OOFDM-SPM and SIPM-OOFDM-DSPM. SIPM-OOFDM-SPM, an improved variant of the SIPM-OOFDM transmission technique proposed in Chapter 3 is explored, for the first time,

over IMDD PON systems. Based on the identified optimum key transceiver design parameters, the SIPM-OOFDM-SPM transmission characteristics have been numerically investigated. It has been shown that the (8-PSK+QPSK)/QPSK encoded-SIPM-OOFDM-SPM signal supports 26.71Gb/s signal transmissions over 25km SSMF IMDD PON systems, and that a 28.6% signal bit rate improvement is achievable compared to the 8-PSK/QPSK-encoded SIPM-OOFDM without increasing the DSP and hardware complexity. In addition, the research work has also indicated that, in comparison with the 32-PSK/QPSK-encoded SIPM-OOFDM technique capable of offering a signal bit rate identical to SIPM-OOFDM-SPM, the proposed technique improves the system power budget and performance tolerance to both chromatic dispersion and fiber nonlinearity. To further improve transmission performance of SIPM-OOFDM-SPM, SIPM-OOFDM-DSPM has been investigated over SSMF IMDD PON systems. Optimum key transceiver parameters have been identified, based on which, the SIPM-OOFDM-DSPM transmission performance characteristics have been explored. It is shown that, with preserved DSP and hardware complexity, (8-PSK+QPSK)/(BPSK+QPSK) SIPM-OOFDM-DSPM offers an 11% improvement in signal bit rate compared to (8-PSK+QPSK)/QPSK-encoded SIPM-OOFDM-SPM, and a 1.8dB received optical power gain compared to 32-PSK/8-PSK-encoded SIPM-OOFDM operating at the same signal bit rate.

References:

[1] M. Alam and Q. Zhang, ‘‘Non-orthogonal multiple access with sequence block compressed sensing multiuser detection for 5G,’’ *IEEE Access, DOI:10.1109/ACCESS.2018.2877477,* (Early Access), Oct. 2018.

[2] L. Chen, F. Halabi, R. P. Giddings, and J. M. Tang, “Subcarrier index-power modulated optical OFDM with superposition multiplexing for IMDD transmission systems,” *J. Lightw. Technol.*, vol. 34, no. 9, pp. 2228–2234, Oct. 2016.

[3] Z. Ding, Z. Yang, P. Fan and H. V. Poor, ‘‘On the performance of non-orthogonal multiple access in 5G systems with randomly deployed users,’’ *IEEE Signal Processing Letters,* vol. 21, no.12, pp.1501-1505, Dec. 2014.

[4] S. Timotheou and I. Krikidis, ‘‘Fairness for non-orthogonal multiple access in 5G systems,’’ *IEEE Signal Processing Letters,* vol. 22, no.10, pp.1647-1651, Oct. 2015.

[5] L. Chen, F. Halabi, J. Zhang, R. P. Giddings, and J. M. Tang, “Subcarrier index-power modulated-optical OFDM with dual superposition multiplexing for directly modulated DFB-based IMDD PON systems,” *IEEE Photon. J.*, vol. 10, no. 6, Dec. 2018.

[6] F. Halabi, L. Chen, R. P. Giddings, A. Hamié, Y. Dumas, P. Freyssinet, C. Aupetit-Berthelemot and J. M. Tang, ‘‘Subcarrier index-power modulated optical OFDM with dual superposition multiplexing for IMDD PON systems’’, *Optics Commun.*, vol. 433, pp. 190-194, Oct. 2018.

[7] F. Halabi, L. Chen, S. Parre, S. Barthomeuf, R. P. Giddings, C. Aupetit-Berthelemot and J. M. Tang, “Subcarrier index-power modulated optical OFDM and its performance in IMDD PON systems,” *J. Lightw. Technol.*, vol. 34, no. 9, pp. 2228–2234, May 2016.

[8] F. Halabi, L. Chen, S. Parre, S. Barthomeuf, R. P. Giddings, C. Aupetit-Berthelemot and J. M. Tang, “Subcarrier index-power modulated optical OFDM (SIPM-OOFDM) for IMDD PON systems,’’ in *Proc. Optical Fibre Communication (OFC) Conference,* Th3C.1, pp.1-3, Mar. 2016.

[9] R. Giddings, ‘‘Real-time digital signal processing for OFDM-base future optical access networks,’’ *J. Lightw. Technol*., vol. 32, no.4, pp.553-570, Feb. 2014.

[10] G. P. Agrawal, Fibre-Optic Communication Systems, 2nd ed. Hoboken, NJ, USA: *Wiley*, 1997.

5. Multilevel SIPM-OOFDM

5.1 Introduction

To further increase the number of information bits conveyed per subcarrier compared with all the previously proposed techniques [1-4], this chapter introduces a novel signal transmission technique called multilevel SIPM-OOFDM (ML-SIPM-OOFDM) [5]. In this technique, the SIP dimension is expanded by increasing the number of subcarrier power levels to allow more information bits to be conveyed per subcarrier and, thus, improving the signal bit rate of SIPM-OOFDM. It should be noted that, multi-level (ML) could also be applied easily in both SIPM-OOFDM-SPM [2] and SIPM-OOFDM-DSPM [3, 4] as the ML-associated operating principles, their DSP elements and corresponding performance advantages are very similar for these transmission techniques. For simplicity but without losing any generality, in this chapter special attention is therefore focused on ML-SIPM-OOFDM only.

In ML-SIPM-OOFDM, within an OFDM symbol, each subcarrier is set at one of the four predefined power levels according to an incoming data sequence. Following that, the corresponding subcarrier is encoded using one of the following four signal modulation formats: BPSK, QPSK, 8-PSK and 16-PSK. Generally speaking, a high (low) signal modulation format is taken on a high (low) power subcarrier. To further improve the signal bit rate and system adaptability, adaptive bit loading (ABL) [6, 7] is also applicable in ML-SIPM-OOFDM. For typical SSMF IMDD PON systems, it is shown that ML-SIPM-OOFDM enables a 30% improvement in signal bit rate compared to QPSK/8-PSK-encoded SIPM-OOFDM. In addition, in comparison with 16-PSK-encoded conventional OOFDM, ML-SIPM-OOFDM enhances the signal bit rate by 13% without degrading the minimum received optical power required at a BER of 1.0×10^{-3}. Finally, further 9% and 10% ML-SIPM-OOFDM transmission bit rate enhancements are also feasible when use is made of ABL and subcarrier count doubling, respectively.

Table 5.1. *ML-SIPM-OOFDM Encoding Process*

SIP Dimension PRBS Stream	Subcarrier Power Level	Modulation Format*
0 0	First P_1	BPSK
0 1	Second P_2	QPSK
1 0	Third P_3	8-PSK
1 1	Fourth P_4	16-PSK

*without adaptive bit loading

5.2 Operating Principle

The ML-SIPM-OOFDM operating principle is similar to the previously reported SIPM-OOFDM technique [1], except that the DSP functions for data encoding (decoding) in the ML-SIPM-OOFDM transmitter (receiver) are considerably modified as detailed below. In addition, to distinguish the received power level of each individual subcarrier in the ML-SIPM-OOFDM receiver, training sequence-based new DSP functions are also developed to detect the subcarrier power status and subsequently calculate three corresponding subcarrier power thresholds for each subcarrier.

In the ML-SIPM-OOFDM transmitter, the four subcarrier power levels are referred to as P_1, P_2, P_3 and P_4 to represent the first, second, third and fourth subcarrier power level,

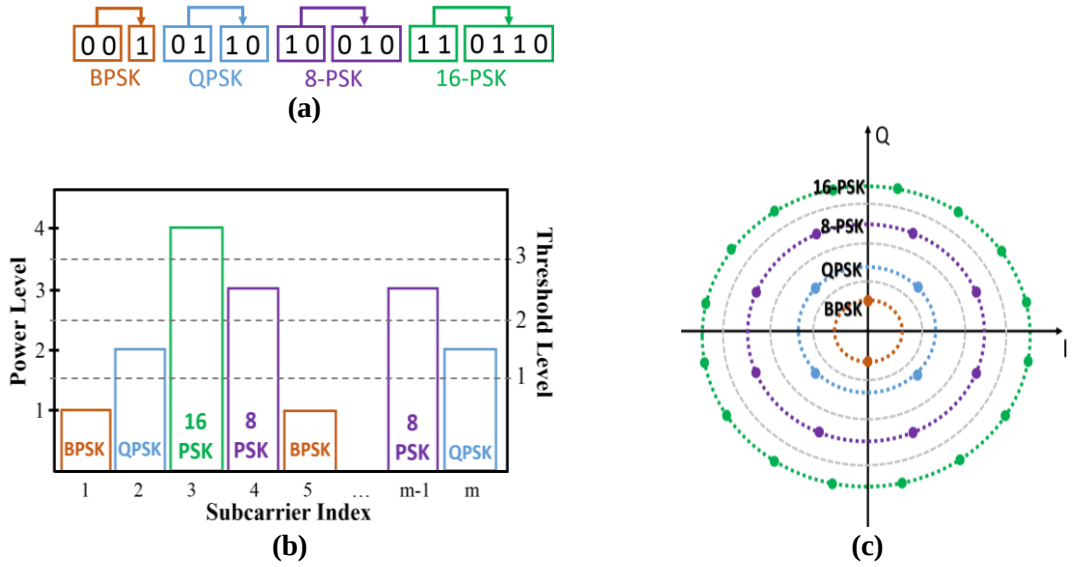

Fig.5.1. (a) ML-SIPM-OOFDM data-encoding process in the transmitter. (b) Schematic diagram showing how a subcarrier of different power levels in the transmitter is encoded using BPSK, QPSK, 8-PSK, or 16-PSK. Three subcarrier power thresholds are also represented using lines that lie between each two distinct subcarrier power levels. (c) Overall ML-SIPM-OOFDM constellation.

respectively. For simplicity, these subcarrier power levels are assumed to satisfy $P_{j+1}>P_j$ with j=1,2,3. To encode an incoming PRBS stream, when ‘’00 (01)’’ bits are encountered, the corresponding subcarrier power is set at P_1 (P_2), and the following 1(2) bits of the PRBS stream are truncated and subsequently encoded using BPSK (QPSK), as presented in Table 5.1. The resulting BPSK (QPSK)-encoded complex number is finally assigned to the subcarrier. On the other hand, when ‘’10 (11)’’ bits are encountered in the PRBS stream, the corresponding subcarrier power is set at P_3 (P_4), and the following 3(4) bits of the PRBS stream are truncated and subsequently encoded using 8-PSK (16-PSK). The resulting 8-PSK (16-PSK)-encoded complex number is assigned to the subcarrier. Such data-encoding procedures ensure that all the information-bearing subcarriers are always active, and more importantly, each information-bearing subcarrier is capable of carrying not only two extra bits per subcarrier in the SIP information-bearing dimension but also relevant information bit(s) in the conventional subcarrier-information-bearing dimension. Examples concerning the above-described encoding procedures are illustrated in Fig.5.1(a) and Fig.5.1(b), and the overall ML-SIPM-OOFDM constellation is also presented in Fig.5.1(c). Here it is worth mentioning the following two aspects: i) a specific subcarrier contained in an individual ML-SIPM-OOFDM symbol is encoded by randomly utilising one of these four signal modulation formats. For a long PRBS stream, the probability of encoding a specific signal modulation format on any subcarrier is 0.25. This implies that the occurrence probability of a particular constellation point presented in Fig.5.1(c) is different for different signal modulation format. This is verified in Fig.5.7.(b); ii) apart from the 30 constellation points, each of these four subcarrier power levels in Fig.5.1(c) can also be regarded as “a constellation point”, as it is capable of carrying two extra information bits in the SIP information-bearing dimension.

In the ML-SIPM-OOFDM receiver, to distinguish the received power level of each individual subcarrier, DSP functions for performing both subcarrier power level detection and subcarrier threshold calculation are implemented by making use of a training sequence that is periodically inserted into the PRBS stream in the transmitter. These DSP functions are located between the FFT and channel estimation/equalization. For a specific subcarrier, its j-th subcarrier power threshold, $P_{T\text{-}j}$, is calculated using the formula expressed below

$$P_{T\_j} = \frac{P_{j+1} + P_j}{2} \quad j = 1,2,3 \tag{5.1}$$

For each subcarrier of the same frequency, $P_{T\text{-}j}$ is averaged over time to reduce the channel noise effect. These three subcarrier power thresholds are utilized to recover the extra information bits conveyed in the SIP information-bearing dimension. Furthermore, these subcarrier power thresholds are also employed to determine the signal modulation format taken on the subcarrier in the conventional subcarrier information-bearing dimension, as shown in Table 5.1. Prior to decoding and recovering the information bits conveyed by the subcarrier in the conventional subcarrier-information-bearing dimension, channel estimation and equalization [8] are also performed using the same received training sequence. As a direct result of the system frequency response roll-off effect associated with typical IMDD PON systems, both P_j and $P_{T\text{-}j}$ are subcarrier index-dependent.

From the above-described ML-SIPM-OOFDM operating principle and as discussed in Chapter 4, it is easy to understand that the maximum ML-SIPM-OOFDM signal bit rate is also subcarrier count-dependent. For an IMDD transmission system, the ML-SIPM-OOFDM signal bit rate, R_b, can be mathematically expressed as:

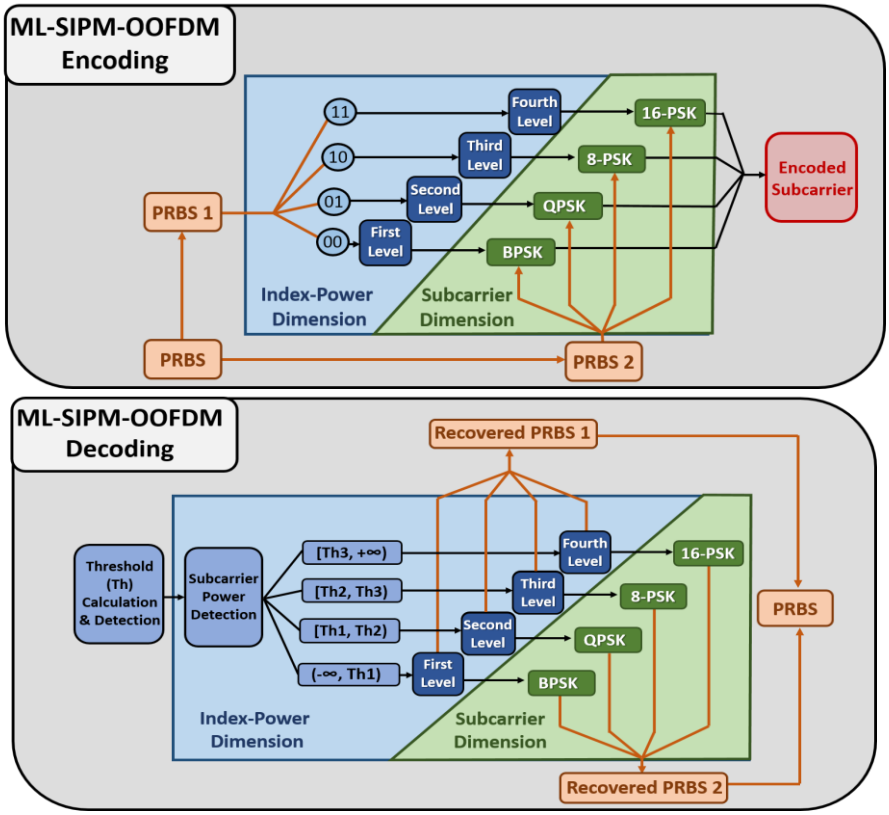

Fig.5.2. ML-SIPM-OOFDM signal encoding and decoding processes and major DSP functions incorporated in the receiver.

$$R_b = \frac{f_s \sum_{i=1}^{N/2-1} (2 + b_i)}{N(1+\alpha)} \tag{5.2}$$

where f_s is the sampling rate of the DAC/ADC, b_i represents the number of bits conveyed by the i-th subcarrier in the conventional subcarrier information-bearing dimension, 2 reflects the extra 2 information bits carried by the subcarrier in the SIP information-bearing dimension. N is the total number of subcarriers per symbol, and α is the coefficient introduced to take into account the signal transmission bit rate reduction due to cyclic prefix and training sequence.

To summarize the above-described ML-SIPM-OOFDM operating principle, Fig.5.2 is presented, where the signal encoding and decoding processes in both the SIP information-bearing dimension and the conventional subcarrier information-bearing dimension are illustrated using two decision-tree-like diagrams. In addition, major DSP functions incorporated in the receiver are also included in the same figure. To effectively combat the IMDD-induced channel fading effect in a cost-effective manner, ABL widely adopted in conventional OOFDM [6, 7] is also applicable in ML-SIPM-OOFDM IMDD PON systems. To apply ABL in ML-SIPM-OOFDM, the subcarrier power level to be selected still depends on the incoming data sequence, and the aforementioned data coding and decoding procedures in the SIP information-bearing dimension remain unchanged. Whilst, in the conventional

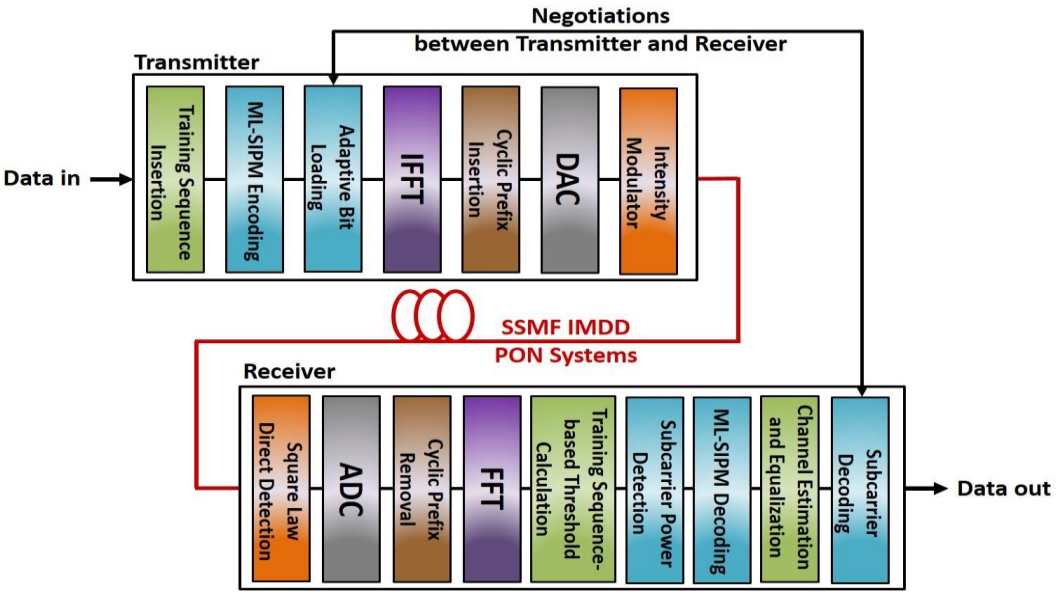

Fig.5.3. Schematic illustrations of the ML-SIPM-OOFDM transceiver architecture and the considered IMDD PON transmission system.

Table 5.2. *Transceiver and Transmission System Parameters*

Parameter	Value
Total number of IFFT/FFT points	64
Data-carrying subcarriers	31
Modulation formats for SIPM-OOFDM	BPSK or QPSK or 8-PSK or 16-PSK
PRBS data sequence length	400,000 bits
Cyclic prefix	25%
DAC & ADC sample rate	12.5GS/s
DAC & ADC bit resolution	9 bits
Clipping ratio	12 dB
PIN detector sensitivity	-19 dBm*
PIN responsivity	0.8 A/W
Fiber length	25km
SSMF dispersion parameter at 1550 nm	16 ps/(nm.km)
SSMF dispersion slope at 1550 nm	0.07 ps/nm/nm/km
Linear fiber attenuation	0.2 dB/km
Kerr coefficient	2.35×10^{-20} m²/W

*Corresponding to 10Gb/s non-return-to-zero data at a BER of 1.0×10^{-9}

subcarrier information-bearing dimension, use can be made of an approach almost identical to conventional OOFDM [8, 9]. As mentioned in Section 2.4, in this approach, according to transmission channel spectral characteristics, negotiations between the transmitter and the receiver are undertaken to determine the highest signal modulation format that can be taken on each subcarrier in order to maximize the signal bit rate at an overall channel BER of 1.0×10^{-3}. As a direct result, each subcarrier at a specific power level no longer corresponds to only a single fixed modulation format specified in Table 5.1, instead, for a subcarrier at a specific power level, the corresponding signal modulation format may vary from BPSK, QPSK, 8-PSK, to 16-PSK, depending upon the channel spectral characteristics. Here, an important exception worth mentioning is that, for the vast majority of cases, high-order signal modulation formats such as 8-PSK and 16-PSK cannot be taken on subcarriers having the first and second power levels, since these relatively low subcarrier power levels considerably reduce the minimum Euclidean distances of these signal modulation formats.

5.3 Optimization of Key Transceiver Parameters

5.3.1 Transceiver Architecture and IMDD PON System

The ML-SIPM-OOFDM transceiver architecture and the IMDD PON transmission system considered in this chapter are illustrated in Fig.5.3. As seen in this figure, the ML-SIPM-OOFDM transmitter consists of several DSP functions that are identical to those employed in

SIPM-OOFDM [1], SIPM-OOFDM-SPM [2], SIPM-OOFDM-DSPM [3, 4] and conventional OOFDM [8]. In particular, new DSP functions are also included to perform the ML-SIPM-OOFDM data-encoding operations described in Section 5.2. In addition, for a specific transmission system, an ABL DSP function is also implemented to ensure the adaptation of highest possible signal modulation formats on any subcarriers in the conventional subcarrier information-carrying dimension. At the output of the IFFT, cyclic prefix addition and DAC are undertaken to produce a final electrical signal, which is then utilised to drive an optical intensity modulator to perform the E/O conversion. To explicitly highlight the salient performance features of the proposed technique, throughout this chapter, an ideal optical intensity modulator based on Eq. (3.2) is also considered. In addition, similar to all previous chapters, a SSMF simulation model based on the widely adopted split-step Fourier method is adopted to model the propagation of optical signals over the IMDD PON systems where the effects of linear loss, chromatic dispersion and fiber nonlinearities are also included. After fibre transmissions, the optical signal is converted to the electrical domain by a square-law photodetector subject to both shot and thermal noise [10].

To numerically simulate the ML-SIPM-OOFDM transmission performance over the IMDD PON system, the adopted key transceiver and system parameters are listed in Table 5.2. Unless stated explicitly in the corresponding text, these parameters are utilised as default throughout this chapter. Similar to SIPM-OOFDM, it is shown in this table that a 12dB clipping ratio is also adopted in ML-SIPM-OOFDM. The use of such a clipping value is verified in Fig.5.4 where both techniques' CDF curves exhibit an almost identical performance in terms of PAPR (Fig. 5.4(a)) and, as a direct result, the same optimum clipping ratios between these two techniques are observed (Fig.5.4(b)). In calculating Fig.5.4(b), AWGN channels with SNR value of 22dB are considered.

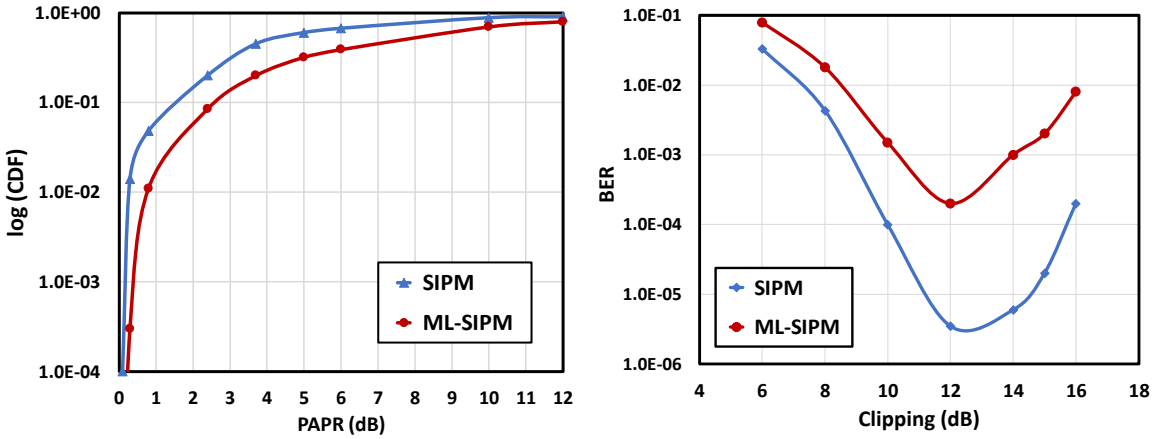

Fig.5.4. (a) Cumulative distribution functions for SIPM-OOFDM, and ML-SIPM-OOFDM. (b) BER performance versus clipping ratio over AWGN channels with SNRs fixed at 22dB.

5.3.2 Optimizations of Subcarrier Power Levels

Due to the fact that each information-bearing subcarrier contains one of the four predefined different power levels, it is therefore envisaged that the adaptation of optimum subcarrier power levels plays a vital role in determining the maximum achievable ML-SIPM-OOFDM transmission performance. As such, special attention in this subsection is first given to optimizing these subcarrier power levels. It is easy to understand that the received absolute optimum subcarrier power at the j-th level, P_j, varies with subcarrier index because of the channel fading effect. To take into account such an effect, in the following optimisation process, instead of employing an absolute subcarrier power level, use is made of a subcarrier power level ratio, PR_j, defined as

$$PR_j = \frac{P_j}{P_1} \quad j = 2,3,4 \tag{5.3}$$

For simplicity, in the transmitter $P_1=1$ is assumed regardless of subcarrier index. Such treatment is valid because channel equalization in the receiver is always conducted on subcarrier basis. In addition, for simplicity without loss of generality, in the optimisation process, AWGN channels are also considered and ABL is excluded.

The adopted numerical optimization procedures are outlined as follows:

1. A subcarrier power level ratio parameter set, $\{b_U\} = \{PR_2, PR_3, PR_4\} = \{3, 5, 7\}$, is adopted as the initial input parameter values.

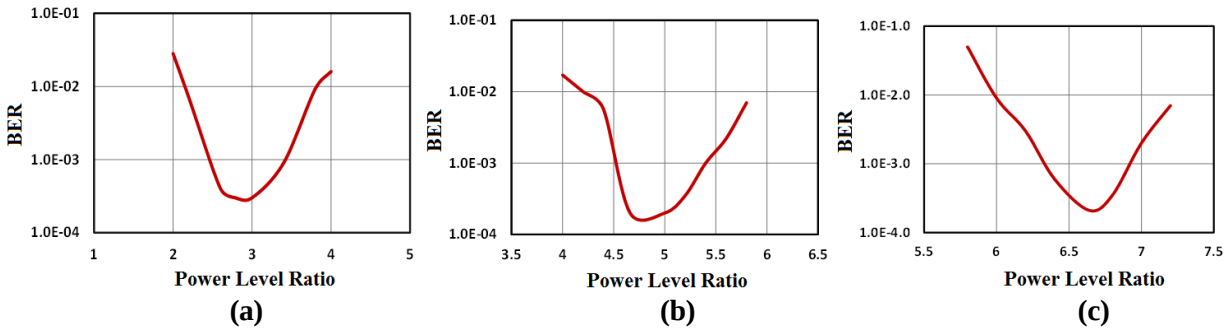

Fig.5.5. Overall channel BER as a function of subcarrier power level ratio. (a) Overall BER versus PR_2 with PR_3 and PR_4 fixed at their optimum values; (b) Overall BER versus PR_3 with PR_2 and PR_4 fixed at their optimum values; (c) Overall BER versus PR_4 with PR_2 and PR_3 fixed at their optimum values. Here, AWGN channels with input ML-SIPM-OOFDM signal SNRs fixed at 18dB are considered in all simulations.

2. Numerical simulations are undertaken with the first element, PR_2, varying within a reasonable range, and all other parameters fixed at their original values. An optimum PR_2 is obtained when a minimum overall channel BER is reached.
3. Numerical simulations are then performed by simultaneously considering the following two conditions: a) the next element in $\{b_U\}$ is selected to vary within a reasonable range, and b) all the previously adopted elements in $\{b_U\}$ remain unchanged except that the elements optimised in this iteration are fixed at their optimum values. An optimum value of the selected element is obtained when a minimum overall channel BER is reached.
4. Step 3 repeats until all the elements contained in $\{b_U\}$ are optimised.
5. By making use of the newly generated parameter set $\{b_U\}$, Step 2, Step 3 and Step 4 are repeated to produce a further updated version of $\{b_U\}$. Such iterative procedure continues until <2% variations of all the elements in $\{b_U\}$ are reached with respect to their corresponding values obtained in last iteration.

Based on the above-mentioned optimisation procedure, after just 3 iterations, the final optimum subcarrier power level ratios are identified, which are $PR_2 = 2.79$, $PR_3 = 4.66$ and $PR_4 = 6.64$. Furthermore, by making use of Eq.(5.1) and $P_1=1$, the three optimum subcarrier power thresholds can also be deduced easily, which are $P_{T-1} = 1.90$, $P_{T-2} = 3.73$, and $P_{T-3} = 5.65$. These six optimum parameters are taken as default values throughout the chapter.

To explicitly demonstrate how the overall channel BER performance varies as a function of individual subcarrier power level ratio, Fig.5.5 is plotted where the electrical AWGN

channels are considered and the input ML-SIPM-OOFDM signal SNRs are fixed at 18dB. In obtaining each of these three figures, except for the variable subcarrier power level ratio, all other two remaining subcarrier power level ratios are fixed at their optimum values. It is shown in Fig.5.5 that for all the cases considered, the overall channel BERs grow with increasing offsets from their optimum values. The occurrence of these optimum subcarrier power level ratios is mainly due to the combined effects of the following three physical mechanisms:

- A variation in the power difference between two adjacent subcarrier power levels alters the accuracy in detecting the received subcarrier power status. This directly affects the BERs corresponding to both the SIP information-bearing dimension and the conventional subcarrier information-bearing dimension via error propagation.
- A variation in the subcarrier power level alters the minimum Euclidean distance of the corresponding signal modulation format taken on the subcarrier. This directly affects BERs because of errors occurring in the conventional subcarrier information-bearing dimension.
- A change to one subcarrier power level causes relevant alterations to all other subcarrier power levels across all subcarriers, as the total ML-SIPM-OOFDM signal power always remains constant.

By making use of the abovementioned physical mechanisms, it is very easy to understand the occurrence of optimum subcarrier power level ratios in both Fig.5.5(a) and Fig.5.5(b). In Fig.5.5(c), for subcarrier power level ratios lower than 6.64, the BER grows with decreasing subcarrier power level ratio, this mainly results from the fast reduction in the minimum Euclidean distance of the 16-PSK constellation. Whilst for subcarrier power level ratios larger than 6.64, the observed BER increase with increasing subcarrier power level ratio occurs because of the fixed electrical signal power-induced reductions in minimum Euclidean distance for the BPSK, QPSK and 8-PSK constellations.

5.4 Transmission Performance

After having completed the optimisations of key transceiver parameters in Section 5.3, the thrust of this section is to explore the maximum achievable ML-SIPM-OOFDM transmission performance over various transmission systems. In addition, the impacts of subcarrier count

and ABL are also investigated on the achievable ML-SIPM-OOFDM signal bit rate versus reach performances.

Table 5.3. *Signal Bit Rate Comparisons*

Modulation Format	Signal Bit Rate (Gb/s)*	Average Bits per Subcarrier
QPSK	11.87	2
8-PSK	17.80	3
SIPM	20.77	3.5
16-PSK	23.73	4
ML-SIPM	26.80	4.5

*31 data-carrying subcarriers are used

By making use of the transceiver parameters listed in Table 5.2 and the optimum parameters identified in Section 5.3, the signal bit rates of SIPM-OOFDM, conventional OOFDM encoded with QPSK, 8-PSK and 16-PSK, as well as ML-SIPM-OOFDM can be calculated very easily, which are summarized in Table 5.3. In this table, the average number of bits transmitted per subcarrier is also listed for each transmission technique considered. It can be seen in Table 5.3 that the proposed technique gives rise to a signal bit rate of 26.80Gb/s, which significantly exceeds 16-PSK-encoded OOFDM and QPSK/8-PSK-encoded SIPM-OOFDM by approximately 13% and 30%, respectively. The fact that ML-SIPM-OOFDM has the ability of significantly outperforming any of these previously proposed transmission

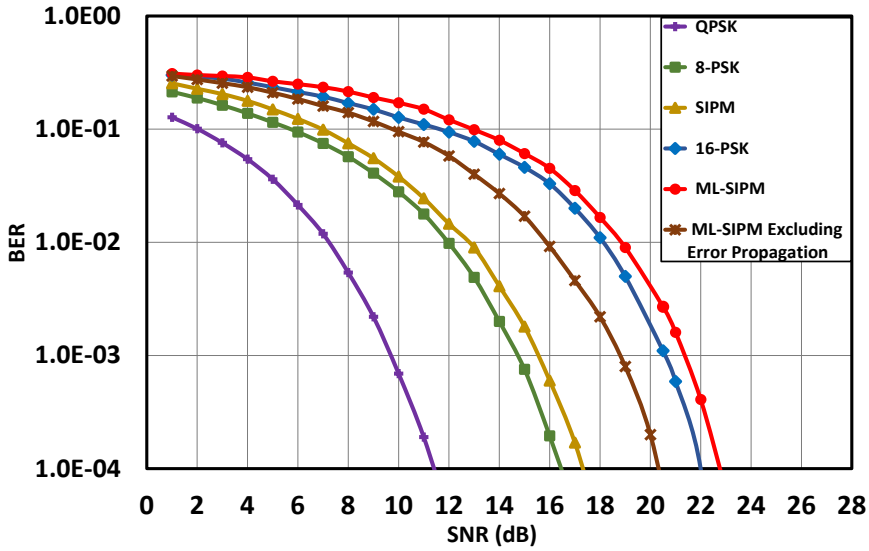

Fig.5.6. Overall channel BER performance versus signal SNR over AWGN channels for ML-SIPM-OOFDM, SIPM-OOFDM and conventional OOFDM encoded using QPSK, 8-PSK and 16-PSK.

techniques encoded using similar signal modulation formats implies that for a specific transmission system, the ML-SIPM-OOFDM-induced improvement in signal bit rate does not compromise considerably the system power budget, as discussed in the following section.

5.4.1 Performance over AWGN Channels and IMDD PON Systems

For achieving specific BERs, the impacts of ML-SIPM-OOFDM on minimum required electrical signal SNR over AWGN channels are presented in Fig.5.6, where BER performance comparisons are made between QPSK/8-PSK-encoded SIPM-OOFDM, conventional OOFDM uniformly encoded with QPSK, 8-PSK and 16-PSK, as well as ML-SIPM-OOFDM. To clearly distinguish the influence of the error propagation effect on minimum required signal SNR at a BER of 1.0×10^{-3}, an error propagation-free ML-SIPM-OOFDM BER curve is also computed and subsequently plotted in Fig.5.6 based on the same approach discussed in Chapter 3. To highlight the ML-SIPM-associated impacts, ABL is excluded for all the cases presented in Fig.5.6. As expected, it is very interesting to note in Fig.5.6 that the 26.80Gb/s ML-SIPM-OOFDM signal has an overall BER developing trend very similar to a 23.73Gb/s 16-PSK-encoded conventional OOFDM signal, and between these two signals, there exists a SNR difference as small as 1.0dB at a BER of 1.0×10^{-3}. This difference is also mirrored between the 20.77Gb/s 8-PSK/QPSK SIPM-OOFDM signal and the 17.80Gb/s 8-PSK-encoded conventional OOFDM signal.

Furthermore, by comparing the ML-SIPM-OOFDM BER curves between the cases of including and excluding the error propagation effect, it is easy to find in Fig.5.6 that the error propagation effect introduces an approximately 2.6dB SNR penalty. More importantly, compared to conventional OOFDM encoded using 16-PSK, error propagation-free ML-SIPM-OOFDM gives rise to a SNR gain as large as 1.7dB. The physical origin of the 1.7dB SNR gain is mainly due to the fact that 16-PSK is just taken randomly on a relatively small portion of the information-carrying subcarriers in ML-SIPM-OOFDM, thus resulting in an increase in the overall minimum Euclidean distances of all signal modulation formats taken on other subcarriers because of the constant signal power employed.

The above results suggest that ML-SIPM-OOFDM has great potential of not only considerably improving the signal bit rate, but also significantly decreasing the minimum required signal SNR, when the present simple subcarrier power-detection algorithms are modified to effectively minimise the error propagation effect. It is also worth mentioning that such error correction algorithms are proposed and extensively investigated in the following chapter.

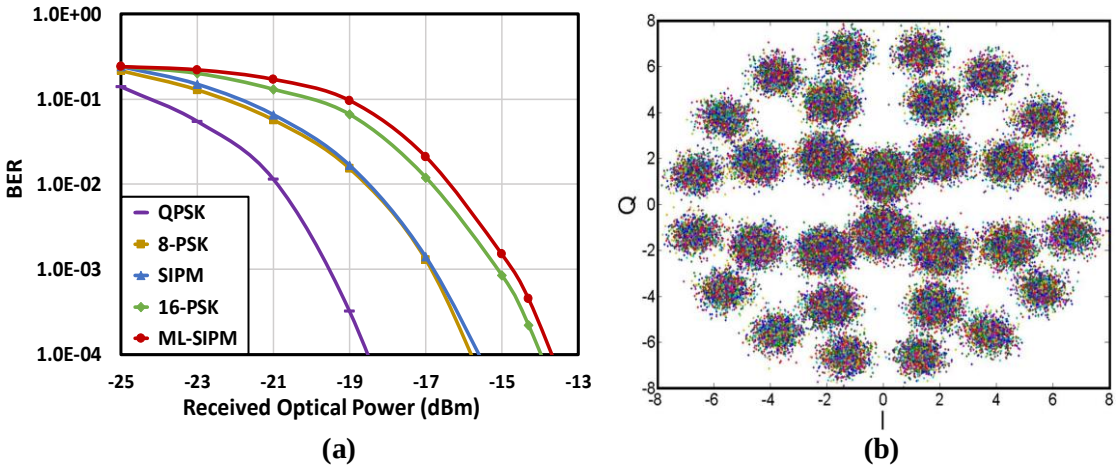

Fig.5.7. (a) Overall channel BER versus received optical power after transmitting through 25km SSMF IMDD PON systems for various transmission techniques. (b) ML-SIPM-OOFDM constellation.

The BER performance of 26.80Gb/s ML-SIPM-OOFDM signal transmission over 25km SSMF IMDD PON systems is presented in Fig.5.7.(a), where the BER performances are also shown for 20.77Gb/s QPSK/8-PSK-encoded SIPM-OOFDM signals, 23.73Gb/s 16-PSK OOFDM signals, 17.80Gb/s 8-PSK OOFDM signals, as well as 11.87Gb/s QPSK-OOFDM signals. In numerically simulating Fig.5.7(a), the optical launch powers are taken to be -9dBm and once again ABL is excluded. Fig.5.7(a) shows that ML-SIPM-OOFDM has a very similar BER performance to 16-PSK OOFDM, and between these two transmission techniques there exists a received optical power difference of approximately 0.5dB at a BER of 1.0×10^{-3}. This agrees very well with the corresponding electrical SNR difference observed in Fig.5.6. Such phenomenon implies that the ML-SIPM-introduced 13% increase in signal bit rate just causes approximately 0.5dB changes to both the received optical power and optical power budget at a BER of 1.0×10^{-3}. Under the same transmission conditions of Fig.5.7(a), the representative ML-SIPM-OOFDM constellations obtained after equalization at a BER of 1.0×10^{-3} are illustrated in Fig.5.7(b). For the same reason discussed in Chapter 4 when describing the SIPM-OOFDM-DSPM constellations, it is noticed in this figure that, the

sizes of the constellation points associated with relatively low signal modulation formats are also larger than those corresponding to relatively high signal modulation formats. In addition, Fig.5.8(a) and Fig.8(b) show that, compared to 16-PSK OOFDM, ML-SIPM-OOFDM does not degrade the system performance tolerances to chromatic dispersion and fiber nonlinearity. In Fig.5.8, the same system conditions used in previous chapters are considered while simulating both chromatic dispersion and fiber nonlinearity.

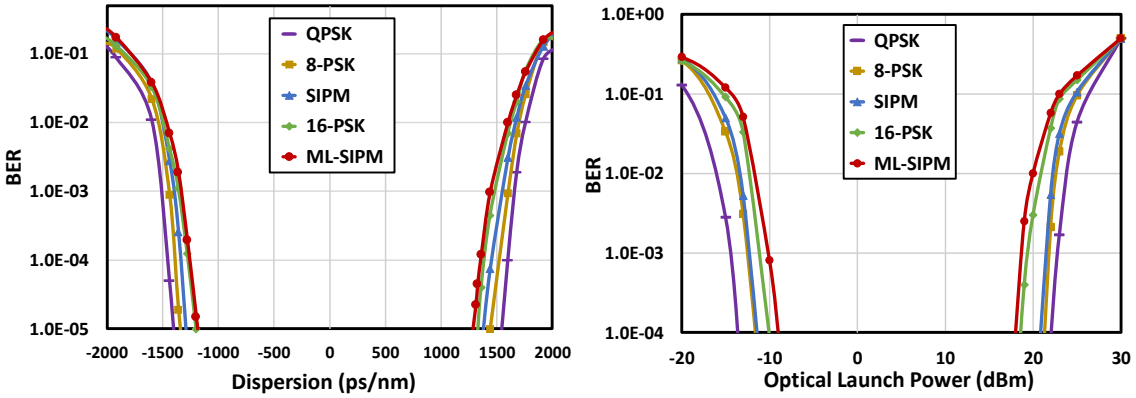

Fig.5.8. Performance tolerance of various transmission techniques after transmitting through SSMF IMDD PON systems (a) chromatic dispersion and (b) fiber nonlinearity.

5.4.2 Impact of ABL and Subcarrier Count

The effectiveness of utilising ABL in improving the ML-SIPM-OOFDM transmission data rate is explored in Fig.5.9 where maximum achievable ML-SIPM-OOFDM transmission bit

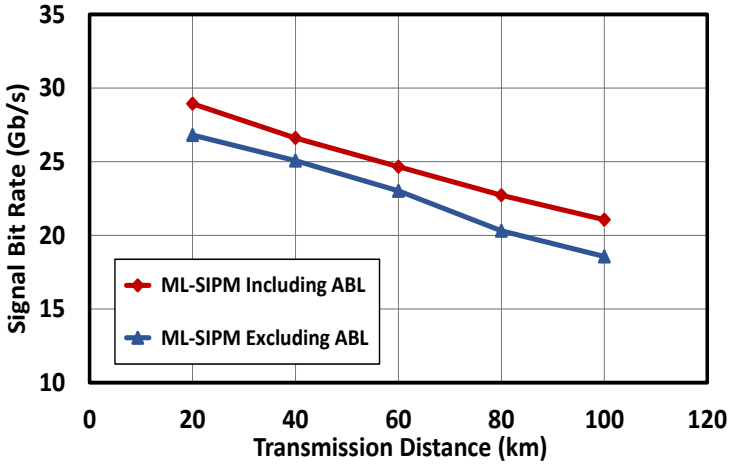

Fig.5.9. Maximum achievable ML-SIPM-OOFDM transmission bit rate as a function of transmission distance over IMDD SSMF PON system. Optical launch powers are fixed at -9dBm. ABL: adaptive bit loading.

rate versus reach performances for fixed optical launch powers of -9dBm are presented for two cases of including and excluding ABL. In implementing ABL, for a given transmission distance, negotiations between the transmitter and the receiver take place to determine the highest signal modulation format that can be taken on each individual subcarrier under the condition that the overall channel BER of $\leq 1.0\times10^{-3}$ is still satisfied. As already stated in Section 5.2, depending upon the channel spectral response experienced by a subcarrier, any power level of a subcarrier may be encoded using signal modulation formats varying from BPSK, to QPSK, to 8-PSK and to 16-PSK. Furthermore, for long transmission distances, the strong channel fading effect may cause high frequency subcarriers to suffer from excessive errors even if the lowest signal modulation formats are taken on them. When such situation occurs, those high frequency subcarriers are dropped completely.

It is shown in Fig.5.9 that for IMDD PON transmission distances up to 100km, ABL is capable of improving the ML-SIPM-OOFDM transmission bit rate by approximately 9% and such improvement is transmission distance-independent. These simulated behaviours agree extremely well with OOFDM experimental measurements reported in [7]. The agreements not only confirm the validity and accuracy of the numerical simulations presented here, but also imply the ML-SIPM-OOFDM capability of perfectly preserving the effectiveness of ABL regardless of transmission distance. On the other hand, very similar to ABL, APL also results in almost identical signal transmission bit rate improvements for ML-SIPM-OOFDM, SIPM-OOFDM and conventional OOFDM. The impact of APL is, however, not shown in this chapter as detailed discussions have already been made in Chapter 3 (Section 3.3).

As discussed in Section 5.2, the achievable ML-SIPM-OOFDM transmission bit rate is a function of subcarrier count. To gain an in-depth understanding of the subcarrier count-dependent ML-SIPM-OOFDM transmission bit rate for various transmission distances, Fig.5.10 is presented, in which the optical launch powers are fixed at -9dBm and ABL is also applied for all the cases. It can be seen in Fig.5.10 that an approximately 10% transmission bit rate enhancement is feasible when the subcarrier count is doubled. As an example, for any transmission distances in this figure, an increase of almost 30% in ML-SIPM-OOFDM transmission bit rate is achievable when increasing the subcarrier count from 16 to 128. In addition, the large subcarrier count-induced transmission bit rate improvement is also independent of transmission distance, as the transmission bit rate curves for different transmission distances exhibit parallel developing trends, as seen in Fig.5.10. Very similar to

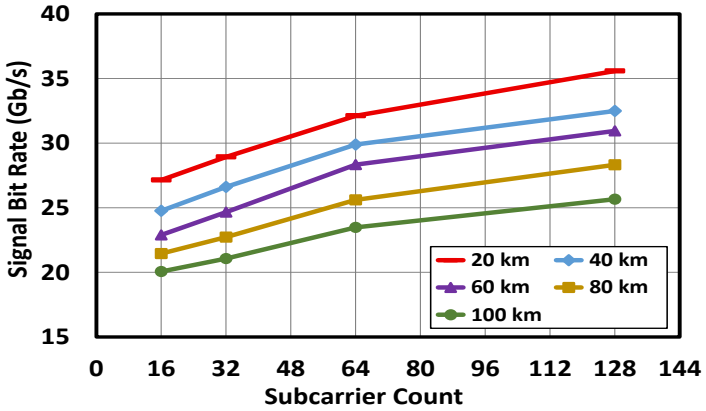

Fig.5.10. Subcarrier count-dependent ML-SIPM-OOFDM transmission bit rate for different transmission distances. Optical powers fixed at -9dBm. ABL is applied for all cases considered.

both ABL and APL, the large subcarrier count-enabled enhancement in ML-SIPM-OOFDM transmission bit rate does not comprise the system power budget. In practical transmission system design, the management of ML-SIPM-OOFDM subcarrier count may provide an effective means to dynamically and adaptively trade the achievable signal transmission bit rate with available transceiver DSP logic resources.

5.5 Conclusion

As a significantly improved variant of the SIPM-OOFDM, SIPM-OOFDM-SPM and SIPM-OOFDM-DSPM techniques that are capable of just carrying one extra information bit per subcarrier in the SIP information-bearing dimension, ML-SIPM-OOFDM has been proposed in this chapter and numerically investigated for the first time. The proposed technique simultaneously conveys four subcarrier power level-supported two extra information bits in the SIP information-bearing dimension. Extensive explorations of ML-SIPM-OOFDM performance characteristics have been undertaken based on which optimum key transceiver parameters are identified. For cost-sensitive IMDD SSMF PON systems, it has been shown that, compared to QPSK/8-PSK-encoded SIPM-OOFDM, ML-SIPM-OOFDM improves the signal transmission bit rate by 30% without increasing the transceiver DSP/architecture complexity. In addition, in comparison with conventional OOFDM encoded using 16-PSK, a 13% increase in ML-SIPM-OOFDM signal bit rate is also feasible without degrading the minimum required received optical power at a BER of 1.0×10^{-3} and also without compromising the transmission performance tolerance towards chromatic dispersion and fiber nonlinearity. Moreover, our results have also indicated that further 9% and 10% ML-SIPM-OOFDM transmission bit rate enhancements are also achievable when use is made of ABL and subcarrier count doubling, respectively.

References:

[1] F. Halabi, L. Chen, S. Parre, S. Barthomeuf, R. P. Giddings, C. Aupetit-Berthelemot, A. Hamié, and J. M. Tang, ‘’Subcarrier index-power modulated optical OFDM and its performance in IMDD PON systems,’’ *J. Lightw. Technol*., vol. 34, no. 9, pp. 2228–2234, May 2016.

[2] L. Chen, F. Halabi, R. P. Giddings, and J. M. Tang, “Subcarrier index-power modulated optical OFDM with superposition multiplexing for IMDD transmission systems,” *J. Lightw. Technol.*, vol. 34, no. 9, pp. 2228–2234, Oct. 2016.

[3] L. Chen, F. Halabi, J. Zhang, R. P. Giddings, and J. M. Tang, “Subcarrier index-power modulated-optical OFDM with dual superposition multiplexing for directly modulated DFB-based IMDD PON systems,” *IEEE Photon. J.*, vol. 10, no. 6, Dec. 2018.

[4] F. Halabi, L. Chen, R. P. Giddings, A. Hamié, Y. Dumas, P. Freyssinet, C. Aupetit-Berthelemot and J. M. Tang, ‘‘Subcarrier index-power modulated optical OFDM with dual superposition multiplexing for IMDD PON systems’’, *Optics Commun.*, vol. 433, pp. 190-194, Oct. 2018.

[5] F. Halabi, L. Chen, R. P. Giddings, A. Hamié, and J. M. Tang, “Multilevel subcarrier index-power modulated optical OFDM with adaptive bit loading for IMDD PON systems,” *IEEE Photon. J.*, vol. 8, no. 6, Art. No. 7907114, Dec. 2016.

[6] E. Giacoumidis, A. Kavatzikidis, A. Tsokanos, J. M. Tang, and I. Tomkos, ‘‘Adaptive loading algorithms for IMDD optical OFDM PON systems using directly modulated lasers,’’ *Opt. Commun. Netw.*, vol. 4, no. 10, pp. 769–778, Oct. 2012.

[7] X. Q. Jin, J. L. Wei, R. P. Giddings, T. Quinlan, S. Walker, and J. M. Tang, ‘‘Experimental demonstrations and extensive comparisons of end-to-end real-time optical OFDM transceivers with adaptive bit and/or power loading,’’ *IEEE Photon. J.*, vol. 3, no. 3, pp. 500-511, Jun. 2011.

[8] R. Giddings, “Real-time digital signal processing for OFDM-base future optical access networks,” *J. Lightw. Technol.*, vol. 32, no. 4, pp. 553–570, Feb. 2014.

[9] E. Giacoumidis, J.L. Wei, X. L. Yang, A. Tsokanos, and J. M. Tang, ‘‘Adaptive-modulation-enabled WDM impairment reduction in multichannel optical OFDM transmission systems for next-generation PONs,*’’ IEEE Photon. J.*, vol. 2, no. 2, pp. 130-140, Apr. 2010.

[10] G. P. Agrawal, Fibre-Optic Communication Systems, 2nd ed. Hoboken, NJ, USA, *Wiley*, 1997.

6. SIPM-OOFDM with Subcarrier Grouping

6.1 Introduction

In all the four previously proposed four transmission techniques, namely SIPM-OOFDM, SIPM-OOFDM-SPM, SIPM-OOFDM-DSPM and ML-SIPM-OOFDM [1-5], each individual subcarrier is used to carry the extra information bit(s). To enable a group of subcarriers to carry the extra information bits instead, this chapter proposes a significantly improved variant of SIPM-OOFDM, termed SIPM-OOFDM with subcarrier grouping (SIPM-SG-OOFDM) [6]. As detailed throughout this chapter, subcarrier grouping enhances the SIPM-OOFDM performance adaptability as it offers improvements in both signal transmission capacity and system power budget.

Similar to SIPM-OOFDM, in this technique all the 8-PSK/QPSK-encoded subcarriers of the two power levels are kept active and, based on the subcarrier-grouping approach discussed in Section 2.5.3, each OOFDM symbol is divided into multiple subcarrier groups. According to an incoming data sequence, the subcarrier power pattern within each subcarrier group is selected from a predefined subcarrier power pattern set. This allows each subcarrier group to bear extra user information bits. For simplicity, throughout this chapter we refer to this dimension as subcarrier group (SG) information-bearing dimension. Compared to SIPM-OOFDM, SIPM-SG-OOFDM offers an increase in signal bit rate by approximately 11%. More importantly, subcarrier grouping also provides SIPM-SG-OOFDM with an additional capability of automatically detecting and subsequently correcting SG information-bearing dimension errors at the receiver without consuming any valuable transmission bandwidth. As a direct result of the zero-overhead error correction capability, the above mentioned signal bit rate improvement is also companied with a 1dB gain in OSNR over 25km IMDD SSMF PON systems, as detailed in Section 6.4.

The major contributions presented in this chapter are summarized as follows: i) exploration and identification of optimum SIPM-SG-OOFDM transceiver design parameters that maximize the signal bit rate for arbitrary subcarrier group sizes, and ii) proposition and exploration of an effective SG-associated automatic error detection and correction technique with zero-overhead and low DSP complexity. Similar to the statement made in Chapter 5,

given that the SG-associated DSP functions could also be applied easily in SIPM-OOFDM-SPM, SIPM-OOFDM-DSPM and ML-SIPMOOFDM, in this chapter, special attention is focused on SIPM-SG-OOFDM only.

6.2 Operating Principle

In general, the operating principles of the proposed SIPM-SG-OOFDM technique are very similar to SIPM-OOFDM [1], except that the SIPM-SG-OOFDM data-encoding (data-decoding) DSP algorithms in the transmitter (receiver) are modified; in the SIPM-SG-OOFDM transmitter, each symbol consisting of a total number of N subcarriers is split into G groups and each group contains n subcarriers, i.e., $N=nG$. To minimise the DSP complexity, simple predefined lookup tables (LUTs) embedded in the transceiver map the incoming data sequence to a specific subcarrier power pattern for each subcarrier group, thus enabling extra information bits to be carried in the SG information-bearing dimension. The total number of bits conveyed by the i-th subcarrier group, B_i, is formulated as $B_i = B_{1i} + B_{2i}$ with B_{1i} representing the bits carried by the conventional subcarrier information-bearing dimension, and B_{2i} representing the extra bits carried in the SG information-bearing dimension. For the conventional subcarrier information-bearing dimension, B_{1i} is given by

$$B_{1i} = n_{Hi} b_H + \ n_{Li} b_L \tag{6.1}$$

where n_{Hi} (n_{Li}) are the number of high (low) power subcarriers within the i-th subcarrier group, and satisfy $n = n_{Hi} + n_{Li}$. b_H and b_L are the number of information bits carried by individual high and low power subcarriers, respectively, in the conventional information-bearing domain. It is well known that, in the SG information-bearing dimension, the total number of bits that can be carried by the i-th subcarrier group, B_{2i}, depend on the total number of possible subcarrier power patterns available in the group. B_{2i} can be expressed as

$$B_{2i} = \left\lfloor log_2(C_n^{n_{Hi}}) \right\rfloor, \text{ where } n_{Hi} < n \tag{6.2}$$

where $C_n^{n_{Hi}}$ denotes the total number of possible subcarrier power patterns and $\lfloor . \rfloor$ denotes the floor function. Clearly, the total number of information-carrying subcarrier power patterns is $2^{B_{2i}}$. When $C_n^{n_{Hi}}=2^{B_{2i}}$, each possible subcarrier power pattern of the $C_n^{n_{Hi}}$ set can be used to map B_{2i} information bits, whilst when $C_n^{n_{Hi}}>2^{B_{2i}}$, redundant subcarrier power patterns occur.

Table 6.1. *Example SIPM-SG-OOFDM Lookup Tables for n=2, 4, and 8*

n=2 (n_H=1, n_L=1)		n=4 (n_H=3, n_L=1)		n=8 (n_H=7, n_L=1)	
SG bits	Pattern	SG bits	Pattern	SG bits	Pattern
0	L H	00	H H H L	000	H H H H H H H L
1	H L	01	H H L H	001	H H H H H H L H
		10	H L H H	010	H H H H H L H H
		11	L H H H	011	H H H H L H H H
				100	H H H L H H H H
				101	H H L H H H H H
				110	H L H H H H H H
				111	L H H H H H H H

Table 6.1 illustrates the information-carrying subcarrier power-pattern examples for three subcarrier group sizes. For the simplest case of *n*=2, to encode an incoming PRBS stream, when ‘‘1(0)’’ bit is encountered, the corresponding subcarrier power pattern within a given subcarrier group is set high-low (low-high). This enables one extra information bit per group carried in the SG information-bearing dimension. On the other hand, in the conventional information-bearing dimension, further 5 bits from the PRBS stream are truncated, of which the first 3(2) are encoded using 8-PSK (QPSK) and the remaining 2(3) are encoded using QPSK (8-PSK).

At the receiver, to determine the received subcarrier power level, the subcarrier power detection and threshold decision DSP functions are employed, which are identical to those mentioned in Section 3.2. These DSP functions, which are located between the FFT and channel estimation and equalization, first calculate the optimum power threshold for the subcarrier, by making use of a training sequence that is periodically inserted into the user data sequence in the transmitter [1]. The subcarrier power threshold, $P_{threshold}$, is defined as

$$P_{threshold} = \frac{P_{8\text{-}PSK} + P_{QPSK}}{2} \tag{6.3}$$

where $P_{8\text{-}PSK}$ and P_{QPSK} are the received powers of the same subcarrier encoded using 8-PSK and QPSK, respectively. The DSP function of the zero-overhead automatic error correction is described below, and its procedures are illustrated in Fig.6.1. By making use of the identified frequency-dependent subcarrier power threshold, the subcarrier power pattern of a targeted subcarrier group is firstly determined, which is then compared with the predefined subcarrier power pattern set stored in the group associated LUT at the receiver. If the detected subcarrier power pattern belongs to the predefined set, then the group-conveyed information bits are decoded accordingly in both the SG information-bearing dimension and the conventional

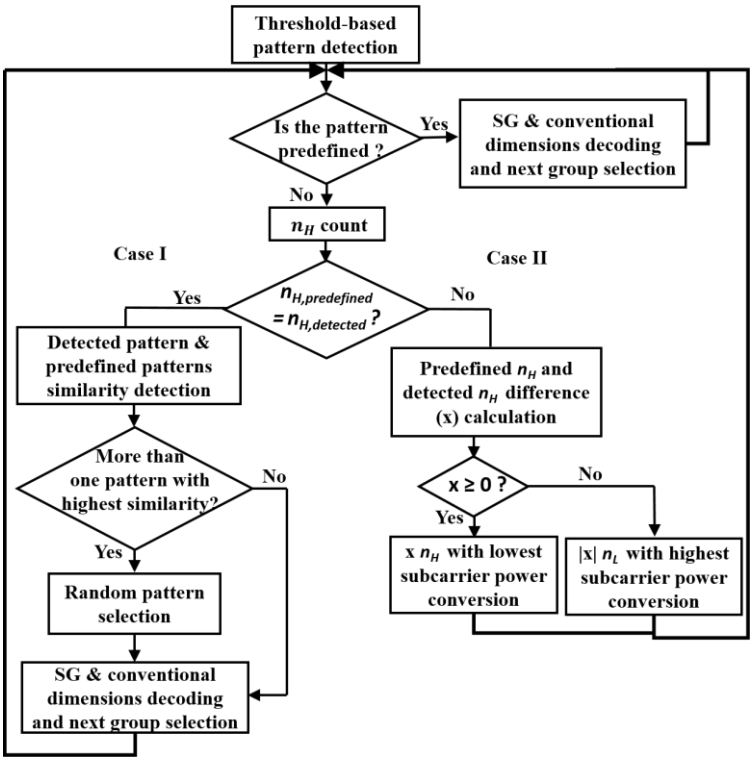

Fig.6.1. Zero-overhead automatic error correction procedure adopted in the SIPM-SG-OOFDM receiver.

information-bearing dimension. On the other hand, if the detected subcarrier power pattern of the group does not belong to the predefined subcarrier power pattern set, calculations of the total number of high power subcarriers occurring in the group are then performed based on which two different cases may occur:

- Case I, where the calculated high power subcarrier number matches the adopted value, i.e., the detected subcarrier power pattern is one of the redundant subcarrier power patterns. For specific n and n_{Hi}, each individual redundant subcarrier power pattern can be made known easily, together with its similarity with respect to each of the predefined subcarrier power pattern. Here the subcarrier power pattern similarity is defined as the minimum number of necessary subcarrier power status changes required to convert the present subcarrier power pattern to a targeted predefined one. For this case, the predefined subcarrier power pattern with the highest similarity with respect to the detected pattern is selected to replace the detected one. Whilst there exist more than one predefined subcarrier power patterns with the same highest similarity with respect to the detected pattern, then a random selection is made from the predefined subcarrier power patterns with the same similarity. Mapping between

the detected subcarrier power pattern and the best matching predefined subcarrier power pattern can be implemented with simple LUTs.

- Case II, where the calculated number of high power subcarriers of the detected group does not match the adopted value, and their difference is assumed to be x. When $x \geq 0$, x high power subcarriers with lowest subcarrier powers are converted to low power subcarriers; whilst when $x \leq 0$, $|x|$ low power subcarriers with highest subcarrier powers are converted to high power subcarriers. After that, the aforementioned DSP procedures can be applied to process the subcarrier group with converted subcarrier power status. The required DSP for Case II can be implemented with simple logic functions such as comparators, multiplexers and combinational logic, thus the increase in overall receiver DSP complexity is minimal. Furthermore, when comparing complexity to OFDM-based wireless systems involving subcarrier index modulation, low complexity is achieved as the wireless systems [7-10] are based on schemes that require complex functions, for example maximum likelihood detectors (complex multiplications), log-likelihood ratio detectors (multiplications, divisions, logarithms and exponentials) and energy-detection (multiplications and divisions).

Based on above discussions, it is easy to understand the following three points:

- For a specific hardware transceiver design, variations in subcarrier grouping can be easily conducted dynamically in the digital domain. As discussed in Section 6.4, such operation alters, to some extent, the transceiver performance in terms of both signal bit rate and system power budget. This implies that subcarrier grouping can improve the transceiver adaptability and performance flexibility.
- The abovementioned SG-induced performance characteristics can be further enhanced when variations in encoding/decoding schemes are also made in the digital domain, which leads to the transmission technique alterations among SIPM-OOFDM, SIPM-OOFDM-SPM, SIPM-OOFDM-DSPM, ML-SIPM-OOFDM and SIPM-SG-OOFDM. Thus, it is practically feasible to design a versatile and elastic transceiver capable of dynamically varying its performance characteristics to always provide optimum performances for different system/traffic status.
- Errors do not propagate across different subcarrier groups and different symbols, as each subcarrier group is treated separately in coding/decoding.

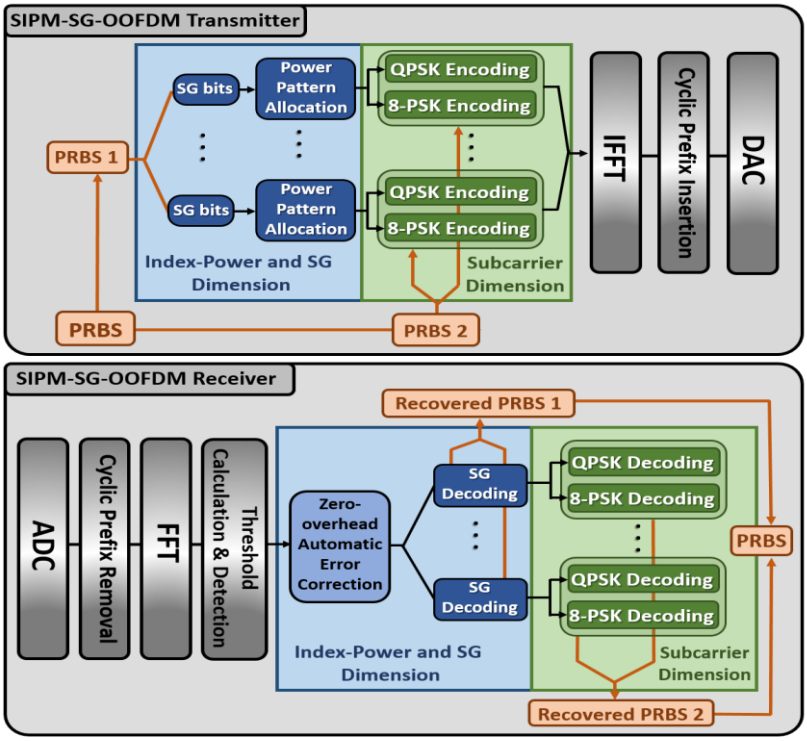

Fig.6.2. Schematic illustration of the SIPM-SG-OOFDM transceiver model

To summarize the above-described SIPM-SG-OOFDM operating principle, Fig.6.2 is presented, where major subcarrier grouping DSP functions incorporated in the transmitter and receiver are illustrated.

6.3 Transceiver Parameter Optimization

The main objective of this section is to identify optimum subcarrier grouping parameters capable of maximizing the SIPM-SG-OOFDM transmission capacity. Based on Eq.(6.1) and Eq.(6.2), the total number of bits that can be transmitted by the *i*-th symbol is

$$B_i = \sum_{i=1}^{G} [n_{Hi} b_H + n_{Li} b_L + \lfloor \log_2(C_n^{n_{Hi}}) \rfloor] \quad (6.4)$$

From Eq.(6.4), it is easy to understand that B_{1i} reaches its maximum when $n_{Hi} = n$, however, this results in B_{2i}=0. On the other hand, B_{2i}, is maximised when $n_{Hi} = n/2$, under which B_{1i} can, however, only reach half of its full potential. To explore the information carrying capacity trade-off between these two information-bearing dimensions, the number of information bits carried by each subcarrier group is plotted in Fig.6.3 for the following

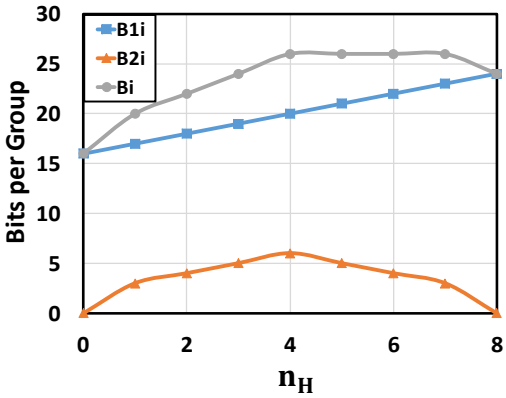

Fig.6.3. Number of bits per group versus n_H when N=32, n=8, and G=4.

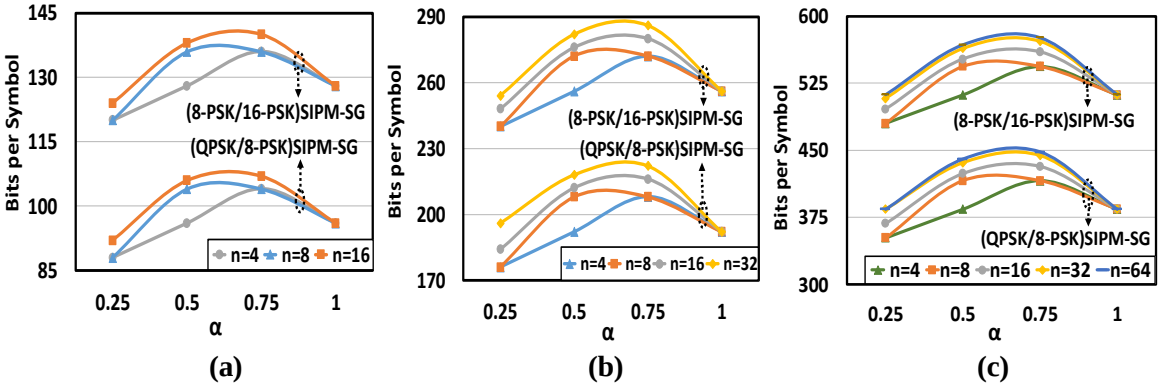

Fig.6.4. Number of bits per symbol versus α for (a) N=32 (b) N=64 (c) N=128.

parameters: N=32, n=8, and G=4. Fig.6.3 indicates that B_i is maximized at an optimum n_{Hi}, termed, n_{Hopt}. To eliminate the impact of subcarrier group size on the performance of different subcarrier grouping schemes, a parameter α is introduced here, which represents the ratio between the total number of high power subcarriers and the total number of subcarriers within a group.

Fig.6.4 is plotted to investigate the α-dependent information bits per symbol. This figure also investigates the α-impact when higher modulation formats are considered on SIPM-SG-OOFDM such as 8-PSK (16-PSK) as low (high) power encoded subcarriers. It can be seen in Fig.6.4(a) that, for different subcarrier group sizes, the maximum information bits per symbol are achieved when α is approximately 0.7. Comparisons between Fig.6.4(a), Fig.6.4(b) and Fig.6.4(c) also indicate that the optimum α remains almost constant regardless of variations in N, n, and the modulation formats used in SIPM-SG-OOFDM. Thus α =0.7 can be regarded as an optimum grouping parameter, which will be considered in all the following numerical simulations. It is also shown in Fig.6.4 that the total number of bits per symbol increases with

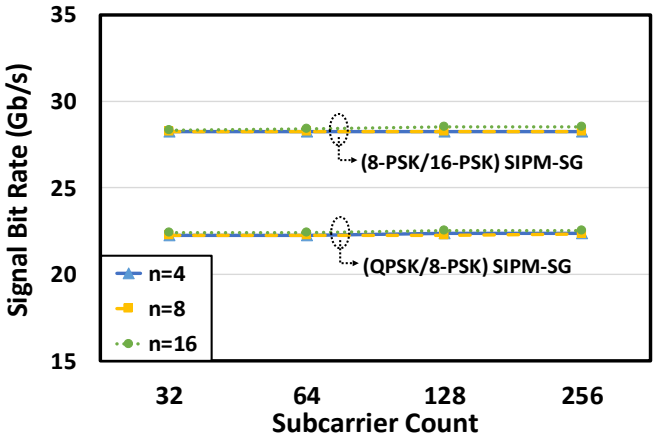

Fig.6.5. Signal bit rate performance of both (QPSK/8-PSK) SIPM-SG and (8-PSK/16-PSK) SIPM-SG versus subcarrier count.

Table 6.2. *Transceiver and Transmission System Parameters*

Parameter	Value
Total number of IFFT/FFT points	64
Data-carrying subcarriers	31
Modulation formats for SIPM-OOFDM	QPSK or 8-PSK
PRBS data sequence length	400,000 bits
Cyclic prefix	25%
DAC & ADC sample rate	12.5GS/s
DAC & ADC bit resolution	9 bits
Clipping ratio	12 dB
PIN detector sensitivity	-19 dBm*
PIN responsivity	0.8 A/W
Fiber length	25km
SSMF dispersion parameter at 1550 nm	16 ps/(nm.km)
SSMF dispersion slope at 1550 nm	0.07 ps/nm/nm/km
Linear fiber attenuation	0.2 dB/km
Kerr coefficient	2.35×10^{-20} m²/W

*Corresponding to 10Gb/s non-return-to-zero data at a BER of 1.0×10^{-9}

n, this, however, does not affect the overall achievable SIPM-SG-OOFDM signal bit rate as shown in Fig.6.5 which explores the signal bit rate performance of both QPSK/8-PSK SIPM-SG-OOFDM and 8-PSK/16-PSK SIPM-SG-OOFDM while increasing *N*. For both cases, Fig.6.5 shows a flat signal bit rate developing trend. More importantly, a 27% increase in signal bit rate is achieved when 8-PSK and 16-PSK are used instead of QPSK and 8-PSK, respectively. For simplicity but without losing any generality, QPSK/8-PSK SIPM-SG-OOFDM is considered in the following parts of this chapter.

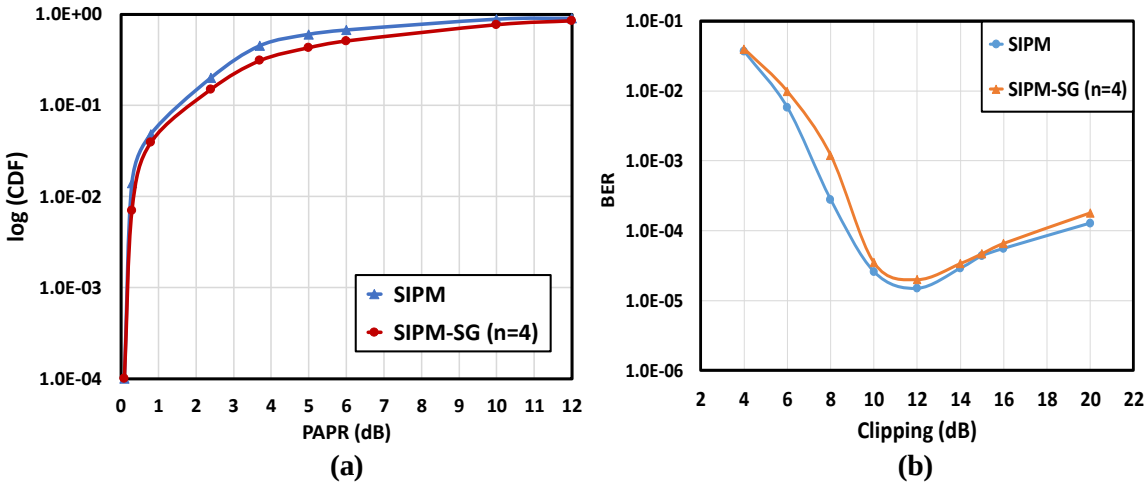

Fig.6.6. (a) Cumulative distribution functions for SIPM-OOFDM, and SIPM-SG-OOFDM. (b) Overall BER versus clipping ratio over 25km SSMF IMDD transmission systems with the optical launch power fixed at -9dBm.

6.4 Transmission Performance

Having discussed the general SIPM-OOFDM-SPM operating principle and based on the identified optimum subcarrier grouping parameters of the previous section, this section detailed numerical simulations are presented. In these simulations, the default transceiver parameters undertaken are listed in Table 6.2. As shown in this table, a clipping ratio of 12dB is used which is the optimum value for SIPM-OOFDM transceivers identified in Chapter 3. The same value is adopted here since, SIPM-SG-OOFDM and SIPM-OOFDM' CDF curves exhibit an almost identical performance in terms of PAPR as shown in Fig.6.6(a). This is also confirmed in Fig.6.6(b), which investigates the impact of the clipping ratio on both SIPM-OOFDM and SIPM-SG-OOFDM transmission performance over 25km SSMF IMDD with an optical launch power of -9dBm. Fig.6.6(b) also implies that the clipping ratio is subcarrier grouping-independent.

6.4.1 Signal Bit Rate

By making use of the transceiver architecture identical to SIPM-OOFDM [1], the SIPM-SG-OOFDM signal bit rate, *R*, is given by

$$R = \frac{\left(\sum_{i=1}^{G-1}\left(nb_H\alpha + nb_L(1-\alpha_{opt}) + \left\lfloor log_2\left(C_n^{n_{Hiopt}}\right)\right\rfloor\right) + \beta\right) f_s}{2N(1+\sigma)} \tag{6.5}$$

Table 6.3. *Signal Bit Rate Comparisons*

Modulation Format	Signal Bit Rate (Gb/s)
8-PSK	17.80
(QPSK/8-PSK) SIPM	20.77
(QPSK/8-PSK) SIPM-SG	23.125
16-PSK	23.73

where $\beta = \left((n-1)b_H\alpha + (n-1)b_L(1-\alpha_{opt}) + \lfloor log_2(C_n^{n_{Hopt}}) \rfloor\right)$ accounts for the information bits conveyed in the final group of a symbol due to 31 data-carrying subcarriers; f_s is the sampling rates of the DAC and ADC, and σ is the coefficient introduced to take into account the signal transmission bit rate reduction due to cyclic prefix and training sequence. By making use of Eq.(6.5), the SIPM-SG-OOFDM signal bit rate can be easily computed and compared with other transmission techniques as summarized in Table 6.3. In this table, it is shown that the proposed technique gives rise to a maximum signal bit rate of 23.125Gb/s (n=4), which exceeds the 8-PSK-encoded OOFDM and the QPSK/8-PSK-encoded SIPM-OOFDM by approximately 30% and 11%, respectively. Moreover, the 8-PSK/QPSK-encoded SIPM-SG-OOFDM signal bit rate is very similar to the 16-PSK/16-QAM-endoded OOFDM signal bit rate, which, however, corresponds to a high minimum received optical power required for achieving a BER of 1.0×10^{-3} [1, 5]. Such an improvement in signal bit rate also indicates that based on identical transceiver architecture, at least >30% variations in

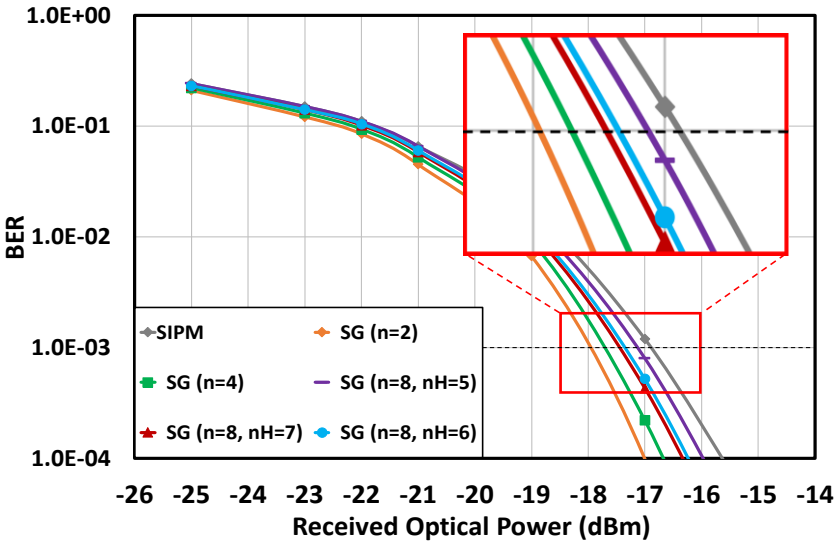

Fig.6.7. Overall channel BER versus received optical power after transmitting through 25 km SSMF IMDD PON systems for SIPM-OOFDM and SIPM-SG-OOFDM for the cases of n=2,4, and 8 (n_H=5, 6, and 7).

signal bit rate are achievable by just altering DSP design configuration. In particular, this signal bit rate dynamic range can also be further increased when use is made of the adaptive group power loading technique.

6.4.2 Performance over SSMF IMDD PON Systems

In this subsection, a VPIphotonics SSMF simulation model is used to explore the 23.125Gb/s SIPM-SG-OOFDM transmission performances over 25km SSMF IMDD PON systems subject to the transceiver/system parameters listed in Table 6.2. Similar to all previous chapters, in all numerical simulations, an ideal intensity modulator based on Eq. (3.2) is used in the transmitter and a PIN is used in the receiver [1]. For fixed optical launch powers of -9dBm, Fig.6.7 shows BER performances of the proposed technique and the SIPM-OOFDM technique. In Fig.6.7, five subcarrier grouping schemes for N=32 are considered, which are: n=2 (n_H=1), 4 (n_H=3), and 8 (n_H=5, 6, and 7), each of these n_H values is close to the identified optimum α value for the corresponding n parameter. It is shown in Fig.6.7 that, compared with 20.177Gb/s SIPM-OOFDM signal, a maximum received optical power gain of approximately 1.0dB is achieved at a BER of 1.0×10^{-3} for the 23.125Gb/s SIPM-SG-OOFDM signal.

To further explore the relationships between the OSNR gain and various subcarrier grouping schemes, Fig.6.8(a) is plotted, which shows a reduction in OSNR gain with increasing n. This is because of the occurrence of an increased redundant pattern status as n increases. As evidenced in Fig.6.8(a), for n=8 with various n_H parameters, the lowest OSNR gain is observed when the redundant pattern status are maximum. This indicates that the maximum

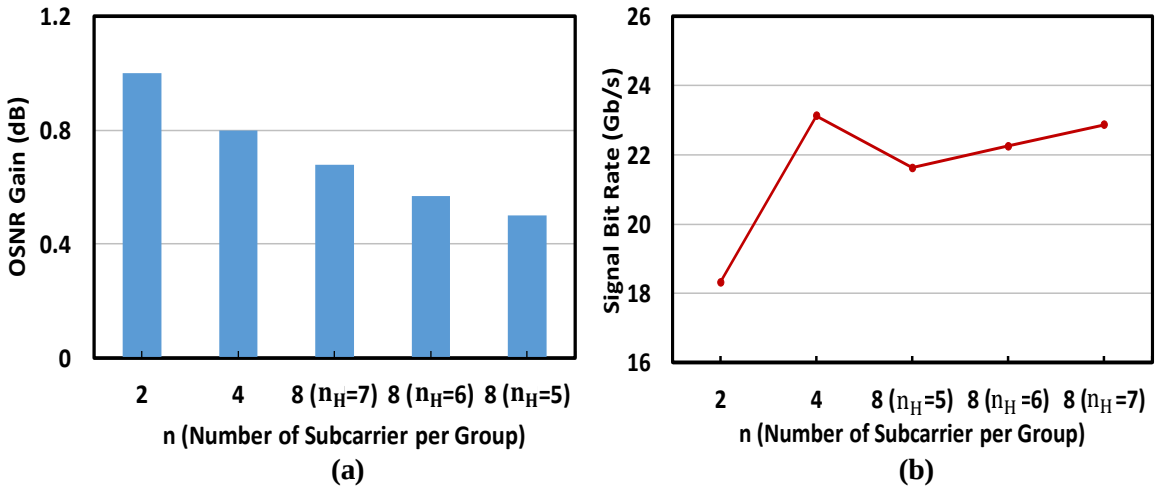

Fig.6.8. (a) OSNR gain for the cases of n=2,4, and 8 (n_H=5, 6, and 7) and (b) their signal bit rates.

1dB OSNR gain is achievable regardless of the grouping size *n*, as long as necessary improvements are made in the encoder/decoder algorithm procedure. For these five cases, Fig.6.8(b) summarizes their corresponding signal bit rate performances. Fig.6.8(b) shows a slight group size-dependent signal bit rate as predicted in both Chapter 4 and Chapter 5.

6.5 Conclusion

This chapter has proposed and numerically investigated an improved variant of SIPM-OOFDM, called SIPM-SG-OOFDM for signal transmissions over 25km SSMF IMDD PON systems. Numerical explorations have been undertaken in the optimum SIPM-SG-OOFDM transceiver design and its corresponding maximum achievable transmission performance over the considered PON systems. Moreover, this chapter has exploited the subcarrier-grouping approach not only to increase the SIPM-OOFDM signal bit rate by 11%, but also, to automatically correct errors at the receiver, which resulted in an OSNR gain of approximately 1.0dB without increasing the transceiver DSP/architecture complexity.

References:

[1] F. Halabi, L. Chen, S. Parre, S. Barthomeuf, R. P. Giddings, C. Aupetit-Berthelemot, A. Hamié, and J. M. Tang, ‘’Subcarrier index-power modulated optical OFDM and its performance in IMDD PON systems,’’ *J. Lightw. Technol*., vol. 34, no. 9, pp. 2228–2234, May 2016.

[2] L. Chen, F. Halabi, R. P. Giddings, and J. M. Tang, “Subcarrier index-power modulated optical OFDM with superposition multiplexing for IMDD transmission systems,” *J. Lightw. Technol.*, vol. 34, no. 9, pp. 2228–2234, Oct. 2016.

[3] L. Chen, F. Halabi, J. Zhang, R. P. Giddings, and J. M. Tang, “Subcarrier index-power modulated-optical OFDM with dual superposition multiplexing for directly modulated DFB-based IMDD PON systems,” *IEEE Photon. J.*, vol. 10, no. 6, Dec. 2018.

[4] F. Halabi, L. Chen, R. P. Giddings, A. Hamié, Y. Dumas, P. Freyssinet, C. Aupetit-Berthelemot and J. M. Tang, ‘‘Subcarrier index-power modulated optical OFDM with dual superposition multiplexing for IMDD PON systems’’, *Optics Commun.*, vol. 433, pp. 190-194, Oct. 2018.

[5] F. Halabi, L. Chen, R. P. Giddings, A. Hamié, and J. M. Tang, “Multilevel subcarrier index-power modulated optical OFDM with adaptive bit loading for IMDD PON systems,” *IEEE Photon. J.*, vol. 8, no. 6, Art. No. 7907114, Dec. 2016.

[6] F. Halabi, L. Chen, R. P. Giddings, A. Hamié, and J. M. Tang, “Subcarrier grouping-enabled improvement in transmission performance of subcarrier index-power modulated optical OFDM for IM/DD PON systems,” *J. Lightw. Technol.*, vol. 36, no. 20, pp. 4792–4798, Oct. 2018.

[7] T. Mao, Z. Wang, Q. Wang, S. Chen, and L. Hanzo, “Dual-mode index modulation aided OFDM,” *IEEE Access*, vol. 5, pp. 50–60, 2017.

[8] X. Zhang, H. Bie, Q. Ye, C. Lei, and X. Tang, “Dual-mode index modulation aided OFDM with constellation power allocation and low-complexity detector design,” *IEEE Access*, vol. 5, pp. 23871–23880, 2017.

[9] S. Dang, J. P. Coon, and G. Chen, “Adaptive OFDM with index modulation for two-hop relay-assisted networks,” *IEEE Trans. Wireless Commun.*, vol. 17, no. 3, pp. 1923–1936, Mar. 2018.

[10] R. Fan, Y. J. Yu, and Y. L. Guan, "Generalization of orthogonal frequency division multiplexing with index modulation," *IEEE Trans. Wireless Commun.*, vol. 14, no. 10, pp. 5350–5359, Oct. 2015.

[11] G. P. Agrawal, Fibre-Optic Communication Systems, 2nd ed. Hoboken, NJ, USA: *Wiley*, 1997.

7. Conclusions and Future Work

7.1 Conclusions

As an attempt to satisfy the requirements of future 5G mobile networks, this dissertation research has introduced multiple information-carrying dimensions into conventional OOFDM by proposing the following signal transmission techniques: SIPM-OOFDM, SIPM-OOFDM-SPM, SIPM-OOFDM-DSPM, ML-SIPM-OOFDM, and SIPM-SG-OOFDM.

In SIPM-OOFDM, it has been shown that the combined subcarrier index and subcarrier power acts as an extra information-carrying dimension, thus the resulting high and low subcarrier power pattern within an OFDM symbol enables extra user information to be conveyed per subcarrier. As a direct result, compared to conventional OOFDM adopting similar signal modulation formats, SIPM-OOFDM improves the signal bit rate performance without compromising the system power budget and without degrading the performance tolerance to both chromatic dispersion and fiber nonlinearity. In SIPM-OOFDM-SPM, the SPM operation is used to maximise the power usage efficiency of high power subcarriers thus improving the SIPM-OOFDM signal bit rate while avoiding any increase in the signal modulation formats. Whereas, in SIPM-OOFDM-DSPM, the SPM operation is used to maximise the power usage efficiency of both high and low power subcarriers thus increasing the SIPM-OOFDM-SPM signal bit rate by adopting even lower signal modulation formats. In ML-SIPM-OOFDM, compared with SIPM-OOFDM, more information bits are conveyed per subcarrier since the number of subcarrier power level can be increased to a predefined ML. As such, ML-SIPM-OOFDM considerably improves the SIPM-OOFDM signal bit rate without increasing the transceiver DSP/architecture complexity. Finally, in SIPM-SG-OOFDM, the subcarrier-grouping scheme is used to allow a group of subcarriers of various power levels to carry extra information bits in the SG information-bearing dimension. Furthermore, SIPM-SG-OOFDM is equipped with an additional capability of automatically detecting and subsequently correcting errors at the receiver. As a direct result, compared with SIPM-OOFDM, SIPM-SG-OOFDM not only improves the signal bit rate but also the system power budget.

More importantly, it has also been shown that all of these techniques share the same transceiver and hardware design except that slight modifications in the encoding/decoding DSP elements exist in the digital domain. Hence, to accommodate dynamically varying transmission performance characteristics such as signal bit rate and system power budget, an appropriate combination of the ML and SG operating principles in each of the above-mentioned signal transmission techniques is applicable. Clearly, this also implies that a further increase in transceiver design flexibility and system performance adaptability is feasible. Over 25km SSMF IMDD PON systems, results have shown that the proposed signal transmission techniques offer a dynamic range of at least 30% variations in signal bit rate and at least 1.0dB OSNR gain, compared with conventional OFDM, employing similar signal modulation formats, without increasing the transceiver DSP/architecture complexity.

7.2 Future Work

The work presented in this thesis has shown that the proposed signal transmission techniques are promising for IMDD PON systems. To rigorously verify these techniques and subsequently fully explore their potential for practical implementation in future 5G networks capable of providing services for a specific use case, further research is still essential, some of which is summarised below:

1) Real-time experimental demonstrations of adaptive and flexible multi information-carrying dimension OOFDM transceiver

   As discussed in the previous sections, the proposed signal transmission techniques share the same hardware design and only differ in the encoding/decoding DSP elements. Nevertheless, these DSP elements, each corresponding to a technique, can be implemented in transceiver FPGAs in parallel, as their DSP logic resource usages are marginal compared to other functions such as IFFT/FFT. Therefore, depending on the dynamic traffic status and network requirements, such a transceiver is capable to not only dynamically switch from one technique to another but also combine different techniques to satisfy the requirements for a particular scenario. For instance, for power budget-limited transmission systems, the encoding/decoding DSP elements of SIPM-SG-OOFDM can be switched on, which can even be combined with SIPM-

OOFDM-SPM or SIPM-OOFDM-DSPM to further improve the system power budget by enhancing the subcarrier power utilisation efficiency. Whilst for bandwidth-hungry transmission systems with sufficiently large power budgets, the encoding/decoding DSP elements of ML-SIPM-OOFDM can be switched on, which can, once again, be combined with SIPM-OOFDM-SPM, SIPM-OOFDM-DSPM or SIPM-SG-OOFDM to further improve the signal bit rate by maximising the information-carrying dimensions. Offline experimental demonstrations of these transceivers should be conducted to verify the transceiver designs for various application scenarios. After that, real-time transceivers should be experimentally demonstrated because such demonstrations are critical for not only evaluating the true potential of the transceivers, but also for identifying the limitations set by practical hardware that numerical simulations and offline demonstrations may not be able to cover.

2) Experimental demonstrations of 50Gb/s/λ 25km SSMF IMDD PON systems using 10G-class optics

As discussed in Chapter 1, 5G fronthaul/backhaul links may have a very large dynamic variation range in terms of signal bandwidth and system power budget. Moreover, such 5G links also impose strong restrictions in overall system cost. The unique features associated with the transceivers presented in the thesis, including, for example, flexible performances, versatile architectures and excellent cost-effectiveness suggest that the transceivers may be able to address the above challenges faced by 5G fronthaul/backhaul links. As such, the next step in the future work is to explore the feasibility of utilising the abovementioned transceivers in 5G fronthaul/backhaul links with particular focus on experimental demonstrations of 50Gb/s/λ 25km SSMF IMDD PON systems using 10G-class optics. Given the fact that the present market-available low-cost 10G-class optics are bandwidth limited, achieving the targeted 50Gb/s/λ signal transmission over 25km SSMFs is technically challenging, as it requires highly spectral efficient signal transmission techniques and advanced DSP techniques to solve the linear and nonlinear effects associated with the systems. To improve the signal spectral efficiency while maintaining sufficient system power budget, further explorations of extra information-carrying dimensions may be necessary to enable a further reduction in the adopted signal modulation formats while still attaining high signal transmission capacity. To effectively

compensate for various system linear and nonlinearities effects, advanced DSP algorithms should be developed, verified and optimised.

Appendix

Journal Publications

[1] **F. Halabi**, L. Chen, S. Parre, S. Barthomeuf, R. P. Giddings, C. Aupetit-Berthelemot, A. Hamié, and J. M. Tang, ‘’Subcarrier index-power modulated optical OFDM and its performance in IMDD PON systems,’’ *J. Lightw. Technol*., vol. 34, no. 9, pp. 2228–2234, May 2016.

[2] L. Chen, **F. Halabi**, R. P. Giddings, and J. M. Tang, “Subcarrier index-power modulated optical OFDM with superposition multiplexing for IMDD transmission systems,” *J. Lightw. Technol.*, vol. 34, no. 9, pp. 2228–2234, Oct. 2016.

[3] **F. Halabi**, L. Chen, R. P. Giddings, A. Hamié, and J. M. Tang, “Multilevel subcarrier index-power modulated optical OFDM with adaptive bit loading for IMDD PON systems,” *IEEE Photon. J.*, vol. 8, no. 6, Art. No. 7907114, Dec. 2016.

[4] **F. Halabi**, L. Chen, R. P. Giddings, A. Hamié, and J. M. Tang, “Subcarrier grouping-enabled improvement in transmission performance of subcarrier index-power modulated optical OFDM for IM/DD PON systems,” *J. Lightw. Technol.*, vol. 36, no. 20, pp. 4792–4798, Oct. 2018.

[5] **F. Halabi**, L. Chen, R. P. Giddings, A. Hamié, Y. Dumas, P. Freyssinet, C. Aupetit-Berthelemot and J. M. Tang, ‘‘Subcarrier index-power modulated optical OFDM with dual superposition multiplexing for IMDD PON systems’’, *Optics Commun.*, vol. 433, pp. 190-194, Oct. 2018.

[6] L. Chen, **F. Halabi**, J. Zhang, R. P. Giddings, and J. M. Tang, “Subcarrier index-power modulated-optical OFDM with dual superposition multiplexing for directly modulated DFB-based IMDD PON systems,” *IEEE Photon. J.*, vol. 10, no. 6, Dec. 2018.

Conference Publication

[1] **F. Halabi**, L. Chen, S. Parre, S. Barthomeuf, R. P. Giddings, C. Aupetit-Berthelemot and J. M. Tang, "Subcarrier index-power modulated optical OFDM (SIPM-OOFDM) for IMDD PON systems,'' *Optical Fibre Communication (OFC) Conference,* Th3C.1, pp.1-3, Mar. 2016.